NASA CONTRACTOR REPORT

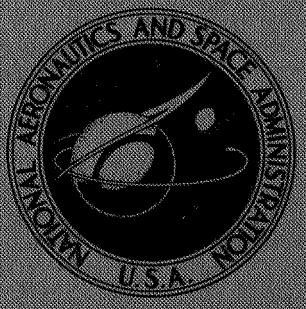

NASA CR-2162

NASA CR-2162

EVALUATION OF CRYOGENIC INSULATION MATERIALS AND COMPOSITES FOR USE IN NUCLEAR RADIATION ENVIRONMENTS

Prepared by
GENERAL DYNAMICS
CONVAIR AEROSPACE DIVISION
Fort Worth, Texas
for George C. Marshall Space Flight Center

NATIONAL AERONAUTICS AND SPACE ADMINISTRATION • WASHINGTON, D. C. • DECEMBER 1972

TECHNICAL REPORT STANDARD TITLE PAGE

1. REPORT NO.	2. GOVERNMENT ACCESSION NO.	3. RECIPIENT'S CATALOG NO.
NASA CR-2162		

4. TITLE AND SUBTITLE	5. REPORT DATE
EVALUATION OF CRYOGENIC INSULATION MATERIALS AND COMPOSITES FOR USE IN NUCLEAR RADIATION ENVIRONMENTS	December 1972
	6. PERFORMING ORGANIZATION CODE

7. AUTHOR(S)	8. PERFORMING ORGANIZATION REPORT #
Listed for each Section separately	FZK-385, 386, 387, 388, 389

9. PERFORMING ORGANIZATION NAME AND ADDRESS	10. WORK UNIT NO.
General Dynamics Convair Aerospace Division Fort Worth Operation Forth Worth, Texas	391
	11. CONTRACT OR GRANT NO. NAS 8-18024
	13. TYPE OF REPORT & PERIOD COVERED Contractor
12. SPONSORING AGENCY NAME AND ADDRESS National Aeronautics and Space Administration Washington, D. C. 20546	14. SPONSORING AGENCY CODE

15. SUPPLEMENTARY NOTES

16. ABSTRACT

This report is comprised of six separate reports generated under this contract covering the following subjects :

1. Composite Materials Test
2. Test of Liquid-Level Sensors and Fissioncouples
3. Test of Valve-Seal Materials
4. Boron-Epoxy Composites
5. Radiation Analysis of Explosive Materials and Bifuels for RNS Applications
6. Test of Thermal Insulation

17. KEY WORDS	18. DISTRIBUTION STATEMENT
Cryogenic Insulation Radiation	

19. SECURITY CLASSIF. (of this report)	20. SECURITY CLASSIF. (of this page)	21. NO. OF PAGES	22. PRICE
Unclassified	Unclassified	177	$3.00

MSFC - Form 3292 (-

*For sale by the National Technical Information Service, Springfield, Virginia 22151

PREFACE

This report was prepared by the Fort Worth operation of Convair Aerospace Division, General Dynamics Corporation, under Contract No. NAS8-18024, Evaluation of Cryogenic Insulation Materials and Composites for Use in Nuclear Radiation Environments, for the George C. Marshall Space Flight Center of the National Aeronautics and Space Administration. The work was administered under the technical direction of the Propulsion and Vehicle Engineering Division, Engineering Materials Branch of the George C. Marshall Space Flight Center, with Dr. R. L. Gause acting as project manager.

TABLE OF CONTENTS

Part I

COMPOSITE MATERIALS TEST

FZK-385

By

R. E. BULLOCK
E. E. KERLIN
J. E. WARWICK

FOREWORD

The radiation effects test described in this report is a part of technology studies conducted at the Nuclear Aerospace Research Facility in support of nuclear rocket vehicle development. The material specimens were irradiated during a test conducted for NASA/SNSO-C in order to take advantage of the higher exposure levels than would be available in the irradiations made under Contract NAS8-18024. This test, designated GTR-20C, was a 6000-MWh irradiation of NERVA materials and components. In addition to the composite materials, two pressure transducers were also irradiated for NASA/MSFC during GTR-20C; results of that test are given in report FZK-372.

The tested composites are research materials and are not readily available; therefore, the authors wish to express their appreciation to the following persons for making them available: Mr. E. C. McKannon of NASA/MSFC for the boron-aluminum tension specimens; Mr. W. G. Scheck of Convair San Diego for the graphite-epoxy tension specimens; and Mr. R. L. Van Auken of the Whittaker Corp. for the fiber-glass reinforced polyquinoxaline.

I. INTRODUCTION

Composite materials are being developed to perform special functions in aerospace vehicles. The special properties of these materials are achieved by careful selection and fabrication of the constituents to take advantage of particularly desirable features of each. A test has been performed to evaluate the effects of reactor radiation on three such materials – a boron-aluminum composite, a graphite-epoxy composite, and fiber-glass reinforced polyquinoxaline. Tension specimens of the boron-aluminum and graphite-epoxy and gaskets of the polyquinoxaline were irradiated during a 600-h run with the Ground Test Reactor (GTR) operating at a power level of 10 MW.

This work was conducted at the Nuclear Aerospace Research Facility (NARF) operated by the Fort Worth operation of the Convair Aerospace Division of General Dynamics for the George C. Marshall Space Flight Center of the National Aeronautics and Space Administration under Contract NAS8-18024. Under Contract NAS8-18024, the Fort Worth operation has performed numerous radiation effects experiments on organic materials and thermal insulations as a part of the technology program supporting the development of a nuclear rocket vehicle.

II. DESCRIPTION OF TEST

2.1 Test Specimens

Three types of composite materials were tested in the experiment described herein: (1) graphite-epoxy, (2) boron-aluminum, and (3) fiber-glass reinforced polyquinoxaline, both plain and Kapton covered. Specimens of these composites were wired to perforated aluminum sheets (7 in. x 9 in.) to make up the four irradiation panels shown in Figure 1.

2.1.1 Graphite-Epoxy Composite

Ten graphite-epoxy tension specimens (6 in. x 0.5 in. x 0.06 in.) were supplied, at the request of Dr, R. L. Gause of NASA/MSFC, by Mr. W. G. Scheck, Convair Aerospace Division of General Dynamics, San Diego operation. Four of these specimens were retained as unirradiated controls and three each were attached to panels 2 and 4 (Fig. 1).

2.1.2 Boron-Aluminum Composite

Twelve boron-aluminum tension specimens (4 in. x 0.5 in. x 0.02 in.) from two different sources were irradiated. Six specimens (1-6), all apparently identical, were provided by Mr. E. C. McKannan of NASA/MSFC; these were all irradiated on panel 1 (Fig. 1). Six (7-12) were provided by Mr. W. G. Scheck

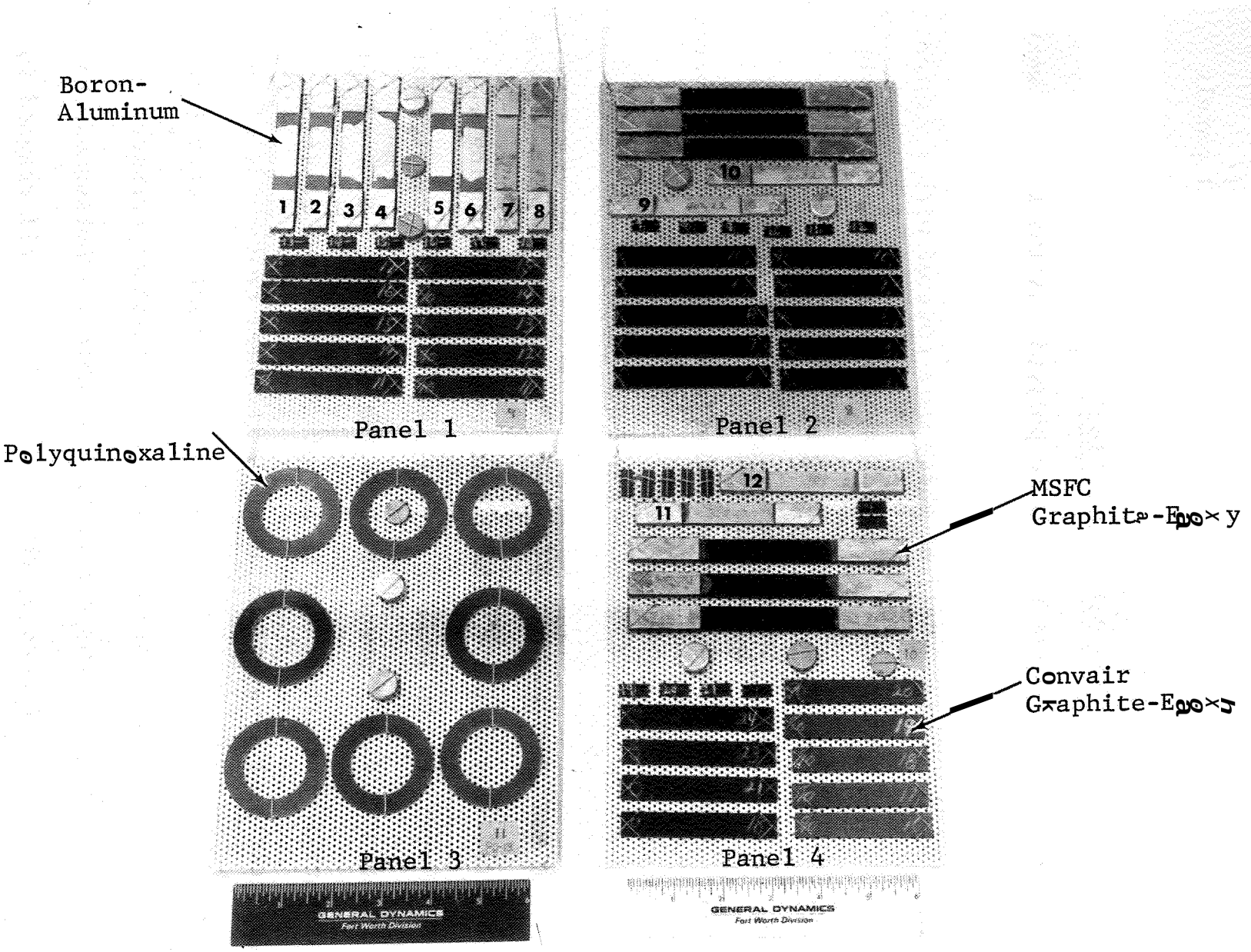

Figure 1 Specimens of Composite Materials Mounted for Irradiation

at the request of Dr. R. L. Gause; two each of these from three different batches of materials were irradiated on test panels 1, 2, and 4 (Fig. 1).

2.1.3 Reinforced Polyquinoxaline

Sixteen fiber-glass reinforced polyquinoxaline gaskets were supplied by Mr. R. L. Van Auken of Whittaker Corporation at the request of Dr. Gause. Half of these were covered with a Kapton film and half were plain. The Kapton-covered gaskets are shown on panel 3 of Figure 1. This panel is doubled like a closed book; it is shown unfolded in Figure 2 after having been irradiated. The plain gaskets are on the left and the Kapton-covered gaskets are on the right.

2.2 Irradiation of Specimens

The four test panels of composite materials described above were irradiated with the Ground Test Reactor (GTR) during a 6000-MWh reactor run from 21 May-19 June 1970. The reactor was operated at its full power of 10 MW for 600 h. All four of the test panels were irradiated in air at the west test position. These test panels were located along the west centerline of the reactor core at various distances from the reactor closet (Fig. 3). Locations of the various test panels and radiation exposure doses at these positions are listed in Table 1. Subsequent to the photograph of Figure 3, the test panels were all wrapped in

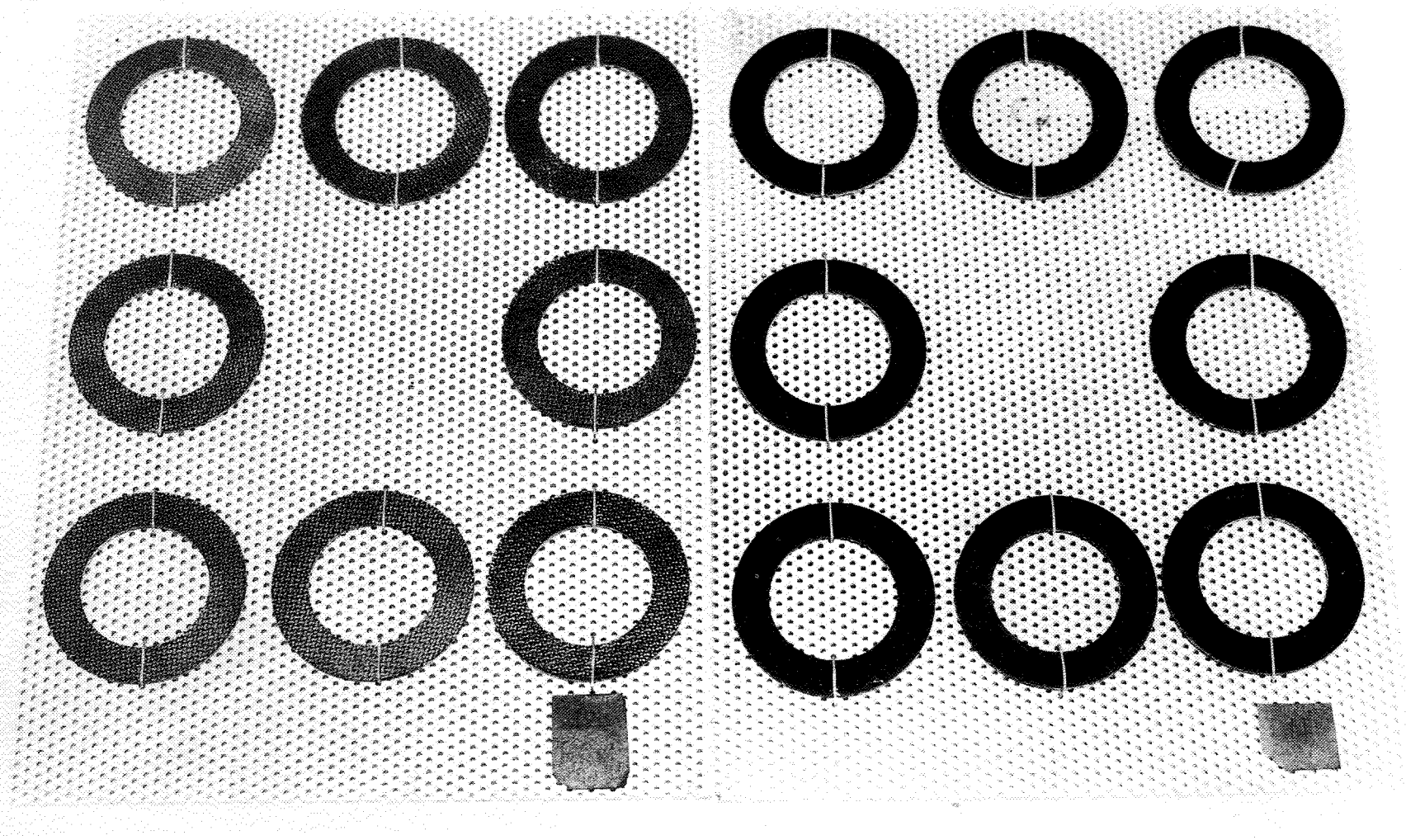

Figure 2 Polyquinoxaline Specimens after Irradiation

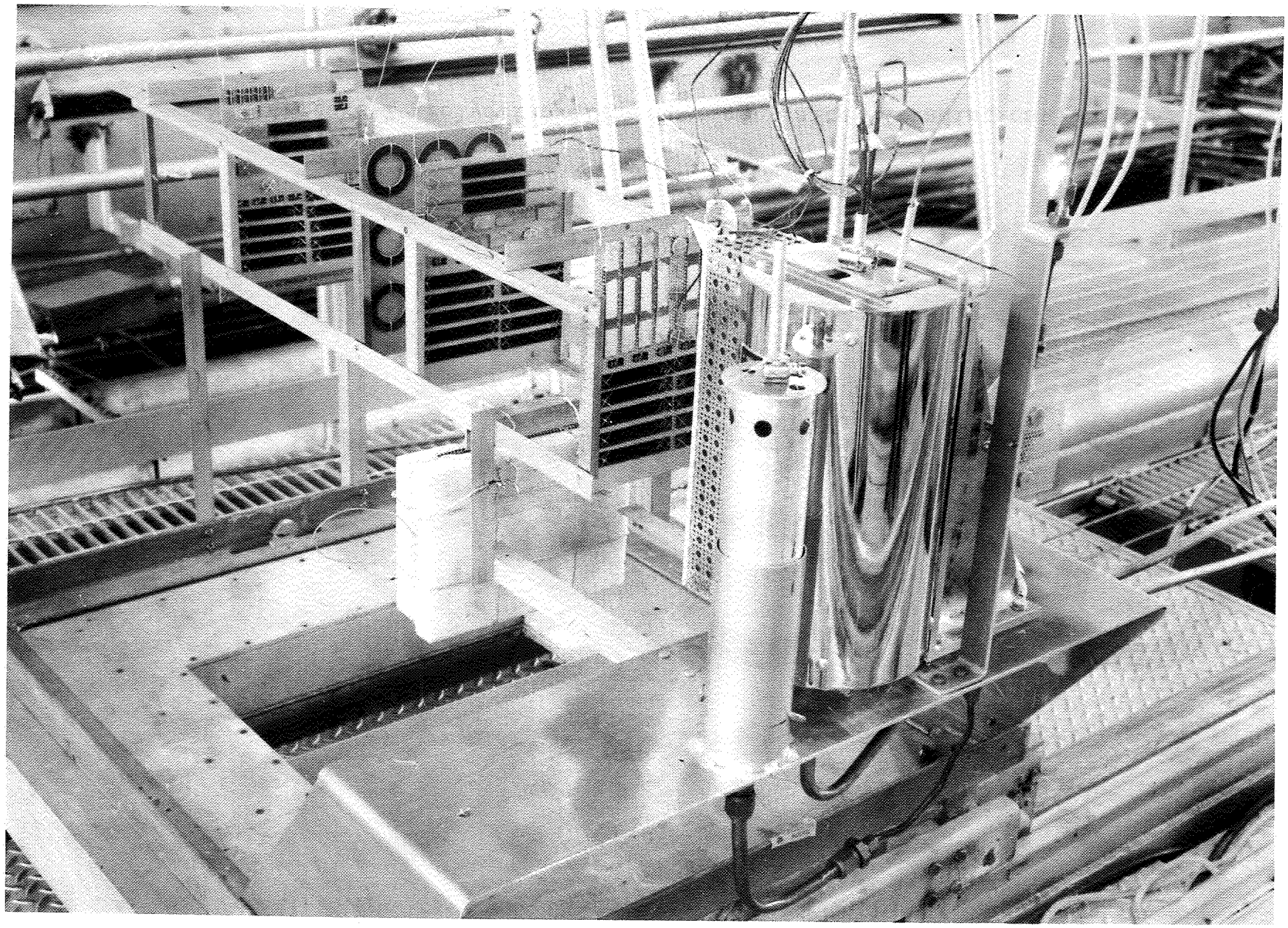

Figure 3 Panels of Test Specimens Mounted the Irradiation Assembly

heavy aluminum foil to minimize radioactive contamination of the specimens during irradiation.

Prior to the 6000-MWh irradiation, a short, low-power mapping irradiation was made for the purpose of measuring neutron fluxes and gamma dose rates. Data from the neutron detecting foils and cobalt glass gamma dosimeters in conjunction with neutron measurements made during the 6000-MWh irradiation were used to determine the radiation exposures.

Table 1

RADIATION DOSES AT *TEST* PANEL POSITIONS

Test Panel	Distance From Reactor Closet (in.)	Fast-Neutron Fluence (n/cm^2) $E > 1$ MeV	Gamma Dose[a] (ergs/g(C))	Thermal-Neutron Fluence (n/cm^2) $E < 0.48$ eV
1	12	7.5×10^{17}	1.0×10^{12}	3.0×10^{16}
2	23	4.2×10^{17}	5.8×10^{11}	3.4×10^{16}
3	28	3.3×10^{17}	4.5×10^{11}	3.3×10^{16}
4	37½	2.9×10^{17}	2.7×10^{11}	3.2×10^{16}

[a]Gamma doses for the 6000-MWh run were calculated by taking the ratios of gamma dose to fast-neutron fluence determined from the mapping irradiation and multiplying these by the measured fast-neutron fluences of column 3.

2.3 Radiation Dosimetry

The fast- and thermal-neutron fluences given in Table 1 were measured during the 6000-MWh reactor run by standard activation techniques. The fast-neutron fluence above 1 MeV was measured with 2-mil nickel foils; the (n,p) reaction with Ni^{58} produces Co^{58} which has a half-life of 71 days. Thermal-neutron fluences were determined by exposing pairs of 100-mil phosphorous disks, one bare and one covered with a 20-mil thickness of cadmium. The cadmium-difference activity of the P32 resulting from the (n,γ) reaction ($T_{\frac{1}{2}}$ = 14.3 d) is used to compute the fluence of neutrons below the cadmium cutoff energy of 0.48 eV.

Because gamma dosimeters suitable for measuring the doses to which the composite specimens were exposed are not available, the gamma doses in Table 1 were obtained by use of a measured gamma-to-neutron ratio. This ratio was measured during the low-dose mapping irradiation and then applied to the fast-neutron fluence of Table 1. This procedure assumes constancy of the gamma-to-neutron ratio in both runs.

2.4 Mechanical Testing of Specimens

2.4.1 Tension Testing

The graphite-epoxy and boron-aluminum tension specimens were mechanically tested at room temperature in the Process

III. TEST RESULTS

3.1 Graphite-Epoxy Specimens

Individual and average tensile strengths of unirradiated control specimens and of specimens irradiated on test panels 2 and 4 (Table 1) are listed in Table 2. These specimens were irradiated at ambient air temperature ($< 120^{o}$F) and were mechanically tested at room temperature. The average tensile strength of the unirradiated controls was 115 ksi, while the irradiated specimens on panels 2 and 4 had average strengths of 111 and 110 ksi, respectively. Thus, no effects of radiation were observed on tensile strengths of graphite-epoxy composites.

Table 2

TENSILE STRENGTHS OF GRAPHITE-EPOXY SPECIMENS

Tensile Strength (ksi)		
Controls	Panel 2	Panel 4
117	112	116
114	103	114
111	120	101
119	111	110
115		

Control Laboratory by utilizing a self-aligning test fixture which gives consistent results for such specimens. All specimens were loaded to failure in an Instron machine at a pull rate of 0.05 in./min. Ultimate tensile strengths (in psi) for these specimens were calculated by dividing the failure loads (lb) by the uniform cross-sectional areas ($in.^2$) of the specimens.

2.4.2 Compression Testing

The fiber-glass reinforced polyquinoxaline gasket specimens were tested at room temperature in the Irradiated Materials Laboratory during April 1971. Two types of compression tests were made on these circular samples. The first consisted of loading the samples between the compression pads of the 20,000-lb Instron tester. After a 15,000-lb load was applied the resulting thickness of the sample was measured. The thickness was again measured one hour after the load was removed.

The second test was a load deflection test performed by use of a special fixture (Fig. 4) loaned by Whittaker Corp. This test fixture was used with the 20,000-lb Instron. A linear variable differential transformer (LVDT) was used as the sensing element to determine the compression-vs-load characteristics. The LVDT output which represents the compression resulting from a load on the jig was recorded as the y coordinate on an x-y plotter and the corresponding load was recorded on the

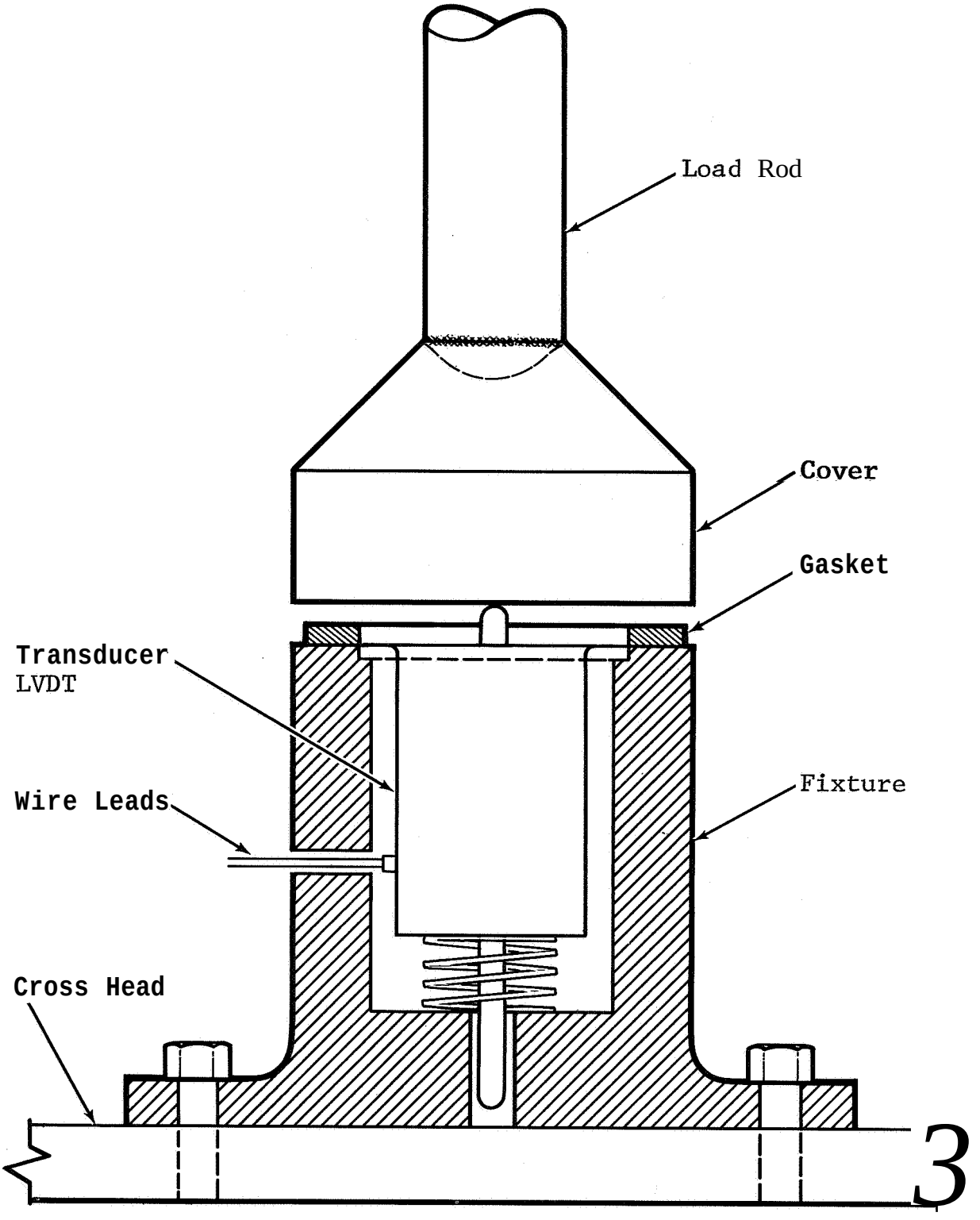

Figure *4* Compression Test Fixture for Gaskets

x coordinate. A block diagram of the excitation and read-out apparatus is shown below:

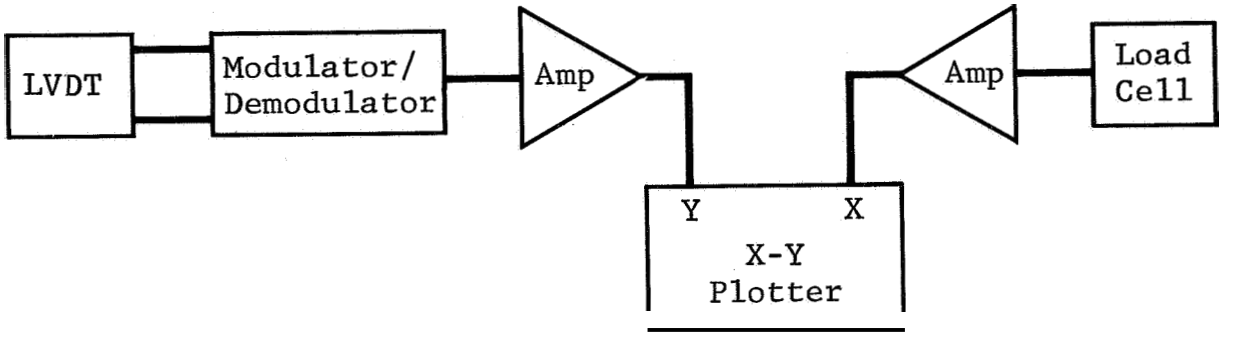

Displacement was calibrated over the usage range of the LVDT by means of a micrometer caliper graduated in 0.0001 in. The ordinate of the x-y plotter was set to full scale for 0.005-in. displacement of LVDT. The abscissa of the x-y plotter was set to full scale for 5000-lb load as detected by the load cell.

The gasket material was initially loaded to 800 lb and the LVDT was set to zero at that point. The load was alternately applied and removed ten times for each specimen. The first, second, and tenth cycles were recorded on the x-y plotter.

3.2 Boron-Aluminum Specimens

Individual and average tensile strengths of controls and of irradiated specimens are given in Table 3. The three pairs of B-A1 specimens supplied by Convair Aerospace Division of General Dynamics, San Diego operation, were from three different batches of material, designated 397 L2, 399 L2, and 402 L2, but all of the specimens were 55% boron filament by volume. There was very little difference in strength from batch to batch, and there was little difference between controls and irradiated specimens. The six irradiated specimens had an average tensile strength of 145 ksi, while the average control strength was 149 ksi. The average tensile strength of the B-A1 specimens provided by NASA/MSFC was 124 ksi. No control values were given, but this strength seems reasonable since these specimens were only 45% boron by volume.

3.3 Reinforced Polyquinoxaline

Individual thickness measurements for the polyquinoxaline specimens compressed under 15,000-lb load are given in Table 4. Table 5 contains the deflection data for the cyclic loading along with the original and final thicknesses. Although there are some indications in this data of radiation effects, the changes in compression properties due to radiation are slight.

Table 3

TENSILE STRENGTHS OF BORON–ALUMINUM SPECIMENS

Panel Number	Batch Number	Tensile Strength (ksi)	
		Controls [a]	Irradiated
1	397L2	131 170 171 153 156	165 130 148
2	402L2	175 169 128 123 149	140 141 141
4	399L2	154 140 129 147 143	148 146 147
1	NASA/ MSFC	–	129 122 123 94 130 143 124

[a] = These control strengths were supplied by Mr. W. G. Scheck in a telephone conversation of 13 August 1970.

Table 4

COMPRESSIBILITY OF POLYQUINOXALINE

Material Type and Specimen Number	Radiation Exposure		Orig. Thickness		Thickness at Load[c]		Final Thickness	
	Gamma Dose (ergs/gm(C))	Neutrons (n/cm^2) E>1.0 Mev	Minimum (in.)	Maximum (in.)	Minimum (in.)	Maximum (in.)	Minimum (in.)	Maximum (in.)
PQ-1[a]								
5	Control	Control	0.059	0.062	0.042	0.043	0.057	0.060
4-1	4.5×10^{11}	3.3×10^{17}	0.049	0.052	0.036	0.037	0.045	0.046
5-1	4.5×10^{11}	3.3×10^{17}	0.051	0.052	0.036	0.037	0.047	0.048
PI-13[b]								
1	Control	Control	0.059	0.061	0.045	0.046	0.056	0.058
4	4.5×10^{11}	3.3×10^{17}	0.059	0.061	0.052	0.053	0.059	0.061
5	4.5×10^{11}	3.3×10^{17}	0.064	0.067	0.052	0.053	0.062	0.064

[b] = Kapton covered fiber-glass reinforced polyquinoxaline
[a] = Plain fiber-glass reinforced polyquinoxaline
[c] = Compression load of 15,000 lb during measurement

Table 5

LOAD DEFLECTION OF POLYQUINOXALINE

Material Type and Specimen Number	Radiation Exposure		Orig. Thickness		Final Thickness		Deflection from 800 lb to 4000 lb		
	Gamma Dose (ergs/gm(C))	Neutron (n/cm^2) E>1.0 MeV	Minimum (in.)	Maximum (in.)	Minimum (in.)	Maximum (in.)	Cycle 1 (mils)	Cycle 2 (mils)	Cycle 10 (mils)
PQ-1									
6	Control	Control	0.059	0.062	0.057	0.059	2.10	1.15	0.87
1-1	4.5×10^{11}	3.3×10^{17}	0.049	0.051	0.047	0.047	2.15	0.93	0.78
2-1	4.5×10^{11}	3.3×10^{17}	0.050	0.052	0.048	0.048	2.45	0.90	0.78
3-1	4.5×10^{11}	3.3×10^{17}	0.047	0.051	0.045	0.048	2.23	0.88	0.77
PI-13									
2	Control	Control	0.059	0.062	0.059	0.061	2.56	1.27	1.06
1	4.5×10^{11}	3.3×10^{17}	0.063	0.069	0.062	0.068	2.88	1.20	1.08
2	4.5×10^{11}	3.3×10^{17}	0.064	0.067	0.063	0.066	2.65	1.13	1.03
3	4.5×10^{11}	3.3×10^{17}	0.066	0.069	0.065	0.067	3.23	1.12	1.03

Because of the rather small changes and the limited number of specimens tested, the effects cannot be said to be statistically significant. The observations cited below confirm, however, that the integrity of the materials were adversely affected at the exposure levels involved.

One sample of each of the two materials was torn apart. The irradiated Kapton covered gasket **(PI-13)** seemed to delaminate more easily than the control gasket and the Kapton film could be removed much more readily. The irradiated gaskets were also less flexible than the control. The Kapton film removed from the irradiated gasket was very weak and could be torn about as easily as an equal thickness of paper. The film from the un-irradiated gasket was very tough and could be torn only with great difficulty.

The irradiated plain gasket (PQ-1) delaminated much more easily than the control and the laminate material flaked easily. This could account for the observation that irradiated gaskets appeared to be more flexible than the control gasket. The unirradiated laminate material would tear but not flake,

Part II

TEST OF LIQUID-LEVEL SENSORS AND FISSIONCOUPLES

FZK-386

By

W. D. McMILLAN

SUMMARY

An irradiation test has been performed on level sensors suitable for use in gaging the height of liquid hydrogen in a propellant tank. A continuous capacitance probe 40 in. long and several each of point sensors of capacitance, thermal, and magnetostrictive types were irradiated in a liquid hydrogen dewar and evaluated for accuracy of measurement both during and between irradiation cycles. The Ground Test Reactor was operated at several power levels up to 5 MW, to investigate radiation rate effects, and for a sufficient time to expose the sensors to a radiation dose exceeding that predicted for ten missions of the Reusable Nuclear Shuttle. The irradiation was conducted in five cycles with the dewar being allowed to warm to about 55°F after each irradiation. Data were obtained by varying the liquid hydrogen level and observing the output and/or resistance of the sensors. Dielectric properties of the capacitive sensors were also measured.

The continuous capacitance probe began showing a radiation rate effect at a 1-MW power level ($\sim 3 \times 10^7$ ergs/gm (C)-h) due to an apparent increase in capacitance. The magnitude of this effect depended upon the length of probe exposed to gaseous hydrogen as well as the radiation rate. At 5 MW, the probe indicated a level of 35 in. when the actual level was 24 in. No permanent radiation effect was observed.

Thermal point sensors having resistance elements of gold-plated platinum wire and nickel-iron wire were essentially unaffected by the irradiation, Some problems were encounted with unirradiation control units, however. The thermal point sensor having a germanium element indicated a change in resistance with prolonged irradiation. Significant temporary radiation effects were observed during the cycles imparting the highest total neutron exposure, This effect became significant at a neutron fluence of about 2×10^{14} n/cm^2 (E > 1 MeV).

The magnetostrictive point sensors performed satisfactorily throughout the test.

The capacitance point sensors exhibited rate effects similar to those of the continuous probe. It was observed that sensors in the hydrogen gas would intermittently indicate liquid.

Fission thermopile assemblies consisting of ten uranium and ten bismuth beads were included in this test. However, all units failed by open circuit during the initial thermal cycling and no further information was obtained.

I. INTRODUCTION

An irradiation test has been performed for the purpose of evaluating liquid-level sensors for potential use on a nuclear powered vehicle. The sensors were irradiated in liquid hydrogen and thermal cycled after each of five irradiation steps at power levels up to 5 MW with the Ground Test Reactor. Data were taken during irradiation to evaluate rate effects and after each irradiation step to determine permanent damage effects. Eighteen point sensors of thermal, capacitance, and magnetostrictive types and one 40-in. long continuous capacitance probe were tested.

This work was conducted at the Nuclear Aerospace Research Facility (NARF) operated by the Fort Worth operation of the Convair Aerospace Division of General Dynamics for the George C. Marshall Space Flight Center of the National Aeronautics and Space Administration under Contract NAS8-18024. Under Contract NAS8-18024, Fort Worth operation has performed numerous radiation effects experiments on organic materials and thermal insulations as a part of the technology program supporting the development of the Nuclear Rocket Vehicle.

II. DESCRIPTION OF TEST

2.1 Test Articles

2.1.1 Liquid-Level Sensors

Three types of level sensors - thermal, capacitive, and magnetostrictive - suitable for use in liquid hydrogen were evaluated. The thermal and magnetostrictive devices were discrete (point) sensors and the capacitance sensors were of both point and continuous types. Table 1 identifies the sensors which are described by type below.

Table 1
LIQUID-LEVEL SENSORS

Type	Manufacturer	Model No.	Quantity
Thermal (point)	Acoustica Associates	STS 505	6
Thermal (point)	United Control Corp.	2641	3
Thermal (point)	Scientific Instruments	3	3
Magnetostrictive (point)	Conrac Corp.	UP1004S-5	3
Capacitance (point)	Transonics	L4447	3
Capacitance (continuous)	Transonics	116945	1

Thermal (point) - a discrete liquid-level sensor that consists of some type of resistance element whose resistance undergoes a step change when the cryogenic medium is changed from liquid to gas. The sensors were fabricated by three manufacturers and employ different resistance elements - gold-plated platinum wire, nickel-iron wire, and p-type germanium,

Capacitance (continuous) - a continuous liquid-level sensor that consists of concentric cylinders forming an air gap capacitor. Operation of the system is based upon detecting the difference in capacitance obtained when the sensor is gradually transferred from a liquid (high dielectric constant) environment to a gas (low dielectric constant) environment.

Capacitance (point) - a discrete liquid-level sensor that operates on the same principle as the continuous capacitance senspr. The sensors consist of four coplaner concentric rings. An off/on signal is provided by associated circuitry when the capacitance changes due to the presence or absence of liquid between the rings.

Magnetostrictive (point) - a discrete liquid-level sensor using the principle of damped oscillation. Signal levels are so adjusted as to maintain oscillation in the nickel rod only when the probe (sensor) tip is exposed to a compressible fluid such as gaseous hydrogen. As soon as the probe tip encounters a non-compressible fluid such as liquid hydrogen, the vibration is damped so that oscillation stops.

2.1.2 Fissioncouples

The fission thermopile assemblies (Phillips Petroleum Co,) consist of ten uranium beads and ten bismuth beads, each 0.03 in. in diameter. The uranium beads enriched to 93% U^{235} contain a total of approximately 0.15 g of uranium and 10% by weight of molybdenum. Each uranium and bismuth bead has a chromel-constantan thermocouple attached, and the thermocouples are connected in series. The beads, potted in Al_2O_3, are enclosed in an aluminum tube about 2 in. in length and 0.25 in. in outer diameter, The four units were potted in polyurethane cylinders having thicknesses of between 150 and 450 mils,

The fission thermopile assemblies failed (open circuit) during the initial thermal cycling of the test dewar. Post-irradiation measurements at room temperature also indicated open circuits within the assemblies. No further information was obtained on the fissioncouples,

2.2 Test Conditions

The level sensors were mounted in a liquid hydrogen dewar and irradiated during five cycles at several reactor power levels. The level of hydrogen in the dewar was varied from time to time throughout the test in order to check the operati-on of the continuous probe and to change the point sensors from the liquid to gaseous environment. After each irradiation step the dewar was allowed to boil dry of liquid and warm to about 55°F.

The reactor power level was varied between 0.01 and 5 MW in order to determine if radiation rate effects significantly altered the sensor outputs. The total radiation exposure level was selected to exceed that predicted for ten missions of a Reusable Nuclear Shuttle powered by a 1500-MW NERVA.

Initial checkout of the sensors was in liquid nitrogen (2 cycles). In addition to the five irradiation cycles, the sensors were thermally cycled in liquid hydrogen three times prior to irradiation and twice after completion of the irradiation.

2.3 Measurements

Data were obtained before the irradiation and during and following each irradiation cycle. Data were obtained both with and without the radiation field by observing the outputs when the sensors were in liquid and in gaseous hydrogen. The level indication for the point sensors was obtained by shutting off the liquid supply and allowing the level to drop below the sensors' positions. The level indication of the continuous probe was compared to that of the point sensors during the boil-off period.

In addition to the liquid and gas phase signal outputs, these measurements were made:

- Resistance of the germanium sensor (Scientific Instruments) during each boil-off cycle
- Capacitance, dissipation factor, and conductivity over the frequency range of 1 to 10 kHz for the capacitance sensors
- Insulation resistance of the sensors

2.4 Dosimetry

The neutron fluxes incident on the liquid-level sensors were measured with sulfur foils. Sulfur foils were located adjacent to the individual sensors at the three levels in the hydrogen dewar. These foils were removed after completion of the irradiation, and their induced radioactivities were measured. The neutron fluxes ($E > 2.9$ MeV) were then calculated. The neutron fluxes ($E > 1$ MeV) were calculated by application of the GTR spectral factor:

$$\frac{(E > 1 \text{ MeV})}{(E > 2.9 \text{ MeV})} = 2.85.$$

The gamma doses received by the liquid-level sensors during the irradiation were not measured. These doses were calculated by multiplying the neutron fluences by previously determined gamma-to-neutron ratios,

III. EQUIPMENT AND PROCEDURES

3.1 Reactor Facility

The irradiation was performed with the 10-MW Ground Test Reactor (GTR), The below-grade tank for this water-moderated thermal reactor has a closet-like structure built into its north wall. The test assemblies are placed in the irradiation cell adjacent to the three faces (designated north, east, and west) of the closet into which the reactor is moved when an irradiation is carried out. The outer faces of the closet are plated with a 20-mil thickness of cadmium to attenuate thermal neutrons.

The test assemblies are lowered into their irradiation positions by means of an overhead crane. Lines and cables are routed over the north wall of the irradiation cell from the control room or the grade-level ramp as required. The cryogen manifold incorporating the control valves and purge fixtures was located on the north ramp. Liquid hydrogen was supplied to the manifold from a transport trailer.

3.2 Test Assembly

The test articles were irradiated in a cylindrical, vacuum-jacketed dewar approximately 51 in. in height and 22 in. in outer diameter, The dewar had a capacity of about 60 gal, The size of the dewar was such that it would contain the continuous liquid-level probe *(40* in, in length) and point sensors located at three levels. This allowed one set of sensors to be positioned above the liquid level, One set was placed near the bottom of the dewar and the third set was near the center of the dewar on the centerline of the reactor core, The arrangement within the dewar is illustrated in Figure 1. Figures 2 and 3 are views of the probe assembly and point sensors as mounted on the irradiation fixture. Figure 4 shows the dewar assembly during an LH_2 cycle prior to installation in the irradiation cell,

The dewar lid contained penetrations for hydrogen fill and exhaust- lines, electrical feed-through connectors, and safety items. The sensor support bracket was also attached to the lid.

A liquid-level system was used to continuously monitor and control the liquid level in the dewar. A probe consisting

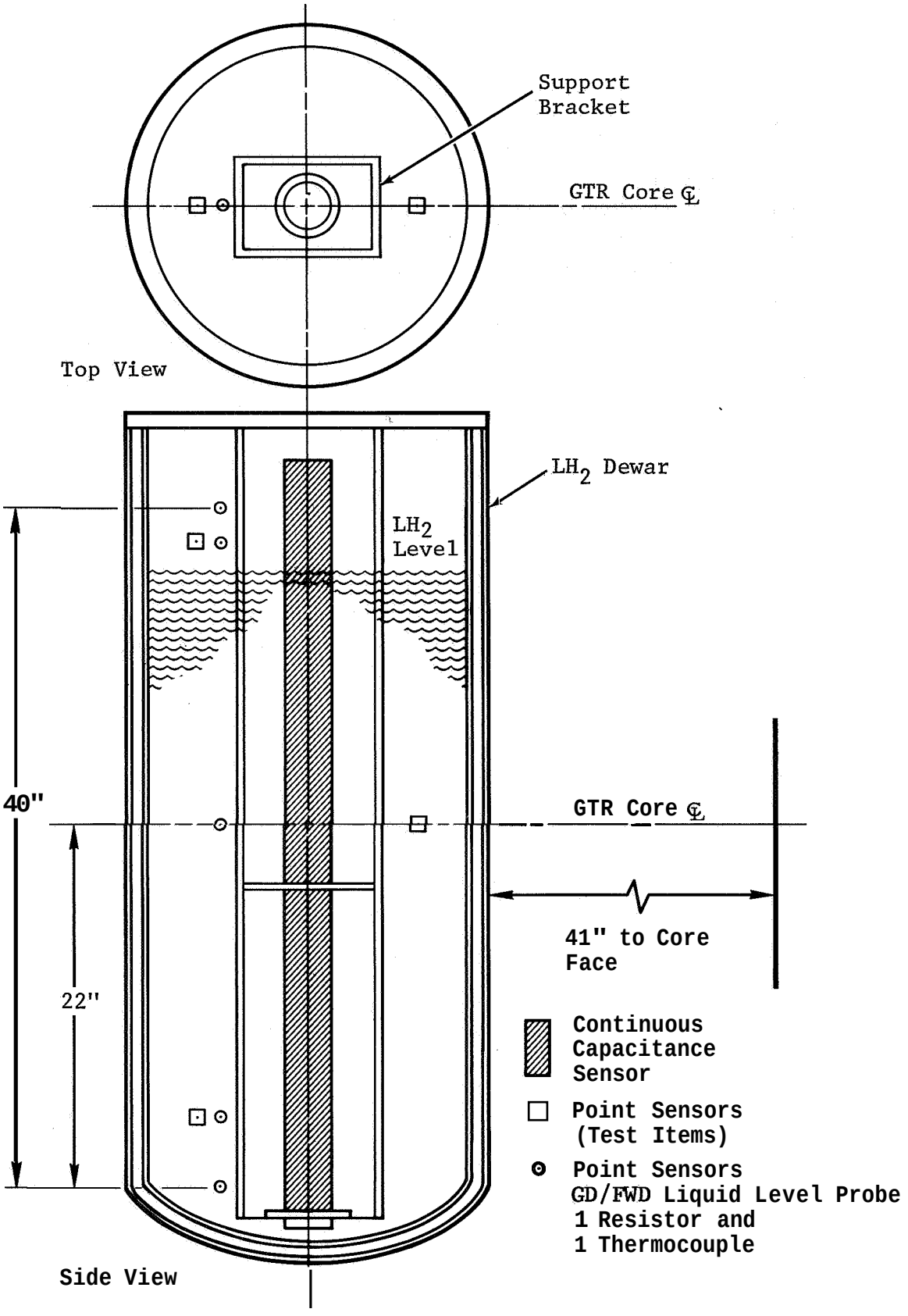

Figure 1 Experimental Setup

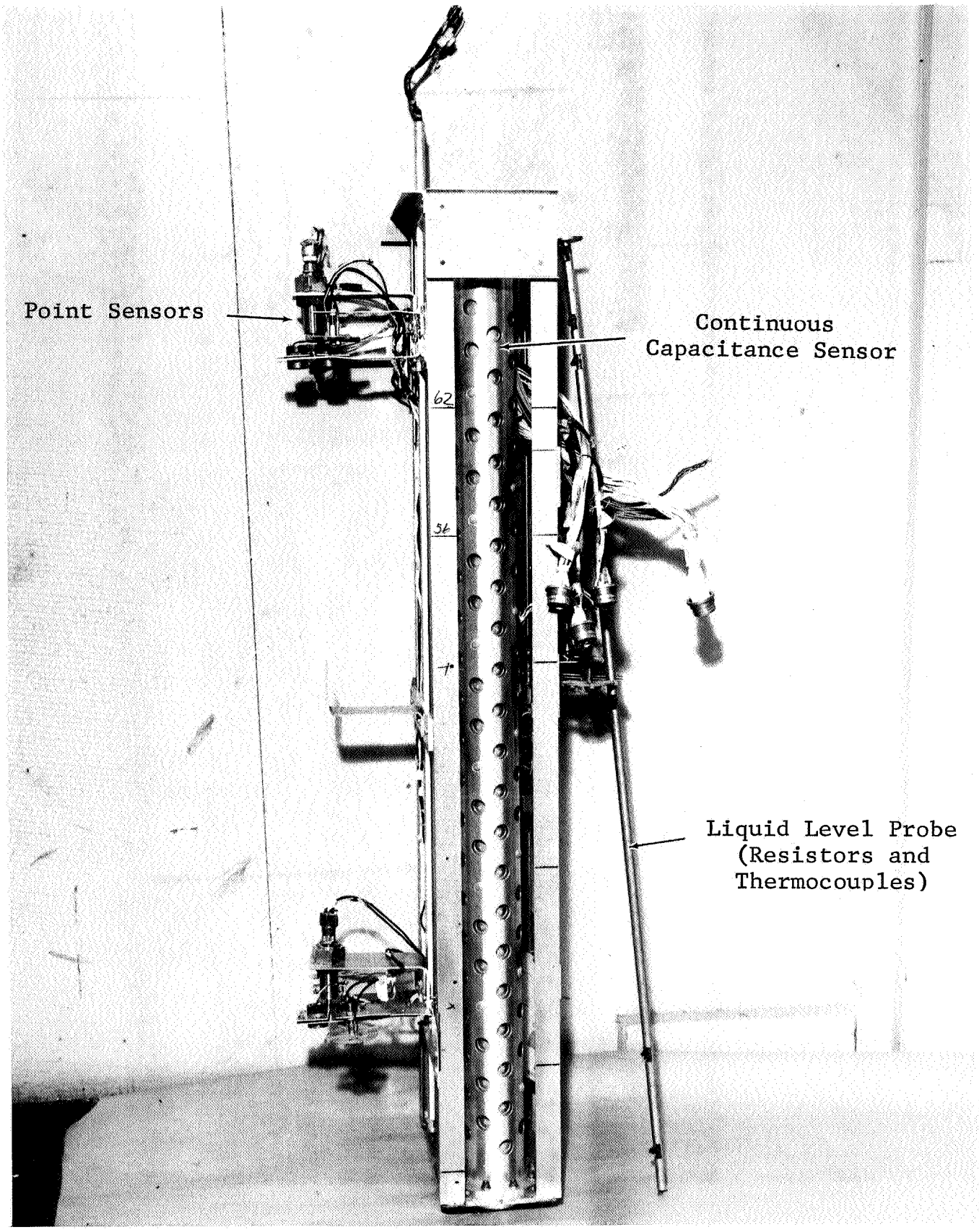

Figure 2 Probe and Point Sensor Assembly

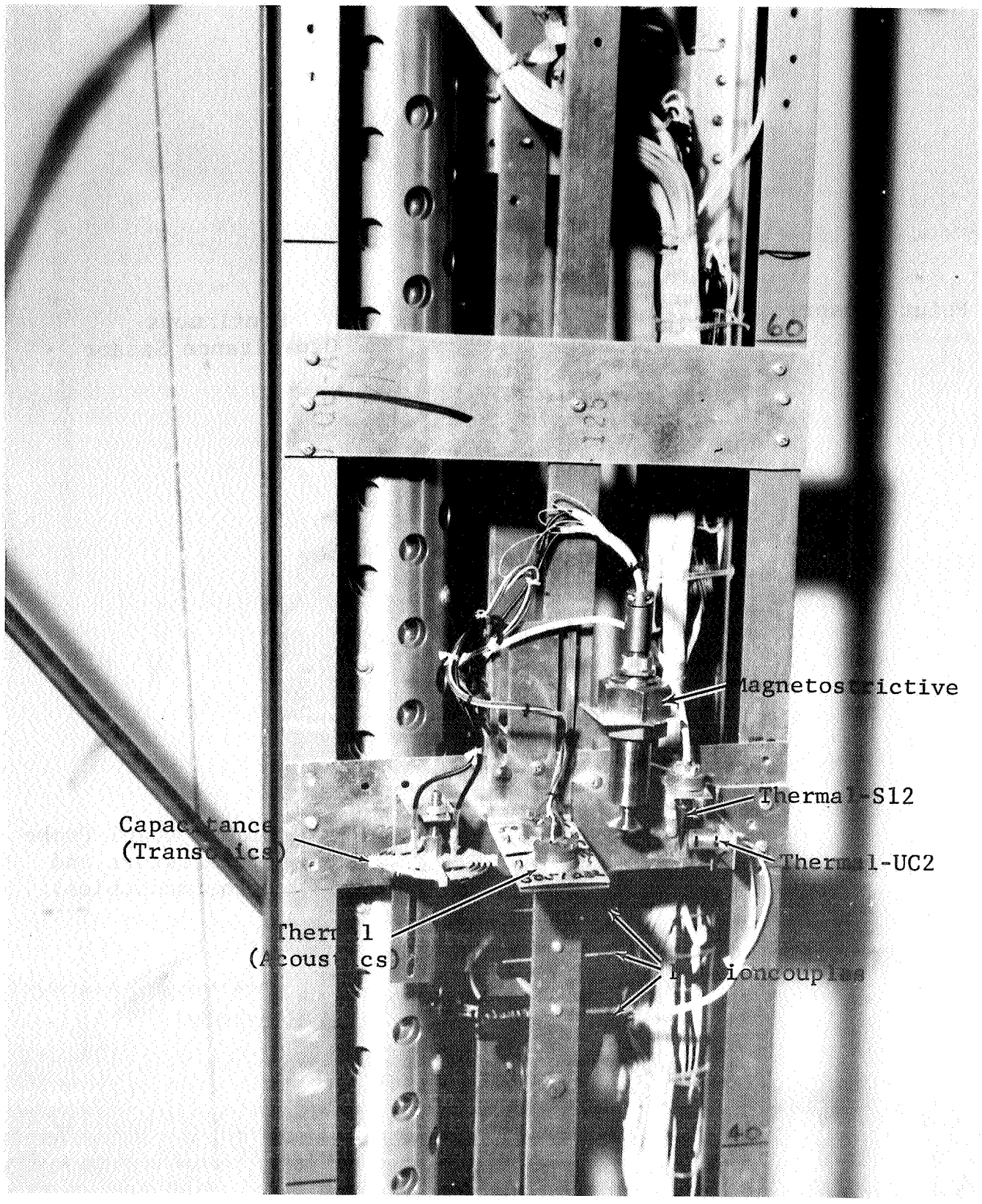

Figure 3 Detail of Sensor **Assembly**

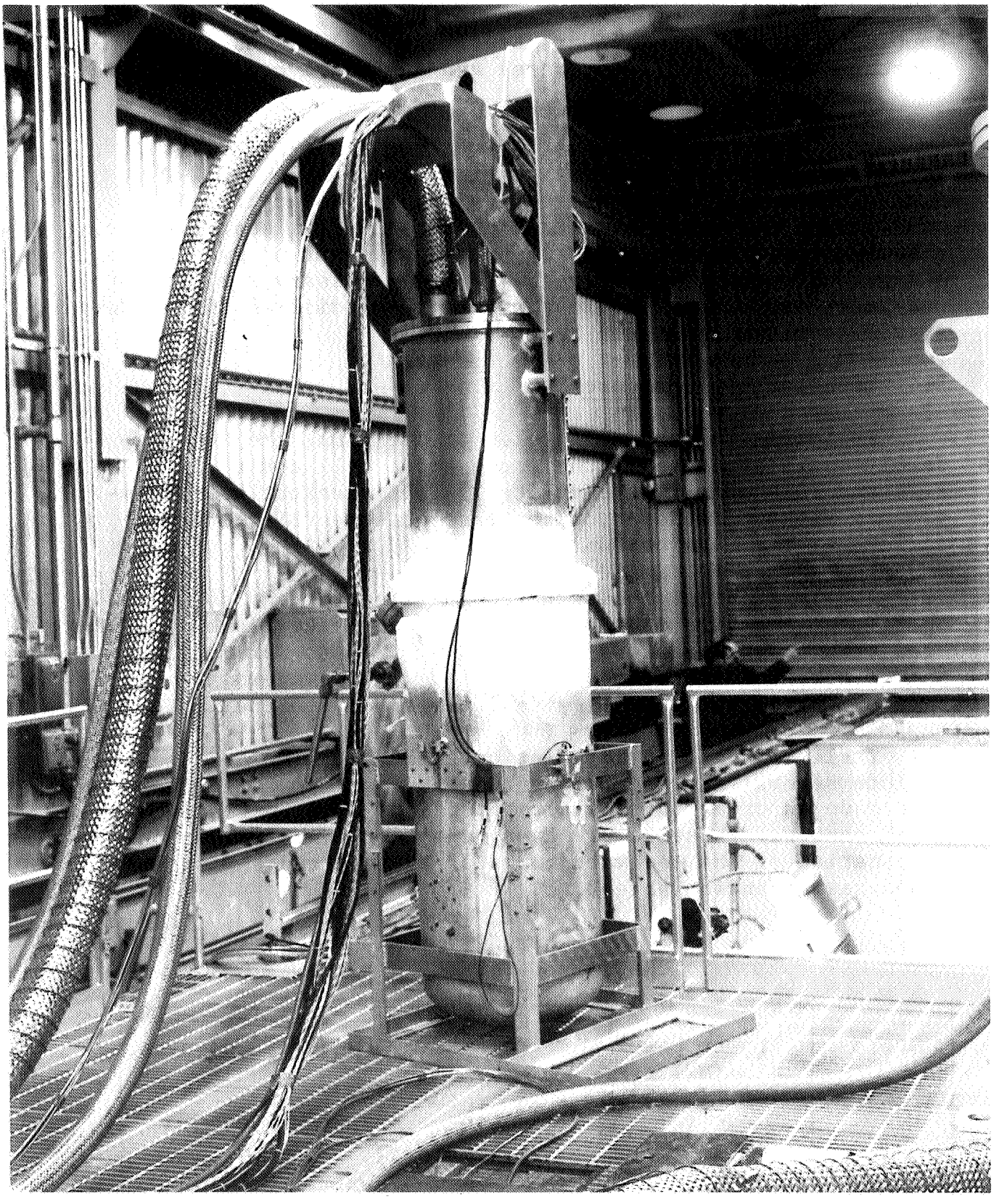

Figure *4* Dewar Assembly

of five resistors (plus a reference resistor) and five thermocouples mounted in the dewar (Figs. 1 and 2) was used in conjunction with an indicator panel and a Bristol control unit.

3.3 Measurement Equipment

Instruments used in data taking were a Dymec 2010-D digital data-acquisition system, a General Radio 1615-A capacitance bridge, a Hewlett-Packard 4329A resistance meter, a Space Craft, Inc. digital capacitance measuring system and a digital to analog converter, and the necessary strip-chart recorders and display indicators. A block diagram of the data system is shown in Figure 5,

3.4 Irradiation Procedure

Following two thermal cycles on the ramp, the test assembly was positioned in the irradiation cell and a third LH_2 fill and leak check was completed. This checkout was accomplished without incident, except, as noted earlier, for the failure of the fissioncouples.

The irradiation cycles were scheduled for and completed on five consecutive days. Data were taken after each irradiation step and the sensors were then allowed to warm to ambient temperature before the next LH_2 fill. The dewar was maintained inerted with helium at all times between the LH2 cycles.

Table 2 gives the irradiation schedule. Table 2 does not include several short duration runs at lower power levels which were made in order to obtain rate effects data on the liquid-level sensor. These lower-power runs have been included in the computation of the megawatt hours of Table 2 and the radiation exposures given in Table 3,

Table 2
IRRADIATION SCHEDULE

Cycle	Power Level (MW)	Energy Release (MWh)	Cumulative Energy Release (MWh)
1	0.1	0.05	0.05
2	1.0	1.56	1.61
3	1.0	4.6	5.2
4	3.0	13.1	19.3
5	5.0	29.3	48.6

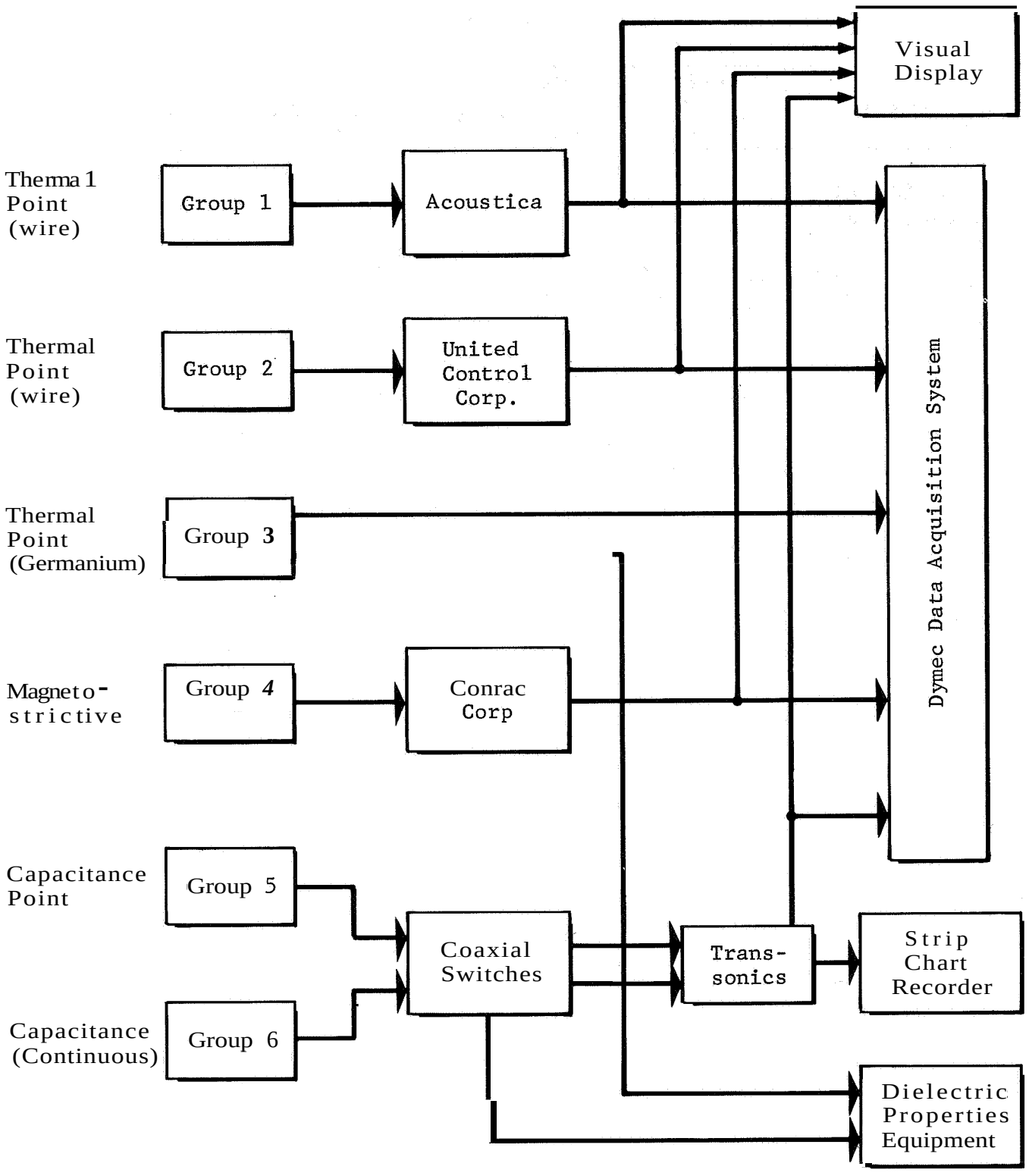

Figure 5 Block Diagram of Data Acquisition System

Table 3

DOSIMETRY DATA

Sensor	Neutron Fluence E > 1 MeV		Gamma Dose	
	(n/cm^2)	(n/cm^2-MWh)	(erg/g(C))	(erg/g(c)-MWh)
Continuous Capacitance:				
Max.	1.74(15)	3.59(13)	2.8(9)	5.8(7)
Min,	3.24(14)	6.67(12)	5.2(8)	1.1(7)
Upper Group	1.21 (15)	2.48(13)	1.9(9)	3.9(7)
Center Group	1.69(15)	3.48(13)	2.8(9)	5.8(7)
Lower Group	2.68 *(14)*	5.51 (12)	4.2(8)	8.6(6)

3.5 Test Procedure

Preirradiation calibrations and operational checks were made on each sensor and the liquid-level system as necessary to determine that it opereted properly and to obtain baseline data. Data for the point sensors were obtained by filling the dewar with LH2 to a level slightly above the sensor and then allowing the liquid to boil off until the sensor was in the vapor above the liquid. The level indicated by the continuous probe was compared with that indicated by the point sensors as they emerged from the liquid.

Data were taken periodically and/or continuously during the irradiation and periodically between irradiation cycles. A fill and boil-off cycle was conducted during and after each irradiation to obtain data on the indication of level change as the sensors emerged from the liquid, or as the length of sensor in liquid changed in the case of the probe.

The postirradiation procedure was similar to the preirradiation procedure. Two fill and boil-off cycles with LH_2 were conducted. The sensors were then removed from the test assembly and visually examined.

IV. RESULTS AND DISCUSSION

4.1 Continuous Capacitance Sensor

The continuous capacitance sensor and its associated electronics (the digital system and digital to analog converter) functioned throughout the irradiation test but erroneous outputs were observed due to radiation rate effects. The electronics portion of this liquid-level system was not irradiated.

The results will be discussed in subsections relating to irradiation cycles. An irradiation cycle consisted of a basic reactor run (Table 2) and shorter runs at lower reactor power levels to test for radiation rate effects. The effects will be discussed in terms of megawatts of reactor power. Gamma dose rates and neutron fluences can be obtained from the information in Tables 2 and 3.

4.1.1 Irradiation Cycle 1

Cycle 1 consisted of a basic reactor run at 0.1 MW preceded by a short run (4 minutes) at 0.01 MW.

No radiation effects were observed during or after this test cycle. The irradiation portion of this cycle was conducted with the sensor completely immersed in LH_2.

4.1.2 Irradiation Cycle 2

Cycle 2 consisted of a basic reactor run at 1.0 MW preceded by short runs at 0.01 and 0.1 MW.

No radiation effects were observed during the 0.01 and 0.1 runs. A small effect was observed when the power level was increased to 1.0 MW. The fine voltage output of the liquid-level electronics gave an erroneous liquid level increase of about 1 inch and then leveled out. The sensor was almost totally immersed in LH_2 for this portion of the cycle.

During the 1 MW irradiation the LH_2 was allowed to boil off to reduce the level about 6 inches while the fine and coarse voltage outputs were recorded and monitored. The sensor and electronics responded as designed to the liquid level change, though the absolute value of the level was in error by the initial offset.

When the reactor was rapidly shutdown (scrammed) at the end of the run, a pronounced effect was observed. The fine voltage output went into rapid oscillation for about 15 seconds and the coarse voltage output took a step function decrease in voltage of about 10 mV indicating an erroneous immediate decrease in liquid level of about 10 inches. This effect was transient and the postirradiation boil-off and fill cycle data indicated no permanent radiation effect. The results of this *irradiation cycle showed that the transient radiation effect was more pronounced if the sensor was appreciably out of liquid.

4.1.3 Irradiation Cycle 3

Cycle 3 consisted of three reactor runs at 1 MW, two at 0.1 MW, and one at 0.01 MW.

A small perturbation of the fine and coarse voltage outputs was observed as the reactor, operating at 0.01 MW, was traversed into the irradiation position. The perturbation was temporary, about one minute, and consisted of what appeared to be 25 mV of noise on the fine output signal, and 5 mV of noise on the coarse output signal. The sensor was within 4 inches of the full mark (40-inch level) and the liquid level system continued to correctly track the liquid boiloff after the perturbation.

As the reactor power level was increased to 1 MW (sensor still almost full of liquid) an erroneous indication of about 0.5-inch increase in liquid level was observed on the fine voltage output, and as the LH_2 level was lowered to the 21-inch level, the fine and coarse voltage outputs indicated a lowering only to the 29-inch level. When the reactor was retracted from the irradiation position (i.e., away from the irradiation cell) the fine output recorded five sawtooth outputs, and the coarse output five step functions in a time interval of about 1 minute. This response indicated an erroneous rapid lowering of the LH_2 level and recovery of the radiation rate effect. After completion of the reactor retraction (i.e., removal of the radiation field) the coarse output voltage was correct.

The sensor was again exposed to 0.1- and 1-MW radiation rates and erroneous liquid level indications of increases of 2 inches and then 5 inches were observed. Again recovery was observed upon reactor retraction. Another 1-MW run indicated the same results, i.e., 5 sawtooths and step functions from

fine and coarse outputs. The coarse output changed from 46 mV to 64 mV in a period of about 100 seconds, an erroneous indication of a 9-inch liquid level increase.

During this 1-MW run the liquid level was increased to 25 inches. The liquid-level system tracked the level increase but the absolute values were in error. The coarse voltage output indicated 32 inches of liquid. The amount of error decreased as the liquid level increased, The error was reduced to about 3 inches as the sensor was nearly full of liquid. Also, a smaller transient effect was observed, the equivalent of the 3-inch error, when the reactor was scrammed. Again, no permanent radiation effect was observed during post cycle 3 testing.

4.1.4 Irradiation Cycle 4

Cycle 4 consisted of a basic reactor run at 3 MW preceded by runs at 0.01 and 0.10 MW and followed by a run at 0.01 MW.

No radiation effect was observed as the reactor, operating at 0.01 MW, was traversed into the irradiation position. The LH_2 was at the 25-inch level of the sensor. As the reactor power level was increased to 0.10 MW the fine voltage output increased from 25 mV to about 90 mV, which is a false indication of liquid level increase of about 1.5 inches. After the reactor power was level at 0.10 MW, the fine and coarse voltage outputs tracked the liquid level increase correctly as the dewar was being filled.

A very pronounced effect was again observed when the reactor power was increased to 3 MW. Six sawtooth and step functions were observed from the fine and coarse outputs indicating an erroneous rapid fill from the 22-inch to the 32-inch level. The liquid-level system responded to level changes but the values were in error. At the 24-inch level the system indicated a level of 33 inches. As discussed previously, the amount of error was a function of liquid level in addition to reactor power. The amount of error decreased from about 10 inches to essentially zero as the sensor became totally immersed in liquid. Rate effects and recovery of the accuracy of the level system response was observed when the reactor was retracted from the irradiation position.

4.1.5 Irradiation Cycle 5

Cycle 5 consisted of a basic reactor run at 5 MW preceded and followed by lower power level runs. The radiation effects observed were very Similar to those observed during cycle 4, that is, no effect at 0.01 MW and an erroneous fill indication as the reactor power was increased to 5 MW. Before the power increase, LH2 was at the 30-inch level; immediately after the increase the indicated level was 37 inches. This error was less than the 3-MW error; however the liquid level was significantly higher (30 inches instead of 22 inches). As the liquid level was decreased to the 24-inch level, the error increased from 7 inches to 11 inches. As the dewar was filled with LH2 the error was reduced until the level indication was 1 inch too high.

4.1.6 Summary of Radietion Effects on the Continuous Capacitance Svstem

The capacitance system used as a continuous liquid-level measuring system exhibited a high degree of radiation rate sensitivity under conditions of high reactor power level (1 MW or greater) combined with a liquid level several inches below the full level. No permanent radiation effects were observed.

The error in liquid level indication is attributed to an apparent increase in capacitance as additional charge carriers are produced by the high intensity radiation fields (primarily gamma radiation). The liquid-level indication of the sensor is related directly to the capacitance existing between the two electrodes of the sensor; therefore as the capacitance increases due to the radiation field, the sensor system responds as though the liquid level were increasing, and conversely when the radiation field is removed the sensor will indicate an erroneous lowering of the liquid level, Dielectric property measurements, presented in the following subsection, gave evidence of the radiation rate effect on capacitance.

4.2 Dielectric Properties of the Continuous Probe

Dielectric property measurements of the continuous liquid-level system were made under conditions of several radiation rates and liquid levels as shown in Table 4. Measurements of capacitance and dissipation factor (at 1 kHz and 10 kHz), and resistance of the system were made, The results of the

Table 4

DIELECTRIC PROPERTIES OF CONTINUOUS CAPACITANCE PROBE

Data Cycle	Power Level (MW)	Liquid Level (in.)	Capacitance (pf)		Dissipation Factor		Resistance (megohms)
			1 kHz	10 kHz	1 kHz	10 kHz	
prairradiation	0	0	314	-	0 0004	--	5000
preirradiation	0	25	349	349	0 007	0.0005	400
cycle 3	0.10	25	351		0 057	--	80
cycle 3	1.0	25	413	368	0.173	0 002	30
cycle 5	3.0	25	624	377	0 52	0.0075	18
cycle 5	3 0	19	910	363	0 80	0 007	12
cycle 4	3 0	17	533	364	0 39	0 005	17
cycle 4	3.0	40	445	386	0 145	0 001	30
postirradiation	0	40	385	385	0.005	0 002	1500
postirradiation	0	0	313.5	313.4	0 0004	0 0005	1300

measurements show significant radiation rate effects. Increases in capacitance and dissipation factor and decreases in resistance were observed. The magnitude of the radiation rate effects was dependant upon the reactor power level, the liquid level, and the oscillator test frequency. The largest effects were observed at the higher power levels with low liquid levels and low oscillator frequency (1 kHz). It can be seen from Table 4 that at a constant liquid level an apparent increase in capacitance was observed and resulted in erroneous outputs of the liquid-level system as discussed in Section 4.1. The observed effects are believed to be caused by the generation of charge carriers, primarily by the gamma radiation. Mobility sensitivity can be seen by comparison of the 1-kHz and 10-kHz measurements.

4.3 Thermal (Point) Sensors - Acoustica Associates Model STS 505

The Acoustica thermal point sensors were not affected by the radiation exposure of this test. However, the associated control units (not irradiated) failed to respond to the resistance change of the sensors; therefore, resistance measurements were made throughout the test instead of monitoring output voltages from the control units.

Typical test data is shown in Table 5. The resistance of the sensors decreased about 100 ohms, from around 106 ohms to approximately 6 ohms, with a decrease in temperature from 55-60°F to that of liquid hydrogen (-423°F). Some variations in resistance values as seen in Table 5 are due to temperature variations

4.4 Thermal (Point) Sensor - United Control Model 2641

The United Control thermal point sensors were unaffected by the radiation exposure. Two of the control units exhibited temporary malfunction at the end of irradiation Cycle 5.

4.5 Thermal (Point) Sensor - Scientific Instruments Model 3

The Scientific Instruments germanium point sensors were operational throughout the test. They indicated a change in resistance as a change occurred in the temperature of the environment.

Significant temporary radiation effects were observed. The sensor exposed to the highest neutron fluence increased

Table 5

RESISTANCE OF SENSE ELEMENTS - ACOUSTICA ASSOCIATES MODELS 505

Data Cycle	Power Level (MW)	Temperature (°F)	Resistance (ohms) A1	A2	A3	A4	A5	A6
preirradiation	0	-423	6.06	6.04	6.08	6.10	5.98	6.08
preirradiation	0	55 to 60	103.8	104.4	105.2	106.4	104.8	104.7
cycle 1	0 100	-423	6.03	6.04	6.07	6.09	5.96	6.05
post cycle 1	0	-423	6.10	6.07	6.09	6.11	5.99	6.09
post cycle 1	0	45 to 50	103.1	104.7	103.9	105.1	102.7	103.8
cycle 2	1.00	-423	6.09	6.09	6.08	6.09	5.98	6.08
post cycle 2	0	-423	6.09	6.05	6.07	6.10	5.97	6.08
post cycle 2	0	50 to 55	103.8	105.3	104.7	105.8	103.7	104.5
cycle 3	1.00	-423	6.34	6.35	6.08	6.10	6.00	6.13
post cycle 3	0	-423 to -400	9.07	9.35	6.07	6.09	5.98	6.11
post cycle 3	0	50 to 55	103.7	105.4	104.9	105.9	103.8	104.8
cycle 4	3.00	-423	6.10	6.06	6.09	6.11	6.00	6.13
post cycle 4	0	-423	6.10	6.05	6.09	6.11	5.99	6.09
post cycle 4	0	50 to 55	103.8	105.4	105.1	105.9	103.9	105.0
cycle 5	5.00	-423	6.08	6.04	6.09	6.11	5.99	6.10
post cycle 5	0	-423	6.09	6.04	6.08	6.10	5.98	6.09
post cycle 5	0	70°	106.2	108.1*	108.1	108.7	106.8	107.9

significantly in resistance while in LH2 during Cycles 4 and 5, the highest fluence cycles. Recovery from this radiation effect (annealing) was observed during measurements made after the temperature of the sensors had been increased.

Some resistance measurements and associated parameters are shown in Table 6 for sensor SI-2 which was located at the center of the dewar.

4.6 Magnetostrictive (Point) Sensor - Conrac Corp. Model UP1004S-5

The Conrac sensor elements were operational throughout the test. The control unit for one of the sensors had to be adjusted occasionally to obtain the correct voltage outputs in and/or out of liquid.

4.7 Capacitance (Point) Sensor - Transonics Corp. Model L4447

The Transonic capacitance point sensor systems were operational through irradiation Cycle 3. Operation of the systems during irradiation at 3 and 5 MW was intermittent (control unit voltage outputs) and dependent on the liquid level in a manner similar to the data obtained from the continuous capacitance sensor system (Secs. 4.1 and 4.2). There was no physical radiation damage to the capacitance sensors and they continued to sense in and out of liquid environment throughout the test; however, as the liquid level was appreciably lowered beneath a sensor (at high radiation rates), indications of liquid state were intermittently observed.

The results of capacitance, dissipation factor, and resistance measurements that were made agreed with the continuous capacitance sensor measurements with regard to radiation rate effects. Increases in capacitance and dissipation factor and decreases in resistance were observed.

4.8 Conclusions

The continuous capacitance liquid-level system began to have appreciable error in the output at a gamma dose rate of about 3×10^7 ergs/gm(C)-h. A longer probe with a greater length out of the liquid could be expected to show significant error at lower dose rates since the error is a function of length out of liquid as well as of radiation rate. Point sensors of capacitance type show changes in properties similar to that exhibited by the probe while continuing to indicate the

Table 6

RESISTANCE OF GERMANIUM SENSOR SI-2 - SCIENTIFIC INSTRUMENTS MODEL 3

Data Cycle	Temperature (^{o}F)	Neutron Fluence E >1 MeV (n/cm^2)	Resistance (ohms)
Preirradiation	-423	0	94
Preirradiation	55	0	37.5
Cycle 3	-423	6.28 (13)	95
Cycle 3	-423	1.79 (14)	114
Post Cycle 3	-423	1.93 (14)	531
Pre Cycle 4	50	1.93 (14)	37.4
Cycle 4	-423	2.62 (14)	279
Cycle 4	-423	4.23 (14)	403
Cycle 4	-423	5.18 (14)	520
Post Cycle 4	50	6.15 (14)	37.3
Post Cycle 4	-423	6.15 (14)	98
Cycle 5	-423	9.63 (14)	268
Cycle 5	-423	1.00 (15)	1005
Cycle 5	-423	1.17 (15)	1513
Cycle 5	-423	1.25 (15)	1925
Postirradiation	70	1.55 (15)	36.4

presence or absence of liquid; some spurious liquid indication were observed when the sensors were out of liquid.

The thermal sensors having wire elements were satisfactory throughout the test as were the magnetostrictive sensors. The thermal point sensors having germanium elements exhibit a radiation effect that is a function of the neutron exposure. The increased resistance of the germanium elements can be annealed by raising the temperature.

Part III

TEST OF VALVE-SEAL MATERIALS

FZK-387

By

L. W. NELMS

SUMMARY

A test has been performed to evaluate the combined effects of reactor radiation and liquid hydrogen on valve-seal materials of potential usefulness on a nuclear-powered space vehicle. The materials were tested under simulated use conditions as components of two liquid hydrogen valves. The valves were filled with LH_2 during the irradiation and data cycles and then warmed to ambient temperature between cycles. Leakage rates and opening and closing times were obtained before and after each of five irradiation steps at power levels from 0.1 to 5 MW with the Ground Test Reactor. Total radiation doses were sufficient to exceed by an order of magnitude the predicted level at the shutoff valve location in ten missions of a Reuseable Nuclear Shuttle with a 1500-MW NERVA.

One of the valves was a 17-in. S-IC stage LOX shutoff valve which had been modified, under NASA contract, by the Whittaker Corporation for liquid hydrogen service in a radiation environment. The modification consisted principally of replacing radiation sensitive organic materials with more radiation resistant materials, some of which were developed for this use by Whittaker. The replacement materials used as seals, gaskets, O-rings, etc. were Kynar, a composite of Kynar, Teflon, and fiber glass, asbestos, and a polyurethane-base material (Narmco 7343).

The second valve was an off-the-shelf S-II stage LOX and LH_2 fill valve (V7-480450, 8-in. line size) manufactured by North American Rockwell. The organic materials used in this valve as lipseals, seals, bearings, packing, etc. are Mylar, Teflon FEP and TEF, Kel-F, synthetic rubber, Nylon, Viton A, polyurethane, and a Teflon and asbestos composite.

After a total exposure (maximum) of 3.5×10^9 ergs/gm(C) and 4.2×10^{15} n/cm^2 (E >1.0 MeV), performance of the 17-in. valve was still satisfactory with regard to leakage. Mainseal leakage stayed well within specification and shaft-seal and flange-static-seal leakage was essentially zero. In three of eight data cycles the actuator vent leakage was above specifications but it was zero at the end of the test. Some increase in valve opening time occurred as the test progressed and in one instance the valve

stuck closed but opened on the second try. At the end of the test the opening time was 3 to 5 seconds as compared to the specification of 2 seconds. The closing time was consistently less than the 1 second specification, in three instances being 0.2 second,

The S-II stage fill valve received a total exposure (maximum) of 1.1×10^{10} ergs/gm(C) and 7.2×10^{15} n/cm^2 (E > 1.0 MeV). Its performance stayed within specification on all measurements except opening and closing times. In three of seven openings, the time was less than the specified 5 ± 2 seconds; in six of seven closings, the time was less than specification (5 ± 2 sec). Other measurements included actuator pressure decay (increased somewhat as the test progressed) and leakage rates from the actuator Port C (zero), actuator piston seal (zero), actuator rod seal (zero), idler shaft seal (zero), drive shaft seal (zero), and latch cover plate (zero with valve closed). The mainseal leakage varied somewhat from one cycle to the next but always remained far below the specification.

After the irradiation test, both valves were disassembled for inspection. Visual inspection of the seals failed to disclose any signs of damage, All seals were intact and appeared to be in good condition,

I. INTRODUCTION

An irradiation test has been performed for the purpose of evaluating organic seal materials for potential use on a nuclear-powered vehicle, One of the most critical applications of organic materials will be in valves of the propellant feed system. Not only do these seals perform vital functions in the proper operation of the system, but the valves-must of necessity be located near the engine and therefore in relatively high radiation fields. Since some of the best organic materials for use in liquid hydrogen systems are among those most susceptible to radiation damage, it has been evident for some time that more radiation resistant materials. would probably be needed and that definitive and realistic testing would be required. Two useful steps have now been taken in this regard.

Toward the development of radiation resistant seal materials, the Whittaker Corporation has modified a 17-in. S-IC LOX shutoff valve for use with liquid hydrogen in a radiation field. In testing, General Dynamics has evaluated this modified valve and an unmodified S-II stage LH_2 fill valve in the combined environment of liquid hydrogen and reactor radiation. The Whittaker and North American Rockwell valves, which served as test vehicles for the seal materials, were irradiated in several steps and actuated, leak checked, and thermally cycled after each irradiation. The total radiation dose was selected to exceed the predicted lifetime dose in an application on the Reuseable Nuclear Shuttle,

This work was conducted at the Nuclear Aerospace Research Facility (NARF) operated by the Fort Worth operation of the Convair Aerospace Division of General Dynamics for the George C. Marshall Space Flight Center of the National Aeronautics and Space Administration under Contract NAS8-18024. Under Contract NAS8-18024, the Fort Worth operation has performed numerous radiation effects experiments on organic materials and thermal insulations as a part of the technology program supporting the development of the nuclear rocket vehicle.

II. DESCRIPTION OF TEST

2.1 Test Articles

2.1.1 17-Inch Valve

The 17-in. valve (Whittaker Corp, P/N 138025) is of spring-opened, pneumatically-closed, spherical rotary type. It was designed for and used as the emergency shutoff valve between the liquid oxygen tank and the engine turbopump of the S-IC stage of the Saturn V vehicle, The valve is operated by means of a pneumatic actuator which closes the valve visor (gate) when pneumatic pressure is applied to the actuator, and opens the visor by means of an internal spring when pressure is removed. The actuator also operates to retract and advance a visor seal that is forced against the inner portion of the visor by means of a metallic bellows; this completes the sealing features of the valve. A complete description along with drawings, parts lists, checkout procedures, etc. may be found in the maintenance manual (Ref. 1).

The 17-in. valve irradiated and tested by General Dynamics (P/N 138025A) had been modified by the Whittaker Corporation under Contracts NAS8-20784 and NAS8-20955 for liquid hydrogen service in a radiation environment. It was specifically intended to serve as a vehicle for testing radiation-resistant seal materials in a combined radiation and liquid hydrogen environment. The details of the Whittaker programs on seal-material development and modification of the valve are described in References 2 and 3,

The Whittaker modifications consisted of replacing existing seals, insulators, lubricants, and nonmetallic components with radiation-resistant components, All replacement components had to conform to the existing valve geometry envelope, The components replaced and the replacement materials are given in Table 1.

2.1.2 LH_2 Fill Valve

The fill valve (North American Rockwell P/N V7-480450) is a pneumatically actuated gate valve of 8-in. line size used for both LOX and LH_2 service on the S-II stage, The valve is spring opened upon pneumatic withdrawal of a latch pin, Table 2 lists the components made of organic materials.

Table 1

RADIATION SENSITIVE COMPONENTS AND REPLACEMENT MATERIALS FOR 17-INCH VALVE

Subsystem	Component	As Designed		As Modified	
		Part Number	Material	Material	New Part No.
Servoactuator					
	Seal	110189-21	Teflon	NARMCO 7343[a]	110189A-21
	Seal	110189-22	Teflon	NARMCO 7343[a]	110189A-22
	Seal	134387	e	Composite[b]	NR357-65
	Seal	135128	e	Composite[b]	NR357-67
	Gasket	136472	Teflon	Kynar	136472A
	Gasket	136477	Teflon	Kynar	136477A
	Seal	136517	Teflon	Kynar	136517A
	Gasket	136638	Teflon	Kynar	136638A
	Seal	136639	Teflon	Kynar	136639A
	Gasket	136959	Teflon	Kynar	136959A
	Seal	136962	e	Kynar	136962A
	Seal	200500-9	e	Composite[b]	NR357-39
	Seal	200500-10	e	Composite[b]	NR357-41
	Seal	200500-12	e	Composite[b]	NR357-43
	O-ring	200506-2-147	Teflon	Kynar	200506A-2-14
	O-ring	200506-3-27	Teflon	Kynar	200506A-3-2
	Seal	200529-313	e	Kynar	200529A-313
	Seal	200529-342	e	Kynar	200529A-342
	Ring, wear	134410	Teflon	Kynar	134410A
	Ring, wear	134370	Teflon/glass	Kynar	134370A
	Ring, wear	136967	Teflon/glass	Kynar	136967A
	Ring	136968	Teflon	Kynar	136968A
Position Indicator Assy					
	Seal	136457	e	Composite[b]	NR357-33
	Seal	136457-1	e	Composite[b]	NR357-35
	Seal	200500-33	e	Composite[b]	NR357-47

Table 1 (cont'd)

Subsystem	Component	As Designed		As Modified	
		Part Number	Material	Material	New Part No.
	O-ring	200506-2-019T	Teflon	Kynar	200506A-2-019
	Seal	200529-9	Teflon	Kynar	200529A-9
	Insulation	100147-1	e	Kynar	100147A-1
	Insulation	127139	e	Kynar	127139A
	Packing	137482	e	Kynar	137482A
	Sleeve	SS379-12-6	e	Kynar	SS379A-12-6
	Sleeve	SS379-14-10	e	Kynar	SS379A-14-10
	Position Indicator	136700	e	c	c
	Connector	100140-100	e	c	c
	O-ring	d	d	Kynar	100140A-200
	O-ring	d	d	Kynar	100140A-300
Valve Body					
	O-ring	100111AJ14	e	Kynar	100111A
	Washer	134501	e	Kynar	134501A-1
	Washer	d	d	Kynar	134501A-2
	Seal	135129	e	Kynar	135129A
	Gasket	135707	Teflon	Asbestos	135707A
	Seal	136719	e	Kynar coated	136719A
	Seal	136767	e	Kynar	136767A
	Seal	136769	e	Kynar	136769A
	Seal	200500-4	e	Composite[b]	NR357-37
	Seal	200500-25	e	Composite[b]	NR357-47
	Seal	200500-34	e	Composite[b]	NR357-49
	Seal	200500-36	e	Composite[b]	NR357-57
	Seal	200500-38	e	Composite[b]	NR357-51
	Seal	137500	e	Composite[b]	NR357-53
	Seal	200500-40	e	Composite[b]	NR357-55
	Seal	200518-10	e	Kynar	200518A-10

Table 1 (cont'd)

Subsystem	Component	As Designed		As Modified	
		Part Number	Material	Material	New Part No.
	Seal	200518-11	e	Kynar	200518A-11
	Seal, face coated	MC252S2TA	Teflon TFE coated	Kynar coated	MC252S2-A
	Seal, face coated	MC252S4TA	Teflon TFE coated	Kynar coated	MC252S4-A
	Seal, face coated	MC252S6TA	Teflon TFE coated	Kynar coated	MC252S6-A
	Shim	136960	e	Kynar	136960A
	Shim	136961	e	Kynar	136961A
	Bushing	137069	Teflon/glass	Kynar	137069A
	Pad	137328	Teflon/glass	Kynar	137328A
	Lubricant	129358-1	e	MoS_2	129358A-1
	Washer	136317	Teflon/glass	Kynar	136317A
	Ring	MS9058-06	e	Kynar	MS9058A-06

[a]NARMCO 7343 is a polyurethane base material fabricated by Whittaker Corp.

[b]Composite material is mixture of Kynar, Teflon, and fiberglass.

[c]Component eliminated in modified configuration.

[d]Component added in design of modified configuration.

[e]Component is part of an assembly and specific material is not identified in the maintenance manual for this valve.

Table 2

RADIATION SENSITIVE COMPONENTS OF S-II STAGE FILL VALVE (V7-480450)

Part Number	Component	Material	Specification
V7-480391	Lipseal	Mylar	MB 0130-060, Type D-7.5
V7-480453	Lipseal	Mylar	MB 0130-060, Type D-7.5
V7-480474	Ring	Teflon FEP	MB 0130-052
V7-480614	Seal	Mylar	MB 0130-060
MS29512	Packing	Synthetic rubber	MIL-P-5315
ME261-0028	Seal	Teflon coated	
V7-480743	Lipseal, gate	Kel-F	MB 0130-053
ME261-0036	Seal	Teflon TFE jacket	
V7-480492	Spacer	Teflon, 25% asbestos	
V7-480607	Bearing	Teflon FEP	MB 0130-052
ME261-0027	Face coated seal	Teflon coated	
V7-480643	Bearing	Kel-F	AMS 3650
V7-480731	Retainer	Nylon	NYLOK
V7-480732	Retainer	Nylon	NYLOK
V7-480485	Lipseal	Mylar	MB 0130-060
V7-480594	Valve		
V7-480590	Body, seal	Viton A	SR277-70
V7-480640	Indicator		
V7-480394	Spacer	Teflon FEP	MB 0130-052
V7-480322	Washer	Kel-F	MB 0130-053
--	Potting compound	Polyurethane	MB 0120-024

2.2 Test Conditions

Both valves were irradiated in five steps while filled with liquid hydrogen. After each irradiation, a data cycle was run and the valves were purged of hydrogen and allowed to warm to ambient temperature (approx. 50°F). The irradiation steps were at nominal reactor power levels of 0.1, 1.0, 1.0, 3.0, and 5.0 MW each for a duration to give the desired integrated gamma dose. The total reactor operating time was 19 hours and the approximate total time the valves contained liquid hydrogen was 31 hours. Including preirradiation checkout, the valves were subjected to 11 LH_2 cycles.

2.3 Measurements

The effect of the applied environments on the ability of the valve-seal materials to continue to perform their function at LH_2 temperatures was determined from measurements of the leakage rates at certain points on tha valves, from measurements of opening and closing times, and from pressure decay measurements (fill valve only), These measurements were made immediately preceding and following the irradiations.

Temperatures were measured at three locations on the outside of each valve body. Gamma doses and neutron fluences were measured by use of cobalt glass and foils, respectively, Liquid levels within the valves and the attached standpipes were measured and controlled by use of resistor probes and the automatic flow-control system.

2.4 Dosimetry

Neutron fluence measurements were made at various locations on each valve by use of nickel, sulfur, and phosphorous foils. Gamma dose measurements were made at accessible exterior locations using cobalt glass detectors; it was necessary to remove these detectors after the first irradiation to avoid saturation. Neutron-to-gamma ratios at these accessible locations were used to calculate the gamma doses at other locations where neutron foils were exposed but where gamma dosimeters could not be used.

The dosimetry data are given in Table 4 of Section III.

III. EQUIPMENT AND PROCEDURES

3.1 Reactor Facility

The irradiation was performed with the 10-MW Ground Test Reactor (GTR). The below-grade tank for this water-moderated thermal reactor has a closet-like structure built into its north wall. The test assemblies are placed in the irradiation cell adjacent to the three faces (designated north, east, and west) of the closet into which the reactor is moved when an irradiation is carried out. The outer faces of the closet are plated with a 20-mil thickness of cadmium to attenuate thermal neutrons.

The test assemblies are lowered into their irradiation positions by means of an overhead crane. Lines and cables are routed over the north wall of the irradiation cell from the control room or the grade-level ramp as required. The cryogen manifold incorporating the control valves and purge fixtures was located on the north ramp. Liquid hydrogen was supplied to the manifold from a transport trailer.

3.2 Test Assemblies

Since the valves were to be irradiated while filled with LH_2, they were assembled with a blind flange bolted on the downstream valve flange and a vacuum-jacketed standpipe bolted on the upstream valve flange. The standpipe assured that the valves would be completely full of LH_2 and also provided a reservoir to maintain an adequate LH_2 level when flow was shut off for the leakage measurements. To minimize the possibility of hydrogen leakage into the irradiation cell, each valve assembly was totally enclosed in a cylindrical container (shroud) which was continually purged with helium. The 17-in.-valve assembly attached to the shroud cover is shown in Figure 1. The largest flexible line is a 4-in. gas exhaust and the smaller line is the 1.5-in. shroud exhaust. A 0.5-in. flexible LH_2 supply line was used. Smaller copper lines were used for actuation pressure and leakage measurements.

A similar arrangement was used for the fill valve, The unmounted valve is shown in Figure 2 and the test assembly is shown positioned at the west face of the GTR in Figure 3, Figure 4 shows the 17-in.-valve assembly on the work platform above and

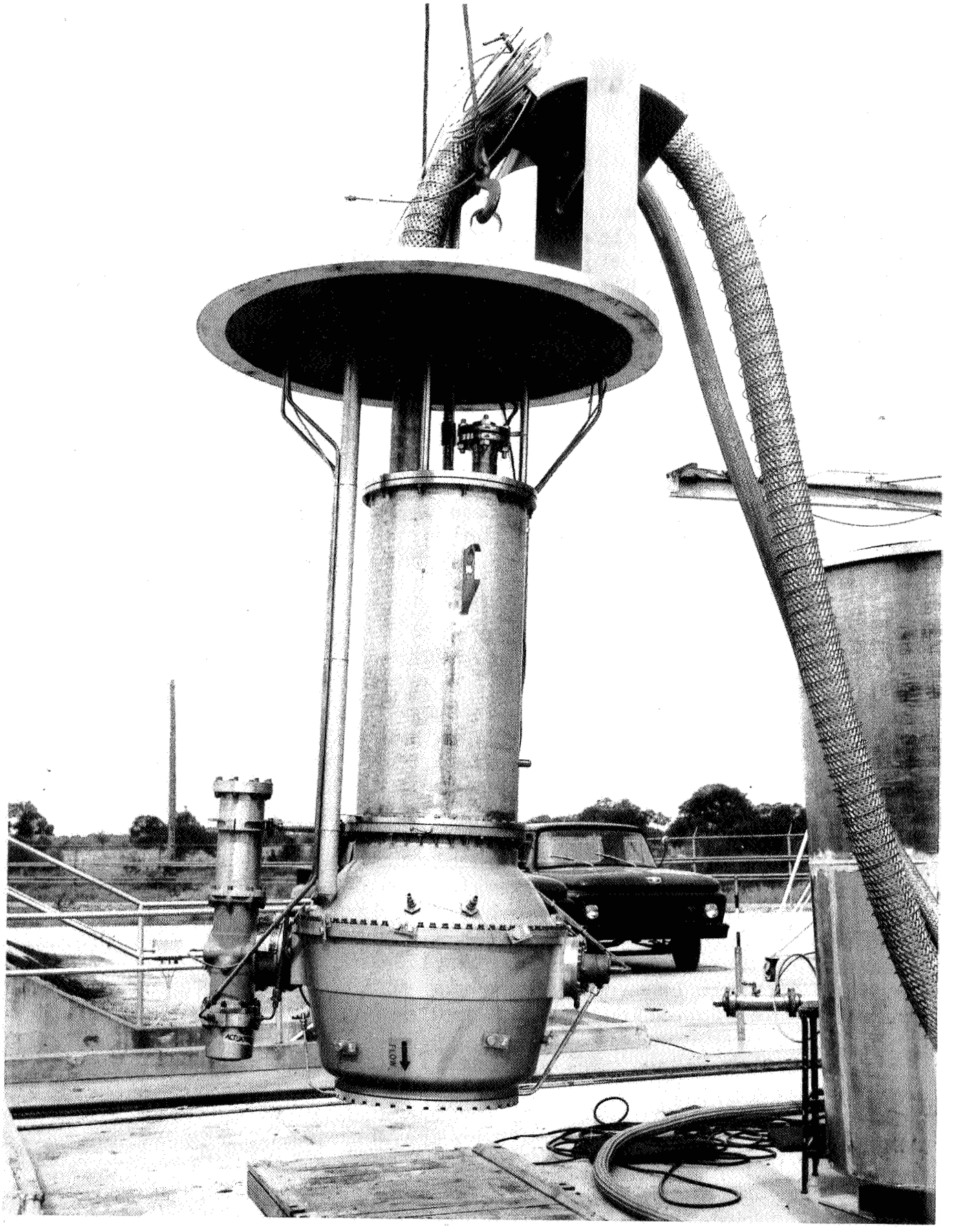

Figure 1 17-Inch-Valve and Standpipe Assembly

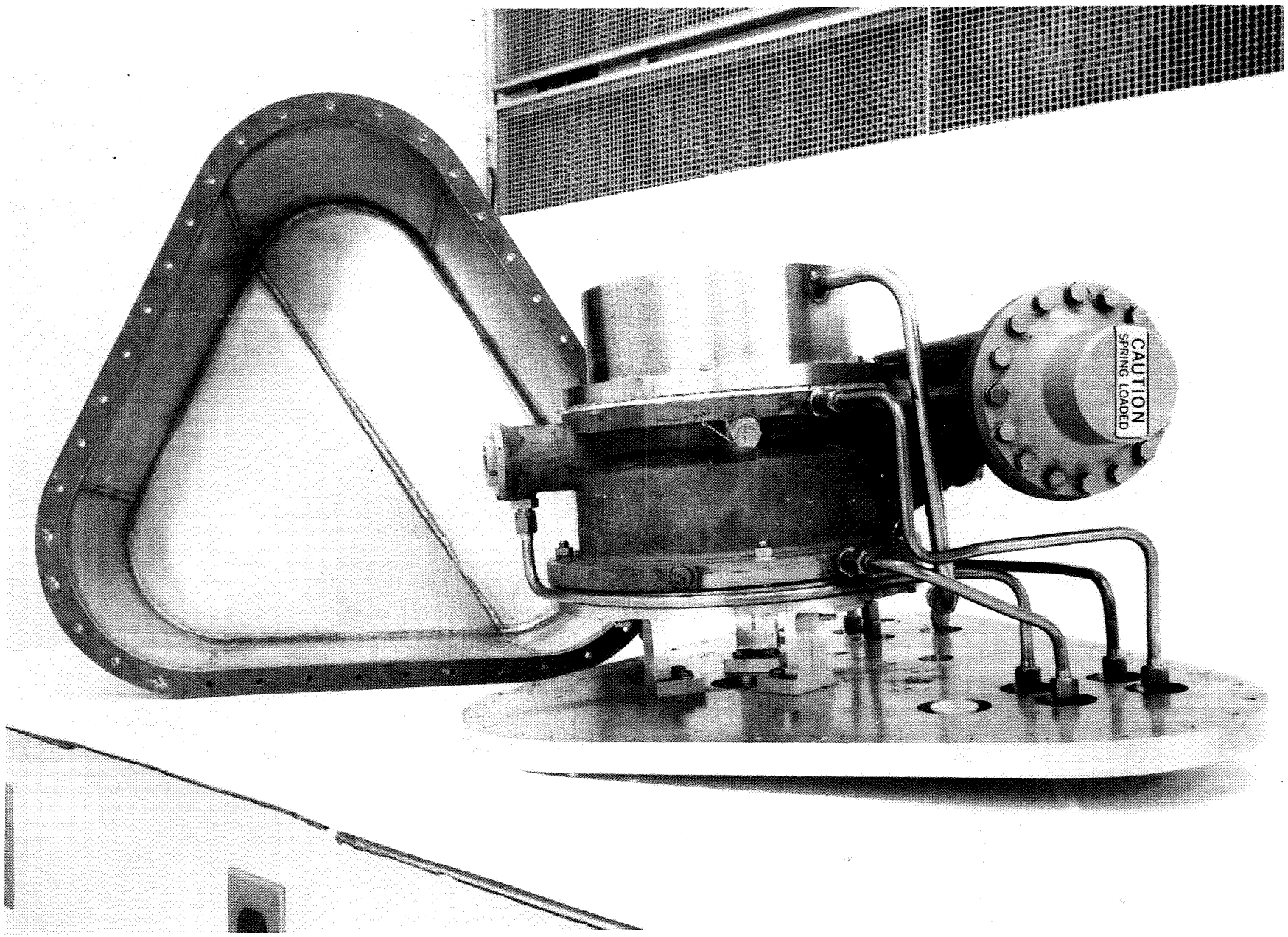

Figure 2 S-II Stage Fill Valve

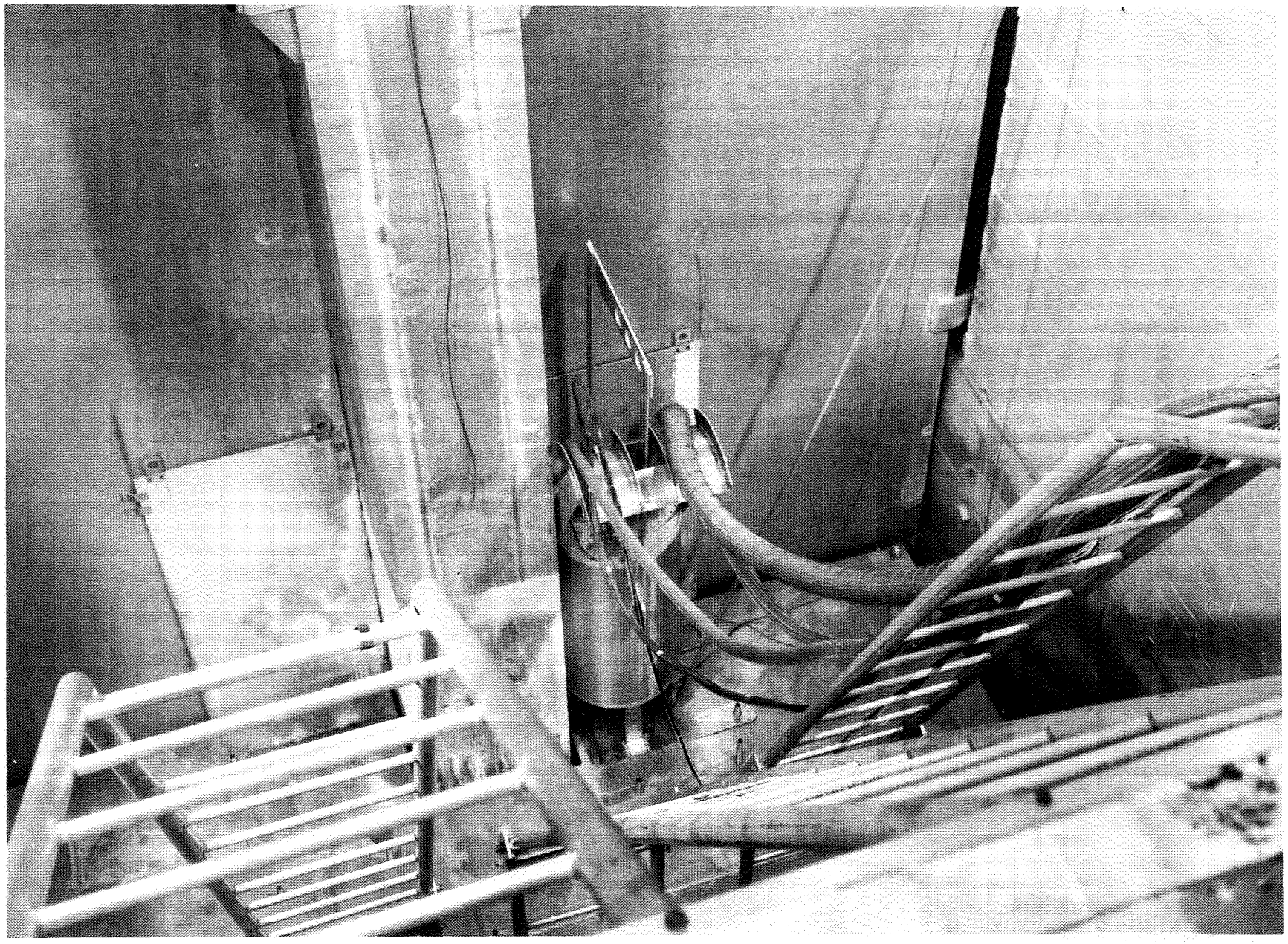

Figure 3 Fill-Valve Assembly in the Irrigation Position

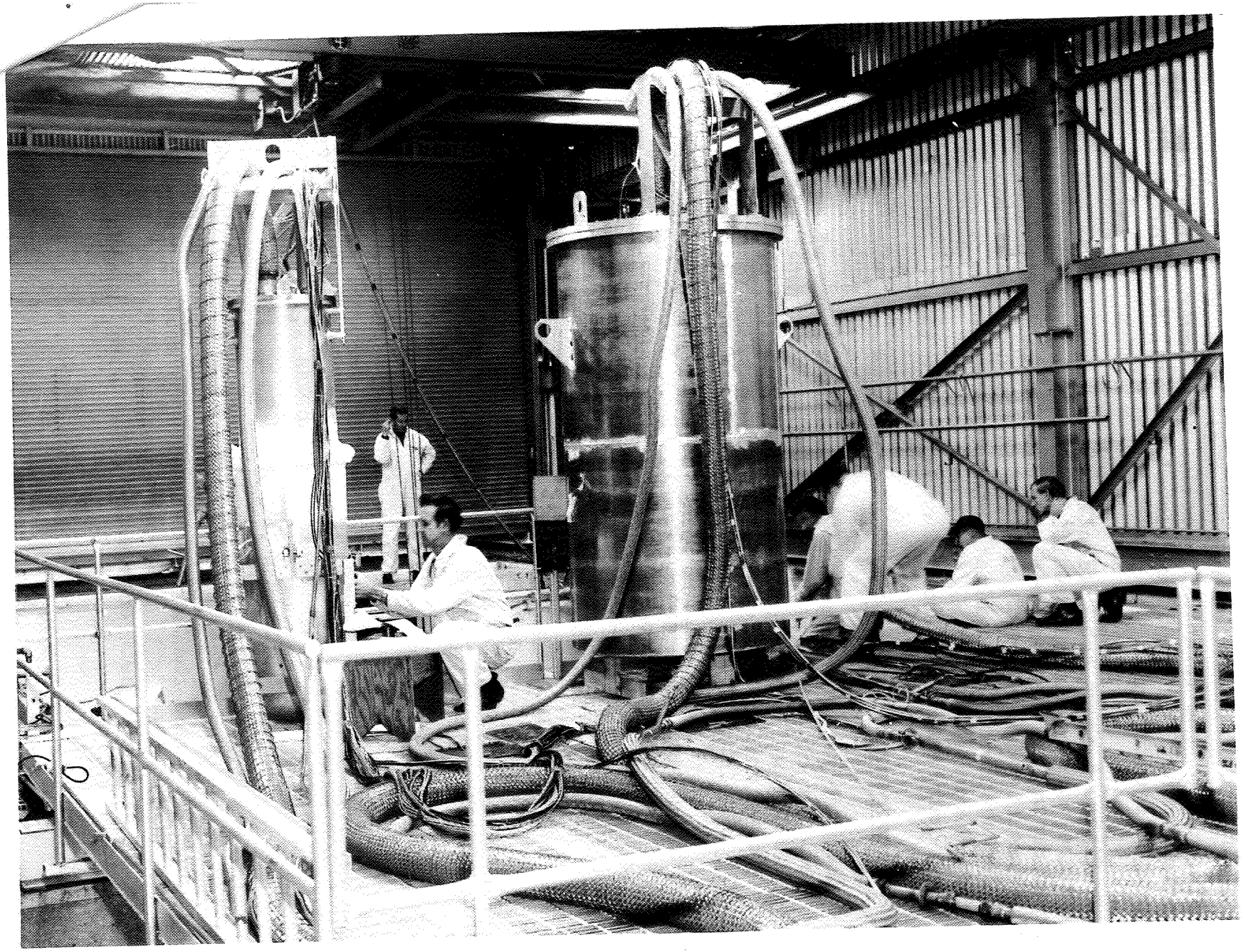

Figure 4 17-Inch-Valve Assembly Ready for Installation in the Irradiation Cell

just north of the irradiation cell. (The dewar on the left in Figure 4 contained the liquid level-sensors, data for which are reported separately.)

Figure 5 shows schematically the valve assembly and shroud with the various lines identified. Figure 6 shows the general experimental arrangement with the fill valve in the west irradiation position and the 17-in. valve in the north position. Control and leakage measurement lines enter the control room where the Leakage Measurements Panel (LMP) was set up. The cryogen and exhaust manifolds were located on the north ramp.

3.3 Measurement Equipment

Leakage rates were measured with flow-meters of several sizes. The smallest of these, a positive displacement meter, is capable of measuring a flow rate of 0 to 1 scfm H_2. The other flowmeters have the following ranges: 0.2 to 3.2 scfm H_2, 2 to 26 scfm H_2, and 15 to 127 scfm H_2.

The Leakage Measurements Panel, shown schematically in Figure 7, incorporated the flowmeters and all the valves, gages, and controls necessary to actuate the valves and completely control the test assemblies.

Valve opening and closing times were measured between break and make of the valve potentiometer open-closing switches. A four channel Sanborn thermal strip-chart recorder equipped with a timing track was used to measure the elapsed time.

3.4 Irradiation Procedure

Following two thermal cycles on the ramp, the test assemblies were positioned in the irradiation cell and a third LH_2 fill and leak check was completed. This checkout was accomplished without incident.

The irradiation cycles were scheduled for and completed on five consecutive days. Data were taken after each irradiation step and the valves were then allowed to warm to ambient temperature before the next LH_2 fill. The valves were maintained inerted with helium at all times between the LH_2 cycles.

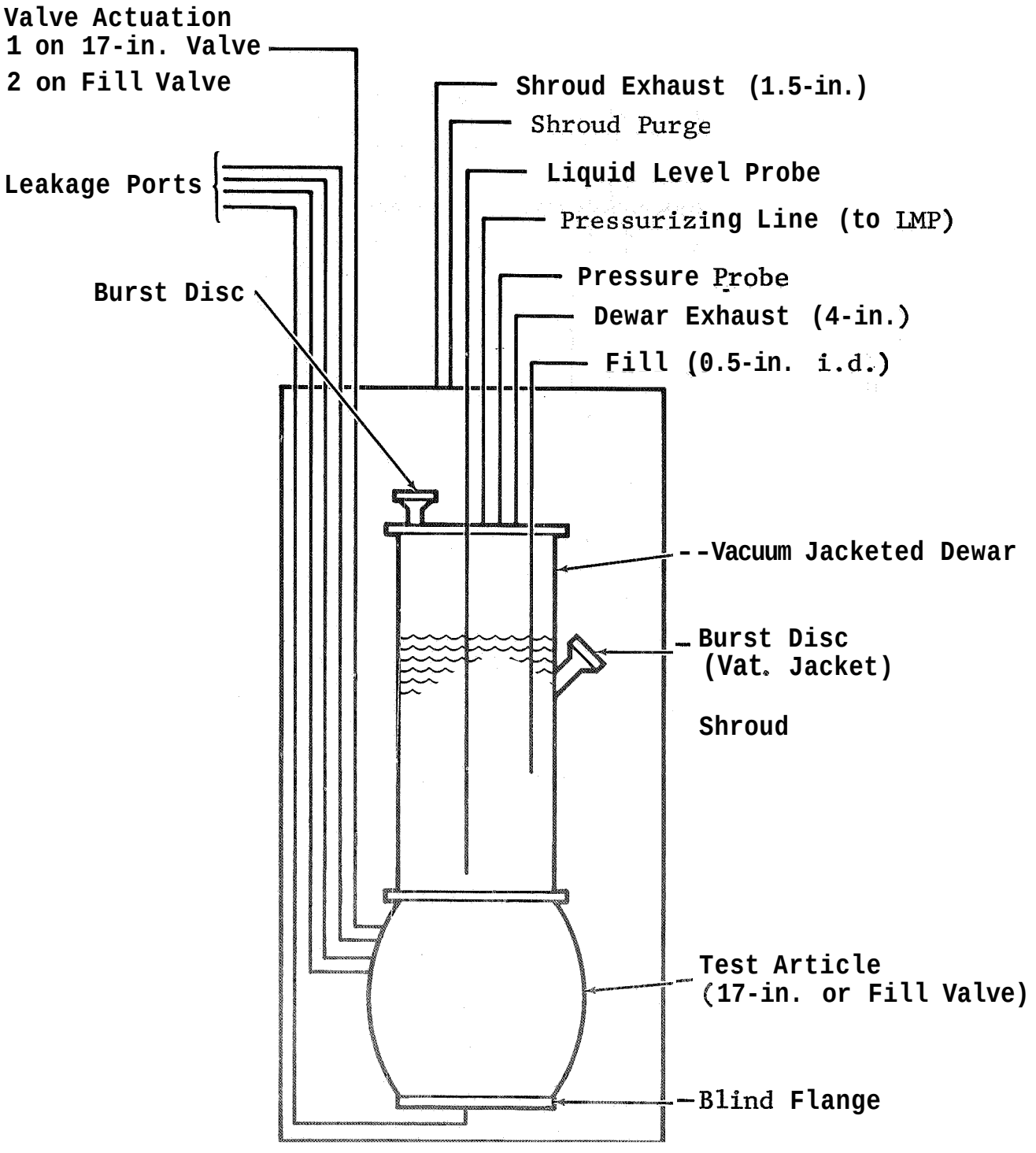

Figure 5 Schematic of Test Assemblies

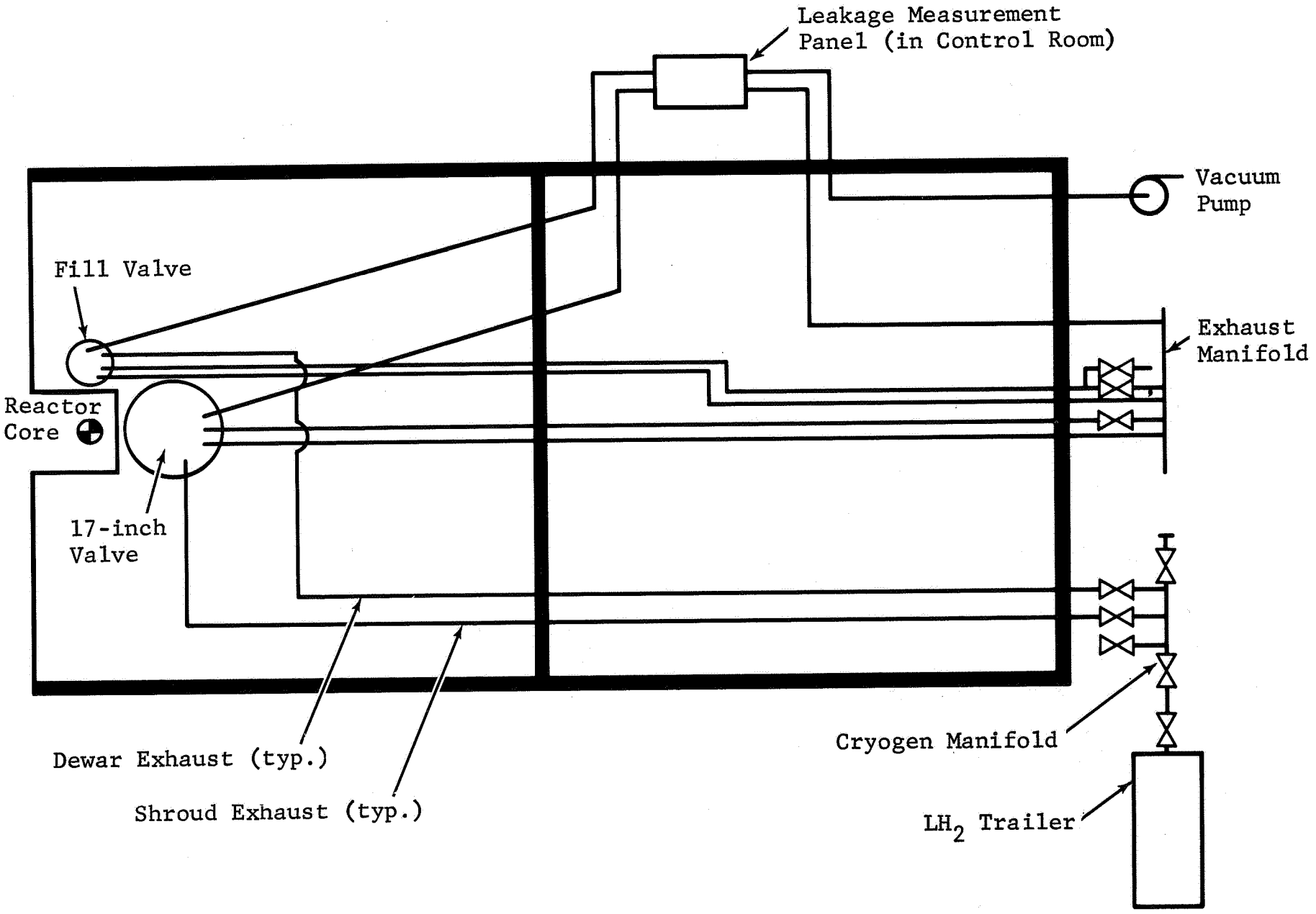

Figure 6 General Experimental Arrangement

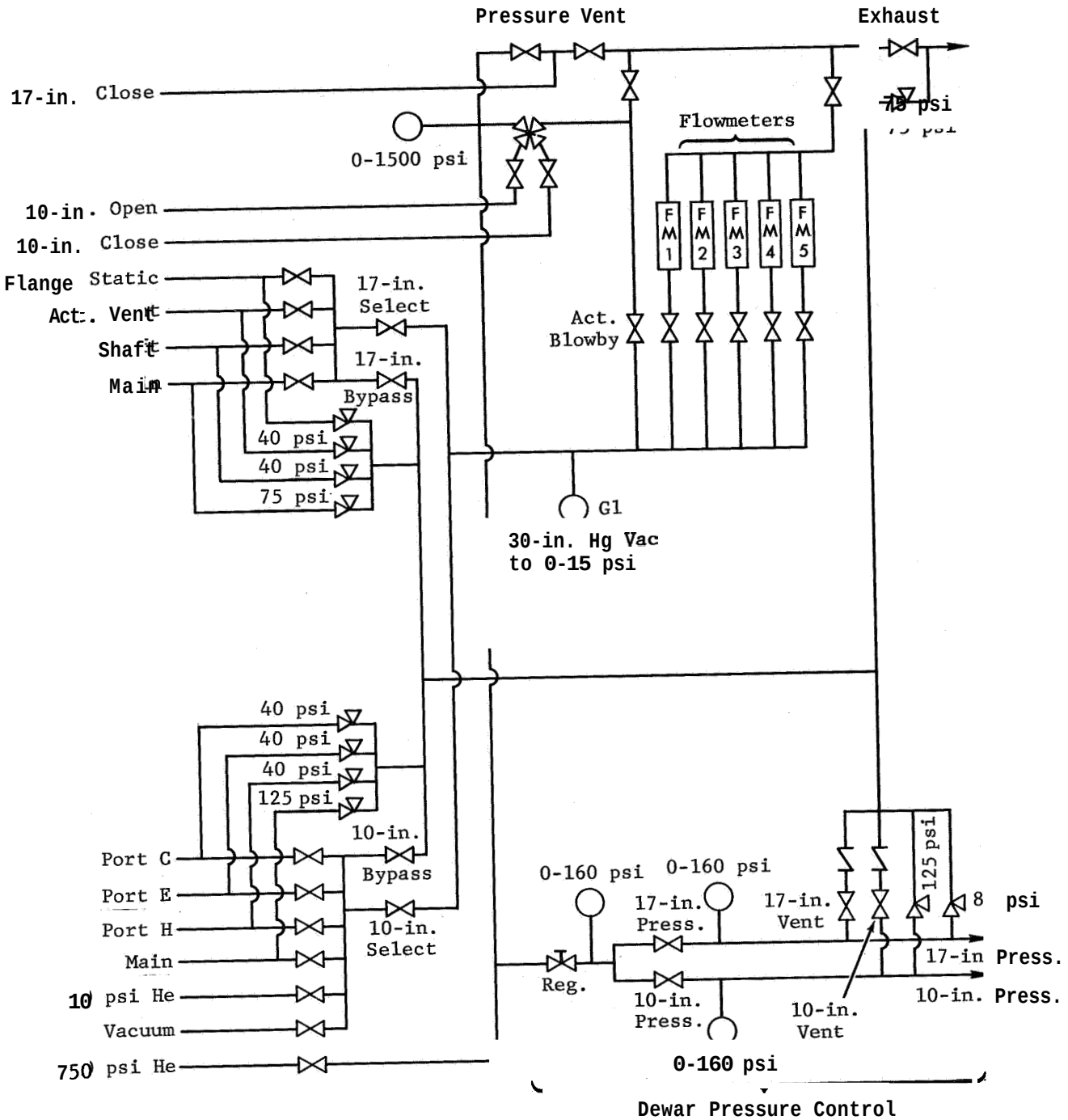

Figure 7 Schematic of Leakage Measurement Panel

Table 3 gives the irradiation schedule. Table 3 does not include several short duration runs at lower power levels which were made in order to obtain rate effects data on the liquid level sensors which were being irradiated simultaneously; these lower-power runs have been included in the computation of the megawatt hours of Table 3 and the radiation exposures given in Table 4,

Table 3

IRRADIATION SCHEDULE

Cycle	Power Level (MW)	Energy Release (MWh)	Cumulative Energy Release (MWh)
1	0.1	0.05	0.05
2	1.0	1.56	1.61
3	1.0	4.60	5.20
4	3.0	13.10	19.30
5	5.0	29.30	48.60

3.5 Measurement Procedure

3.5.1 17-Inch Valve

Each data cycle was accomplished by completing the following sequence of actions:

1. Close 17-in. valve; fill with LH_2.
2. Apply 20-psig test pressure.
3. Measure main seal leakage.
4. Measure actuator vent leakage.
5. Reduce test pressure to 0 psig,
6. Open 17-in. valve; measure time.
7. Apply 20-psig test pressure.
8. Measure shaft seal leakage,
9. Measure flange static seal leakage.
10. Reduce test pressure to 0 psig.
11. Close 17-in. valve; measure time.
12. Refill valve with LH_2.

Table 4

DOSIMETRY **DATA**

Location	Fluence E >1 MeV (n/cm^2)	Gamma Dose (ergs/gm(C))
17-in. Valve Main Seal		
Front	5.4(15)	8.0(9)
1/3 Back	4.4(15)	4.3(9)
2/3 Back	2.3(15)	2.2(9)
Full Back	3.0(14)	3.5(8)
17-in. Valve Flange		
Front	4.7(15)	6.8(9)
1/4 Back	7.6(15)	7.3(9)
1/2 Back	4.7(15)	4.6(9)
3/4 Back	7.0(14)	6.8(8)
Full Back	2.4(14)	2.4(8)
17-in. Valve Actuator		
Midbody	1.1(16)	1.6(10)
Fill Valve Main Seal		
Front	9.3(15)	1.2(10)
1/3 Back	6.5(15)	1.1(10)
2/3 Back	2.3(15)	4.1(9)
Back	1.2(15)	3.0(9)
Fill Valve Actuator		
North End	1.2(16)	1.7(10)
Midbody	1.4(16)	2.0(10)
Southend	5.2(15)	7.8(9)

13. Perform irradiation.
14. Repeat steps 2 through 10.
15. Warm valves to room temperature.

3.5.2 LH_2 Fill Valve

Each data cycle was accomplished by completing the following sequence of actions:

1. Close 10-in. valve; fill with LH_2.
2. Measure actuator pressure decay.
3. Apply 40-psig test pressure.
4. Measure main gate seal leakage.
5. Reduce test pressure to 0 psig.
6. Measure latch cover plate leakage, valve closed.
7. Open 10-in. valve; measure opening time.
8. Measure latch cover plate leakage, valve open.
9. Measure actuator piston rod seal leakage, valve open.
10. Apply 40-psig test pressure.
11. Measure idler shaft seal leakage.
12. Measure drive shaft seal leakage.
13. Reduce test pressure to 0 psig.
14. Close 10-in. valve; measure closing time.
15. Refill valve with LH_2.
16. Perform irradiation.
17. Repeat steps 2 through 13.
18. Warm valve to room temperature.

IV. RESULTS AND DISCUSSION

4.1 17-Inch Valve

Table 5 gives the results of the 17-in. valve irradiation. Main seal leakage stayed well within specification and varied randomly from run to run. Shaft seal and flange static seal leakage remained essentially zero throughout the test. In three of the eight data cycles the actuator vent leakage was well above specification, but it was zero at the end of the test. There was a trend toward increasing valve opening time as the test progressed. In one instance the valve stuck closed but opened on the second try. At the end of the test the opening time was 3 to 5 seconds as compared with the specification of 2 seconds. The closing time remained well within the specification of 1 second in each of the cycles.

It is concluded that the cumulative radiation dosage had little to no effect on leakage from the 17-in. valve. It is believed, however, that the combination of increasing opening time and constant closing time is possibly evidence of the onset of seal functional degradation. The valve opens, and is held open, by pneumatic pressure developed against the actuator piston and closes by an opposing spring load on the actuator piston. Thus, piston seal degradation would tend to increase valve opening time due to gas leakage past the piston without effecting closing time at all.

Visual inspection of the seals failed to disclose any sign of damage. All seals were intact and seemed to be in good shape. Figures 8 and 9 are photographs of the 17-in.-valve seals.

4.2 LH_2 Fill Valve

Table 6 gives the results of the LH_2 fill valve irradiation. Main seal leakage stayed well within specifications and varied randomly from run to run. Actuator pressure decay increased somewhat as the test progressed. Actuator piston seal (valve closed), latch cover plate (valve closed), actuator piston rod seal (valve openj, idler shaft seal (valve open), and drive shaft seal (valve open) all displayed essentially zero leakage throughout the test.

Table 5

DATA FOR 17-INCH VALVE

Measurement	Units	Cycle											Spec. (max)
		Pre 1	Post 1	Pre 2	Post 2	Pre 3	Post 3	Pre 4	Post 4	Pre 5	Post 5	6	
Main Seal Leak	scfm	0.37	-	-	-	1.2	0	0	0	0.31	0.66	0	3.0
Actuator Vent Leak	scim	0	-	-	-	12	20	0	0	26	0	0	2.0
Shaft Seal Leak	scim	0	-	-	-	0	0	0	0	0	0	0	50.0
Flange Static Seal Leak	scim	0	-	-	-	0	0	0	0	0	0	0	5.0
Opening Time	sec	1.4	-	-	-	-	1.9	-	2.5	3.5	3.2*	5.3	2.0
Closing Time	sec	0.60	-	-	-	0.50	-	0.50	-	0.20	0.20	0.20	1.0
Avg Cumulative Gamma Dose**	erg/ gm(C)	0	3.5(6)	3.5(6)	1.1(8)	1.1(8)	3.7(8)	3.7(8)	1.4(9)	1.4(9)	3.5(9)	3.5(9)	
Avg Cumulative Neutron Fluence	n/cm^2	0	4.2(12)	4.2(12)	1.4(14)	1.0(8)	4.5(14)	4.5(14)	1.6(15)	1.6(15)	4.2(15)	4.2(15)	

* Valve stuck for 35 sec on first try. Time shown is for second try.

**Computed

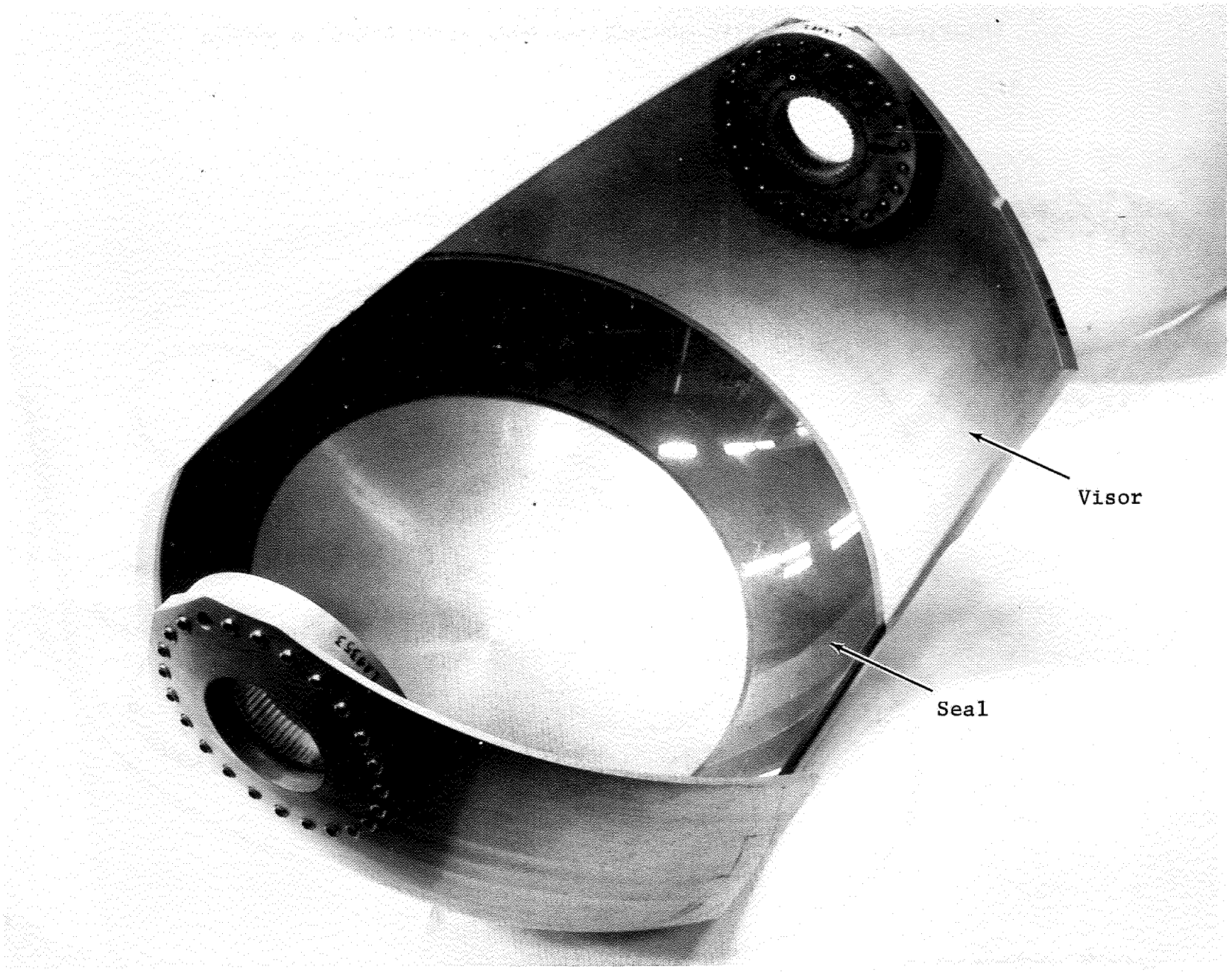

Figure 8 Main Seal from the 17-inch Valve after Irradiation

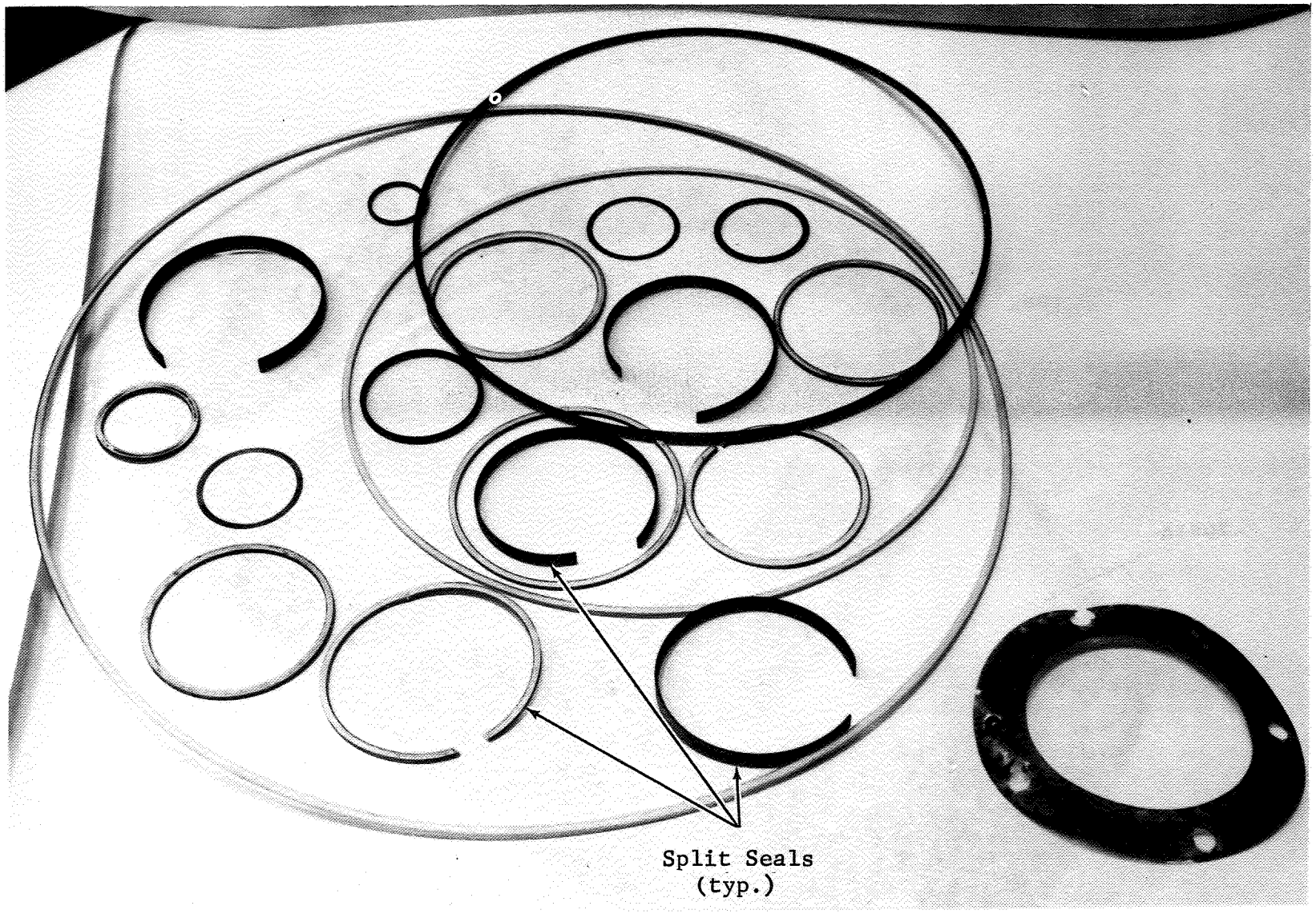

Figure 9 Other Seals from the 17-in. Valve after Irradiation

Table 6

DATA FOR LH_2 FILL VALVE

Measurement	Units	Cycle											Spec. (max)
		Pre 1	Post 1	Pre 2	Post 2	Pre 3	Post 3	Pre 4	Post 4	Pre 5	Post 5	6	
Actuator Pressure Decay	Δ psi	-	-	-	-	65	60	-	-	62	60	70	92
Actuator Pressure Decay, Port C Leak	scim	0	0	-	-	0	0	-	-	0	0	0	100
Main Seal Leak	scim	8.6	0	6.9	0	0	0	0	0	35	10.3	6.9	300
Actuator Piston Seal Leak, Valve Closed	scim	0	0	0	0	0	0	0	0	0	0	0	100
Latch Cover Plate Leak, Valve Closed	scim	0	0	0	0	0	0	0	0	0	0	0	5.0
Actuator Piston Rod Seal Leak, Valve Open	scim	0	0	0	0	0	0	0	0	0	0	0	100
Idler Shaft Seal Leak, Valve Open	scim	0	0	0	0	0	0	0	0	0	0	0	50
Drive Shaft Seal Leak, Valve Open	scim	0	0	0	0	0	0	0	0	0	0	0	50
Opening Time	sec	4.6	-	2.1	1.1	-	3.2	-	3.1	-	3.1	2.6	5±2
Closing Time	sec	-	2.4	1.9	3.5	2.1	-	2.1	-	2.0	-	2.3	5±2
Avg Cumulative Gamma Dose*	erg/ gm(C)	0	1.1(7)	1.1(7)	3.5(8)	3.5(8)	1.1(9)	1.1(9)	4.3(9)	4.3(9)	1.1(10)	1.1(10)	
Avg Cumulative Neutron Fluence	n/cm^2	0	7.4(12)	7.4(12)	2.4(14)	2.4(14)	7.7(14)	7.7(14)	2.9(15)	2.9(15)	7.2(15)	7.2(15)	

*Computed

Valve opening time was less than the specified minimum of 3 seconds in three of the seven openings. Valve closing time was less than the specified minimum of 3 seconds in six of the seven closings. In no case was either opening or closing time as much as the nominal 5-second specification value.

Visual inspection of the seals failed to disclose any signs of damage. All seals were intact and seemed to be in good shape. Figures10 and 11 are photographs of seals from the fill valve.

4.3 Conclusions

The results of this irradiation experiment indicate that the seal materials used in either of the valves would be satisfactory for application at the exposure levels expected in ten missions of a Reuseable Nuclear Shuttle powered by a 1500-MW NERVA. This was anticipated for the 17-in. valve since the materials were specifically chosen to have radiation resistance superior to the replacement materials.

However, the performance of the unmodified S-II stage fill valve shows that even Teflon and Kel-F, materials widely used for cryogenic applications but of rather low radiation resistance, will function to rather high dose levels under certain conditions. The absence of oxygen during the radiation exposure is probably the main factor since oxidation therefore cannot occur. Exposure at cryotemperature may also contribute to the improved radiation resistance, but when the organic material is actually submerged in the cryogen it is the exclusion of oxygen rather than the cryotemperature per se that is the chief benefactor,

Perhaps the most important result of this test is that it graphically illustrates that the environment and test conditions can be all important in evaluating radiation effects. For applications in space at cryotemperature, at the least, the commonly used organic materials may well be entirely suitable for most applications on the nuclear powered vehicle.

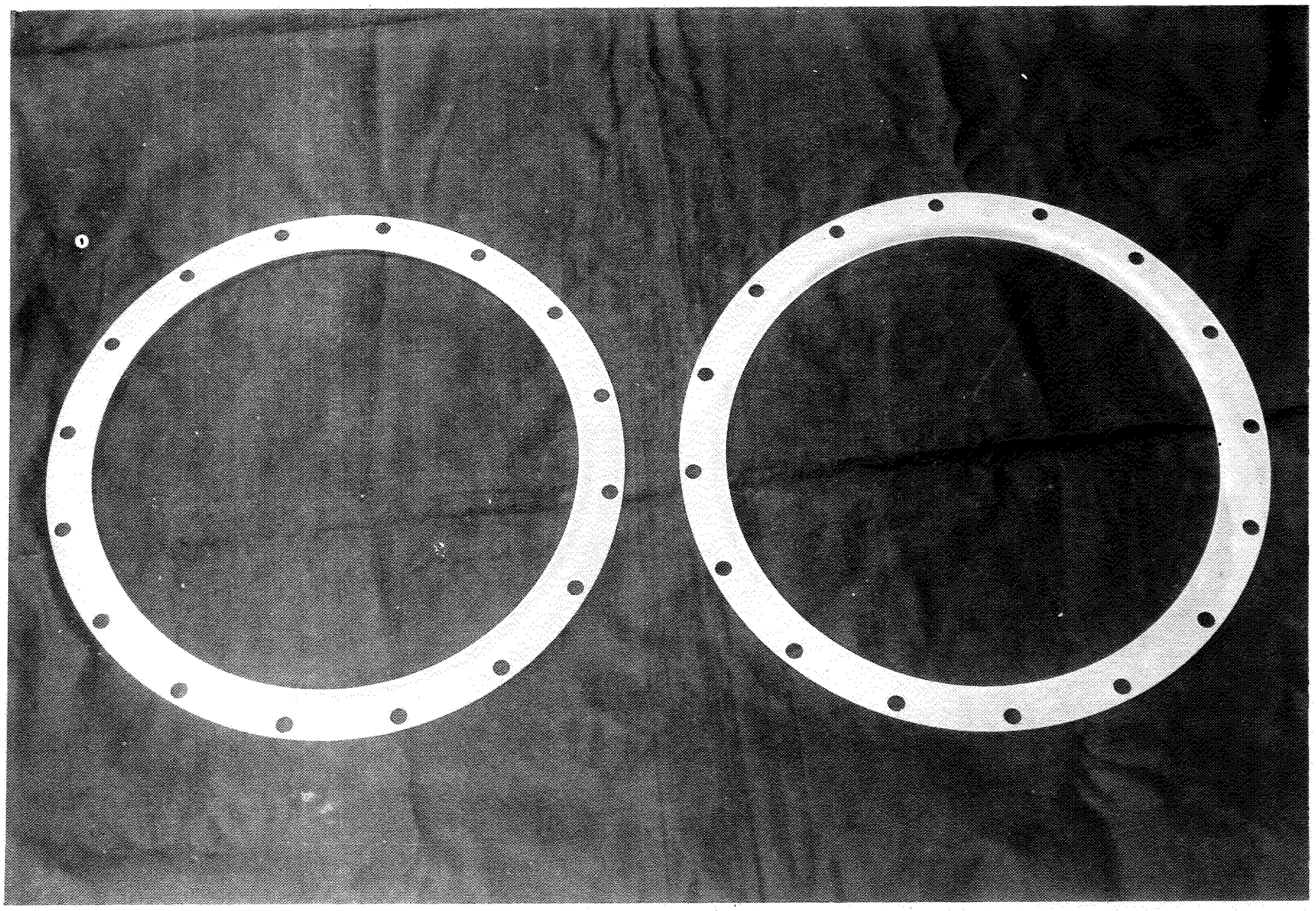

Figure 10 Main Lipseals from the F-111 Valve After Irradiation

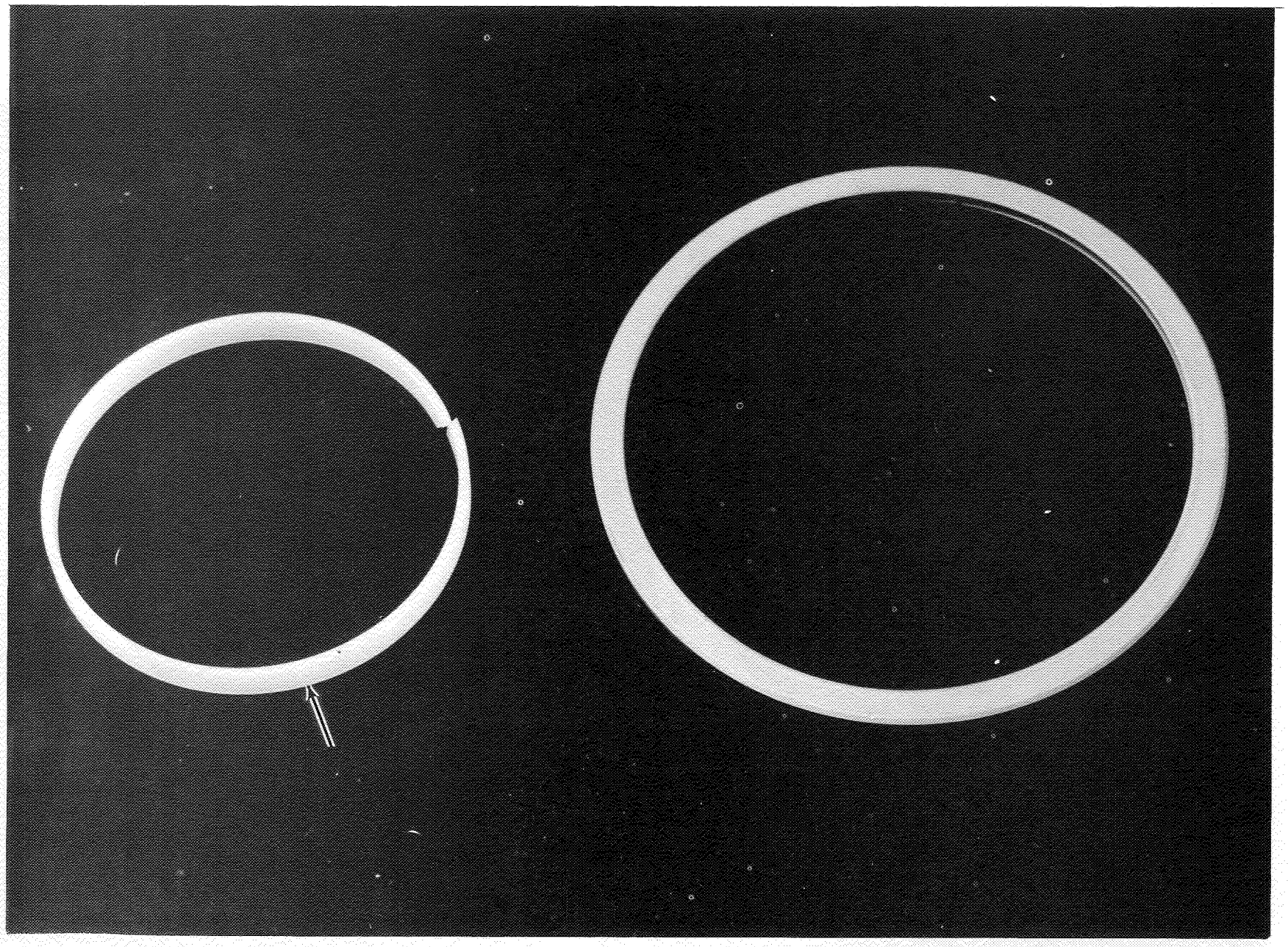

Figure 11 Other Seals from the Fill Valve after Irradiation

REFERENCES

1. Maintenance Manual, Pneumatically Actuated Spherical Rotary Valve, MSFC 20M32010 Series, Manufacturing Engineering Laboratory, George C. Marshall Space Flight Center, Huntsville, Alabama.

2. Van Auken, R. L., Modification of LOX Prevalve, Whittaker Corporation, Research & Development Division, San Diego, California, February 1970.

3. Scheck, W. G., Replacement of Radiation Components on a 17-Inch LOX Prevalve, Whittaker Corporation, Narmco Research & Development Division, San Diego, California, April 1968.

4. Valve Assembly, Propellant Fill, V7-480450-61, and -91, Saturn S-II, Acceptance Test Procedure for, North American Aviation, Inc. Specification MA0201-1955, 21 January 1967.

Part IV

BORON-EPOXY COMPOSITES

FZK-388

By

R. E, BULLOCK

SUMMARY

Light weight, high strength boron-epoxy composites were irradiated in a nuclear reactor and then mechanically tested for strength. These boron-epoxy laminates, made by reinforcing an epoxy matrix with 15 plies of unidirectional boron filaments, were irradiated and tested under three different combinations of temperature which could occur in a nuclear-powered spacecraft using a cryogenic propellant. Specimens of group 1 were irradiated in air or water at ambient temperatures below 80°C and were tested at room temperature, as were specimens of group 2 which were irradiated in liquid hydrogen at -253°C. Specimens of group 3 were irradiated and tested in liquid nitrogen at -196°C without an intermediate warmup. Mechanical strengths of all specimen groups were degraded primarily by thermal neutrons. For equivalent thermal-neutron fluences, flexural strengths in the longitudinal direction (parallel to boron filaments) were best for specimens of group 1, next best for those of group 2, and poorest for those of group 3. This order of degradation seems to be dictated by the more radiation-sensitive interlaminar shear strength, which measures epoxy-to-filament bonding. The order of damage above was reversed for transverse flexural strengths.

I. INTRODUCTION

Unidirectional boron-epoxy composite has considerably higher ratios of tensile strength to weight and elastic modulus to weight than do conventional bulk metals. Therefore, designers are giving this material a great: deal of attention for structural applications in weight-sensitive spacecraft. Much design work has also been done on a nuclear-powered engine for spacecraft under NASA's Nuclear Engine for Rocket Vehicle Application (NERVA) Program. The NERVA engine utilizes hydrogen as a propellant (stored as a liquid) and a nuclear reactor as a heat source. Thus, it is of considerable interest to know how strengths of boron-epoxy composites are affected by mixed-radiation fields from a nuclear reactor, both at normal ambient temperatures and at cryogenic temperatures.

Experiments have been performed in which specimens of boron-epoxy composite were irradiated with the Ground Test Reactor (GTR) in several environments including liquid hydrogen, liquid nitrogen, air, and water. Maximum radiation exposures were more than an order of magnitude higher than those expected forward of the engine tangent plane in ten hours of operation of the NERVA. In addition to varying the irradiation temperature and total radiation exposure, the ratios of reactor radiations (thermal and fast neutrons and gamma rays) were also varied over limited ranges. For example, the irradiation in water was for the purpose of obtaining a high thermal-neutron fluence because boron has a large cross section for thermal neutron capture.

With the exception of some specimens irradiated and tested in liquid nitrogen without warmup, all testing was at room temperature. Specimens were of flexural (longitudinal and transverse) and shear types.

II. DESCRIPTION OF TEST

2.1 Test Specimens

Boron-epoxy specimens for the irradiation test were cut from 15-ply laminated panels which had a thickness of 0.084 in. The boron reinforcements in these panels were 4-mil filaments of natural boron which had been vapor deposited on 0.5-mil cores of tungsten wire. These boron filaments were initially embedded parallel to one another in tacky epoxy-resin tapes (Whittaker Corporation's Narmco 5505) at a density of about 200 filaments per inch of tape width. These tapes were then covered with a 1-mil thickness of woven glass cloth and were partially cured to form 5-mil sheets of composite material. Panels from which test specimens were cut were fabricated by layering 15 of these composite plies together with the same filament orientation. These laminated panels were then fully cured by subjecting them to prolonged heat and pressure to form an epoxy matrix unidirectionally reinforced with close-packed boron filaments (55% filaments by volume and 72% by weight). The finished composite panels had a density of 2 g/cm^3 and were, by weight, about 60 percent natural boron, 28 percent epoxy, and 12 percent natural tungsten.

Flexural specimens 3.0 in. by 0.5 in, were cut from these 0,084-in. panels with their major axes both parallel to the filament direction (longitudinal, or 0° specimens) and perpendicular to it (transverse, or 90° specimens). Interlaminar shear specimens 0.6 in. by 0.25 in. were cut with their major axes lying along the filament direction.

2.2 Test Conditions

The test specimens were irradiated with the 10-MW Ground Test Reactor during irradiations of NERVA materials and components. Panels of specimens were irradiated in air, in water, in liquid nitrogen, and in liquid hydrogen. Temperature of the air specimens was a maximum of $80^\circ C$ and of the water specimens $50^\circ C$. The specimens irradiated in LN_2 and LH_2 were maintained in those cryogens throughout the irradiations, The LH_2-irradiated specimens were allowed to warm to room temperature after completion of the irradiation, while the LN_2-irradiated specimens were maintained in that cryogen until completion of testing,

2.3 Mechanical Tests

All composite specimens were loaded to failure on an Instron machine at a crosshead speed of 0.05 in./min, and load-deflection curves were continuously recorded at a chart speed of 2 in./min. The longitudinal flexural specimens were loaded at their midpoints while bridging a support span of 2.5 in., while transverse flexural specimens were loaded at two points 0.5 in. either side of their midpoints while bridging a 2.0-in. span. Interlaminar shear specimens were loaded at their centers while supported over a 0.4-in. span. The specimens which were irradiated in air or water at ambient temperatures were all mechanically tested at room temperature, as were the specimens which had been irradiated in LH_2. The specimens which were irradiated in LN_2 were also tested in LN_2 without intermediate warmup. This was accomplished by immersing the various test fixtures in a special LN_2 Dewar which was supported by the compression plate of the Instron machine. The specimens were rhen loaded by the downward motion of the Instron crosshead in the usual way, with the weight of the LN_2-filled Dewar and the test fixture being balanced out of the recorded loads,

Ultimate flexural strengths for longitudinal and transverse specimens were calculated from the formulas (Ref. 1)

$$F(0^{\circ}) = \frac{3S}{2wt^2} P$$

$$F(90^{\circ}) = \frac{3s}{4wt^2} P ,$$

and interlaminar shear strengths were calculated from (Ref. 2)

$$S = \frac{3}{4wt} P .$$

Here, P is the failure load (lb) on a specimen of width w (in.) and thickness t (in.), and S is the magnitude of the support span length measured in inches for the flexural specimen in question (2.5 for longitudinal specimens and 2.0 for transverse specimens).

The width and the thickness of each specimen tested at room temperature were measured to the nearest 0.001 in. before and after irradiation, and the dimensions after irradiation were used

in the equations above. Dimensions of the specimens irradiated and tested in LN_2 were measured only before irradiation, and these values were used in strength calculations for those specimens. Dimensions of specimens were very uniform and before irradiation did not differ by much from a thickness of 0.084 in. and a width of 0.500 or 0.250 in. for flexural specimens or shear specimens, respectively. The dimensions of specimens measured before room-temperature testing were increased somewhat by irradiation, probably because of helium-gas formation in the specimens. Thicknesses increased by as much as 6 percent and widths by some few tenths of a percent. Accurate dimensional measurements could not be made after the specimens in LN_2 were tested, for these specimens delaminated severely on warmup.

2.4 Dosimetry

Each test panel was instrumented with ten phosphorus detectors, six bare and four cadmium covered, arranged so that eight values of thermal-neutron fluence ($E < 0.48$ eV) over each test panel were calculated from measured radioactivities of different pairs of detectors. Mean thermal-neutron fluences for each test panel were obtained by averaging the eight measured values for different positions on each panel. One standard deviation from the mean for the eight measured values was less than 20 percent in all cases but one, for which it was 30 percent. Mean fast-neutron fluences ($E > 1.0$ MeV) for each test panel were obtained by averaging values calculated from radioactivity measurements of two nickel foils. One standard deviation from the mean for these two values was less than 15 percent in all cases. Gamma doses were measured with cobalt-glass dosimeters during short preliminary mapping runs. These mapping doses per MWh were then linearly projected over the long test runs to obtain gamma doses.

Table 1 identifies the various test panels by radiation environment and gives the radiation exposures for each. The data are ordered in three groups according to increasing thermal-neutron fluence.

Table 1

RADIATION EXPOSURES FOR THE TEST PANELS

Test Panel No.	Environment	Gamma Dose [ergs/g(C)]	Fast-Neutron Fluence (n/cm^2) $E > 1$ MeV	Thermal-Neutron Fluence (n/cm^2) $E < 0.48$ eV
1	Air	4.0×10^{10}	2.8×10^{16}	4.5×10^{14}
2	Air	5.2×10^{8}	2.8×10^{14}	8.1×10^{14}
3	Air	4.3×10^{10}	3.5×10^{16}	1.3×10^{15}
4	Air	5.0×10^{11}	2.9×10^{17}	7.0×10^{15}
5	Water	3.0×10^{11}	5.7×10^{15}	2.2×10^{16}
6	Air	2.1×10^{12}	8.6×10^{17}	3.0×10^{16}
7	Air	6.5×10^{11}	3.5×10^{17}	3.6×10^{17}
8	Water	1.1×10^{12}	2.0×10^{17}	1.1×10^{18}
9	Water	2.9×10^{12}	5.7×10^{17}	7.0×10^{18}
10	LH_2	2.4×10^{10}	1.1×10^{16}	3.8×10^{16}
11	LH_2	2.1×10^{11}	5.6×10^{16}	1.8×10^{17}
12	LH_2	4.5×10^{11}	2.1×10^{17}	4.8×10^{17}
13	LN_2	1.1×10^{12}	6.4×10^{17}	1.1×10^{17}
14	LN_2	3.3×10^{12}	1.8×10^{18}	1.6×10^{17}

III. RESULTS

Average strengths for the three types of boron-epoxy specimens are listed in Table 2 for the various conditions of irradiation and mechanical testing, and percentage standard deviations for the five specimens of each type are listed in Table 3. The data of Table 2 are listed according to increasing thermal-neutron fluences received by specimens in three groups: group 1 irradiated in air or water at ambient temperatures ($< 80^{\circ}C$) and mechanically tested at room temperature (RT), group 2 irradiated in LH_2 ($20.3^{\circ}K$) and tested at RT, and group 3 irradiated in LN_2 ($77.4^{\circ}K$) and tested in LN_2 yithout intermediate warm-up. Unirradiated control specimens were stored in the various irradiation environments (air, LH_2, and LN_2) for the same length of time as the irradiated specimens and were then mechanically tested at the temperature appropriate for each of the three groups.

The longitudinal flexural strengths and interlaminar shear strengths for the three test conditions are plotted against thermal-neutron fluence in Figure 1, and transverse flexural strengths are similarly plotted in Figure 2. There are not really enough data to plot curves for strengths of specimens in group 3; the tentative curves are drawn more for the purpose of connecting the three data points than'for defining functional strength relationships. It is not possible to completely separate the effects of mixed-field radiations from a nuclear reactor, of course, so that it is not strictly proper to plot any of the strength data against thermal-neutron fluence alone. However, except for the transverse flexural strength at low thermal-neutron fluences and at gamma doses in the range of 10^{10} erg/g(C) (where cross-linking of epoxies are known to occur), all strength data correlate very well with thermal-neutron fluence but not with gamma dose or fast-neutron fluence, so that it is concluded that thermal-neutron fluence is predominately responsible for the observed radiation effects on strengths of boron-epoxy composites.

The longitudinal flexural strengths at room temperature of specimens irradiated in air or water does not begin to decrease until thermal-neutron fluences beyond 4×10^{17} n/cm^2 ($E < 0.48$ eV) are reached, but it then falls off rapidly and is degraded by more than 75 percent at the highest thermal fluence of 7×10^{18} n/cm^2. The room-temperature strength of longitudinal specimens irradiated in LH_2 falls off even more sharply above a thermal fluence of 2×10^{17} n/cm^2 and is degraded by about 50 percent at

Table 2

STRENGTHS OF IRRADIATED BORON-EPOXY COMPOSITES

Test Panel Number	Thermal-Neutron Fluence (n/cm^2) $E < 0.48$ eV	Radiation Environment	Test Temperature	Longitudinal Flex Strength (ksi)	Transverse Flex Strength (ksi)	Interlaminar Shear Strength (ksi)
Control 1	0	Air	RT	226	20.0	14.7
1	4.5×10^{14}	Air	RT	227	23.9	15.3
2	8.1×10^{14}	Air	RT	226	20.3	15.2
3	1.3×10^{15}	Air	RT	223	23.8	15.3
4	7.0×10^{15}	Air	RT	232	19.4	14.9
5	2.2×10^{16}	H_2O	RT	236	*	14.7
6	3.0×10^{16}	Air	RT	240	16.3	10.0
7	3.6×10^{17}	Air	RT	242	6.4	4.5
8	1.1×10^{18}	H_2O	RT	199	*	3.8
9	7.0×10^{18}	H_2O	RT	51	*	2.3
Control 2	0	LH_2	RT	225	20.6	14.8
10	3.8×10^{16}	LH_2	RT	228	22.4	15.2
11	1.8×10^{17}	LH_2	RT	228	13.7	10.8
12	4.8×10^{17}	LH_2	RT	126	7.5	3.2
Control 3	0	LN_2	LN_2	244	21.3	16.7
13	1.1×10^{17}	LN_2	LN_2	143	18.7	3.8
14	1.6×10^{17}	LN_2	LN_2	128	18.0	3.6

*No specimens irradiated.

Table 3

COEFFICIENTS OF VARIATION FOR EACH SPECIMEN GROUP

Test Panel Number	Percentage Standard Deviations*		
	Longitudinal Flex Strength	Transverse Flex Strength	Interlaminar Shear Strength
Control 1	1.1	8.3	4.3
1	3.7	3.3	0.8
2	2.0	6.6	2.6
3	2.6	4.5	1.8
4	2.5	5.8	2.5
5	2.6	-	4.4
6	3.4	4.1	2.1
7	2.7	1.9	16.4
8	6.8	-	6.2
9	9.6	-	5.9
Control 2	1.6	5.7	3.8
10	2.8	3.9	2.1
11	1.5	4.8	1.1
12	9.8	8.3	4.8
Control 3	1.2	6.9	3.6
13	7.8	2.9	4.1
14	9.5	6.4	7.8

*Based on five specimens.

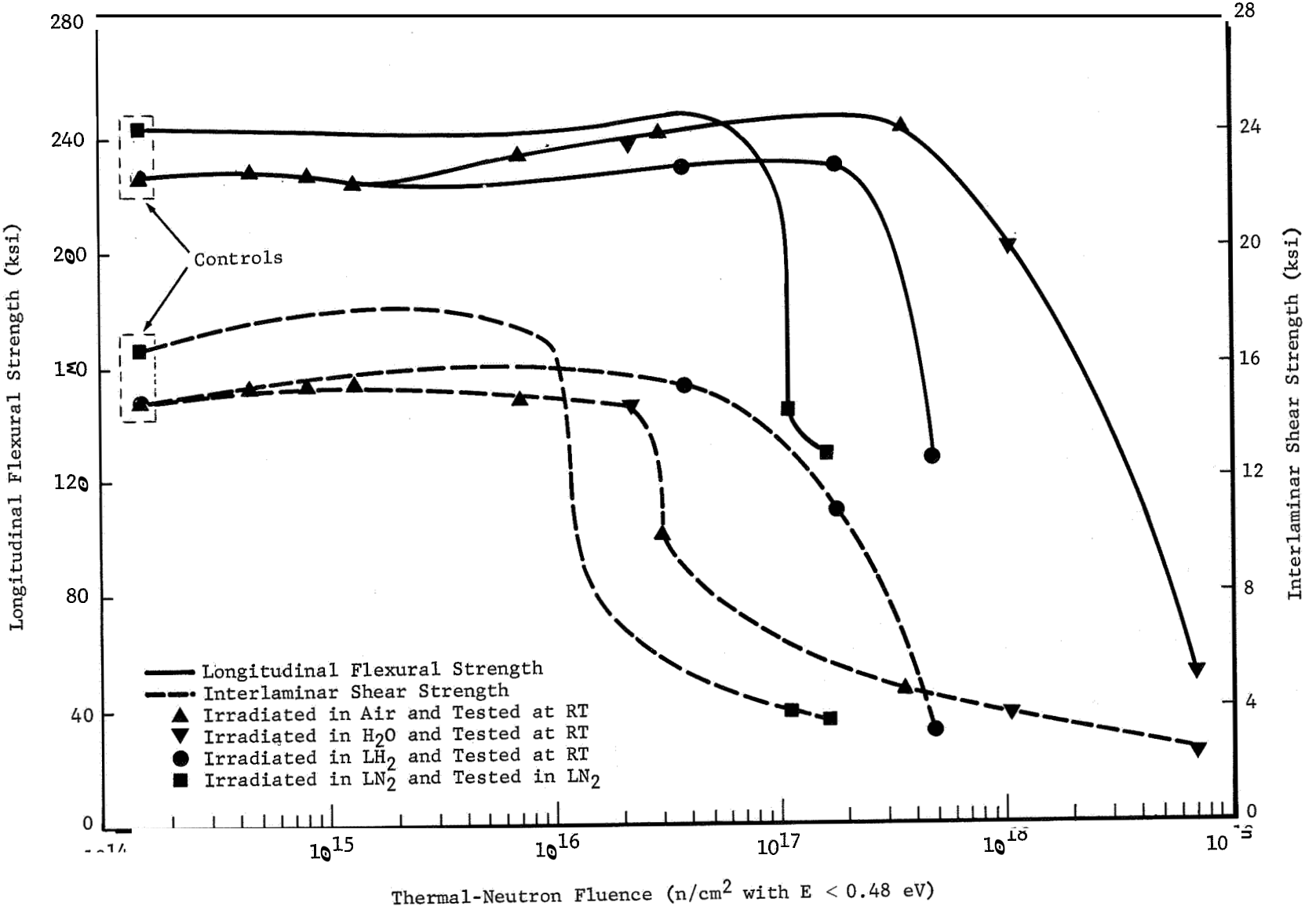

Figure 1 Longitudinal Flexural Strengths and Interlaminar Shear Strengths of Boron-Epoxy Composites Irradiated and Mechanically Tested in Various Environments

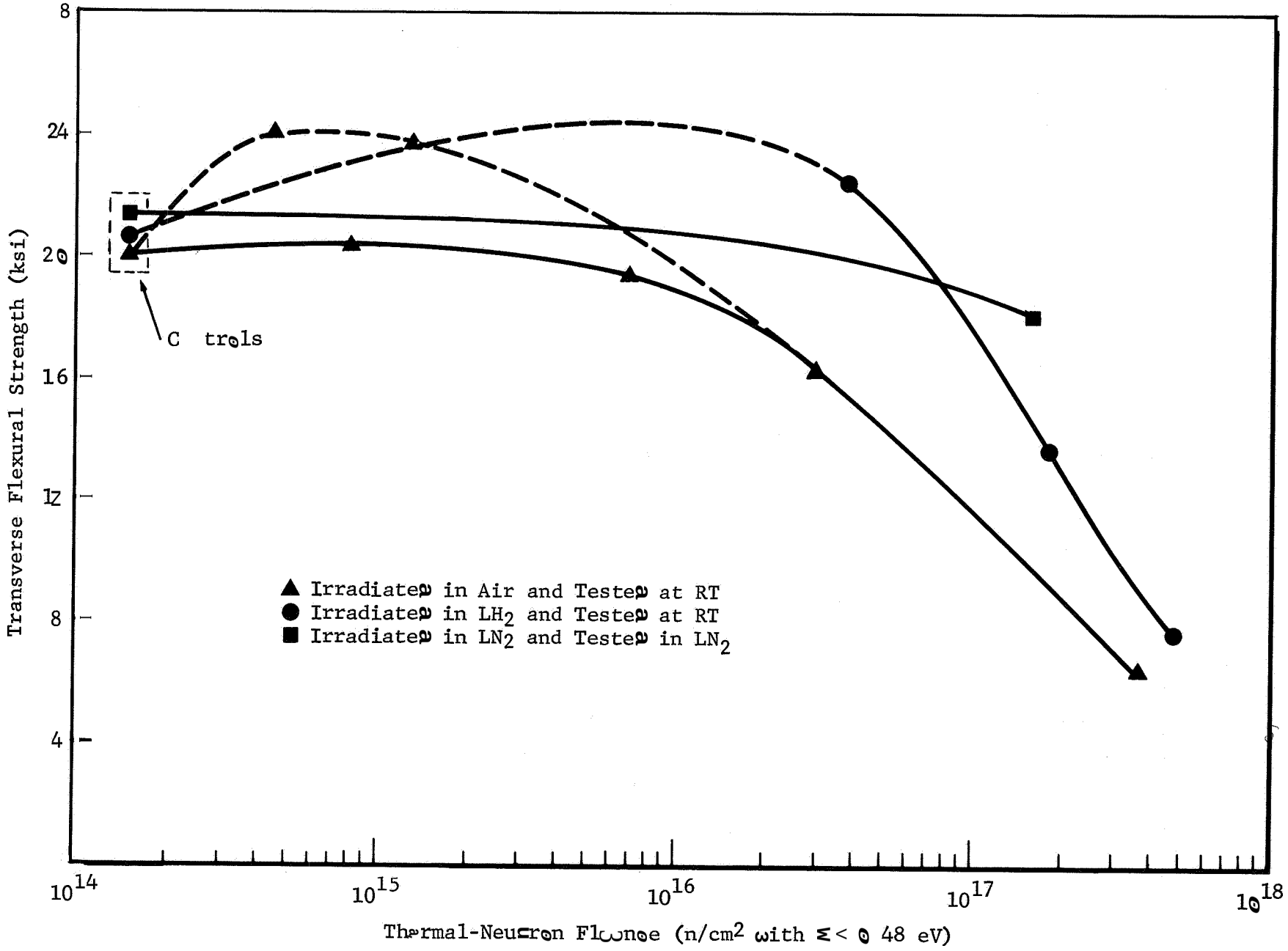

Figure 2 Transverse Flexural Strengths of Boron-Epoxy Composites Irradiated and Mechanically Tested in Various Environments

a fluence of 5 x 10^{17} n/cm^2. The longitudinal flexural strength at LN_2 temperature is degraded still more severely by radiation exposure, being reduced by almost 50 percent at a thermal-neutron fluence of 1.6 x 10^{17} n/cm^2.

The interlaminar shear strengths of boron-epoxy specimens begin to be degraded at thermal-neutron fluences roughly an order of magnitude lower than those for longitudinal flexural specimens for each of the three test conditions. The room-temperature shear strength of specimens irradiated in air or water begins to drop off rapidly beyond a thermal-neutron fluence of 2 x 10^{16} n/cm^2 and is 85 percent lower than the control value at the highest fluence of 7 x 10^{18} n/cm^2, while the room-temperature shear strength of specimens irradiated in LH_2 begins to fall off above a fluence of 4 x 10^{16} n/cm^2 and is reduced by about 80 percent at a fluence of 5 x 10^{17} n/cm^2. The shear strength at LN2 temperature is degraded by about 80 percent at an even lower fluence of 1.6 x 10^{17} n/cm^2.

The transverse flexural strengths of Figure 2 begin to fall below control values for roughly the same thermal-neutron fluences as do the shear strengths for each of the three test groups. The room-temperature transverse strength for specimens irradiated in air begins to fall off first at a fluence of about 1 x 10^{16} n/cm^2 and is 70 percent below the control value at a fluence of 3.6 x 10^{17} n/cm^2, while the room-temperature strength of specimens irradiated in LH_2 begins to fall off next at a fluence of about 4 x 10^{16} n/cm^2 and is reduced by almost 70 percent at a fluence of 5 x 10^{17} n/cm^2. The transverse flexural strength at LN_2 temperature falls off much less rapidly and is only 15 percent below the control strength at a fluence of 1.6 x 10^{17} n/cm^2. The transverse-strength increases at lower fluences (dashed sections of the curves) reflect cross-linking in the epoxy matrix caused primarily by gamma-ray exposures, as mentioned above, and should not properly be plotted against thermal-neutron fluence, but thermal-neutron degradation does eventually take over for higher exposure doses (solid sections of curves).

Flexural moduli were also measured for the longitudinal and transverse specimens; these mean values along with percentage deviations from the means are presented in Table 4. It can be seen that the transverse flexural modulus is much more affected by radiation exposure than is the longitudinal flexural modulus, as is to be expected, and that both moduli generally begin to fall off significantly at the same time that the respective

Table 4

FLEXURAL MODULI OF IRRADIATED BORON-EPOXY COMPOSITES

Test Panel Number	Longitudinal Flexural Modulus (10^6 psi)		Transverse Flexural Modulus 10^5 si	
	Y	s(%)		
Control 1	23.6	1.09	34.1	2.83
1	23.1	2.56	39.4	1.64
2	23.2	3.09	37.2	2.55
3	23.6	2.68	38.4	2.18
4	25.8	1.45	35.1	2.12
5	25.6	3.36	-	-
6	25.3	3.17	24.2	3.26
7	23.9	6.55	23.4	4.71
8	19.5	4.31	-	-
9	14.0	4.32		-
Control 2	23.9	1.25	34.6	2.64
10	24.2	2.36	38.0	1.57
11	23.4	1.65	24.8	1.97
12	20.3	2.53	12.4	5.12
Control 3	19.7	8.21	15.2	6.32
13	19.9	8.60	8.8	9.00
14	19.8	1.53	8.1	6.97

strengths do, but not as rapidly as do the strengths. Thus, strength properties are generally more sensitive to radiation than are stiffness properties, so that moduli will usually be affected only above the exposure thresholds given for strength degradations. The exception to this is for irradiation and testing in LN_2 where the transverse modulus falls off more rapidly than does the transverse strength. The longitudinal modulus also behaves differently here, remaining almost constant with radiation exposure as the strength falls off drastically.

IV. DISCUSSION

4.1 Experimental Data

The longitudinal flexural strength primarily measures the strength of the boron reinforcement filaments, the transverse flexural strength measures the strength of the epoxy matrix of. the composite, and the interlaminar shear strength gives a measure of filament-to-matrix bonding (Refs. 3 and 4). Therefore,. the more matrix-related strength properties are affected first by radiation, as to be expected. The cross-linking of the epoxy matrix by gamma rays probably dominates up to a dose of about 10^{11} ergs/g(C) if the thermal neutron fluence is less than 10^{16} n/cm2. This hardens and stiffens the matrix and apparently gives better bonding with the boron filaments, but the embrittled matrix also causes increased scatter in the measured longitudinal strengths. Matrix degradation by alpha particles and lithium ions from thermal-neutron reactions in boron filaments apparently begins to take over at around 10^{16} n/cm^2, and the transverse and shear strengths decrease significantly, but for a time this allows the less brittle composite to develop more of the strength of the boron filaments in the longitudinal direction (Refs. 5, 6, and 7). Matrix properties are soon degraded to the extent that reinforcement filaments can no longer be properly supported, however, and the longitudinal strength then falls away rapidly above thermal-neutron exposures of 10^{18} n/cm^2. This loss of longitudinal strength is, no doubt, enhanced by degradation of the boron filaments themselves in this region of highest thermal-neutron fluences. The transverse and shear strengths are found to be strongly correlated, in general, but the transverse flexural strength at LN_2 temperature is very little degraded for long radiation exposures in LN_2 which severely degrade shear strengths, and when this happens the longitudinal flexural strength drops markedly; this suggests a relationship between the longitudinal strength and the shear'strength, a plot of which is shown in Figure 3. There appears to be little, if any, correlation between the longitudinal strength and the transverse strength.

According to Figure 3, the longitudinal strength initially increases gradually as the shear strength is reduced by radiation exposure, but it peaks and then falls off extremely rapidly once the shear strength falls below a value of about 4 ksi. Having the correlation curve of Figure 3, which holds for all

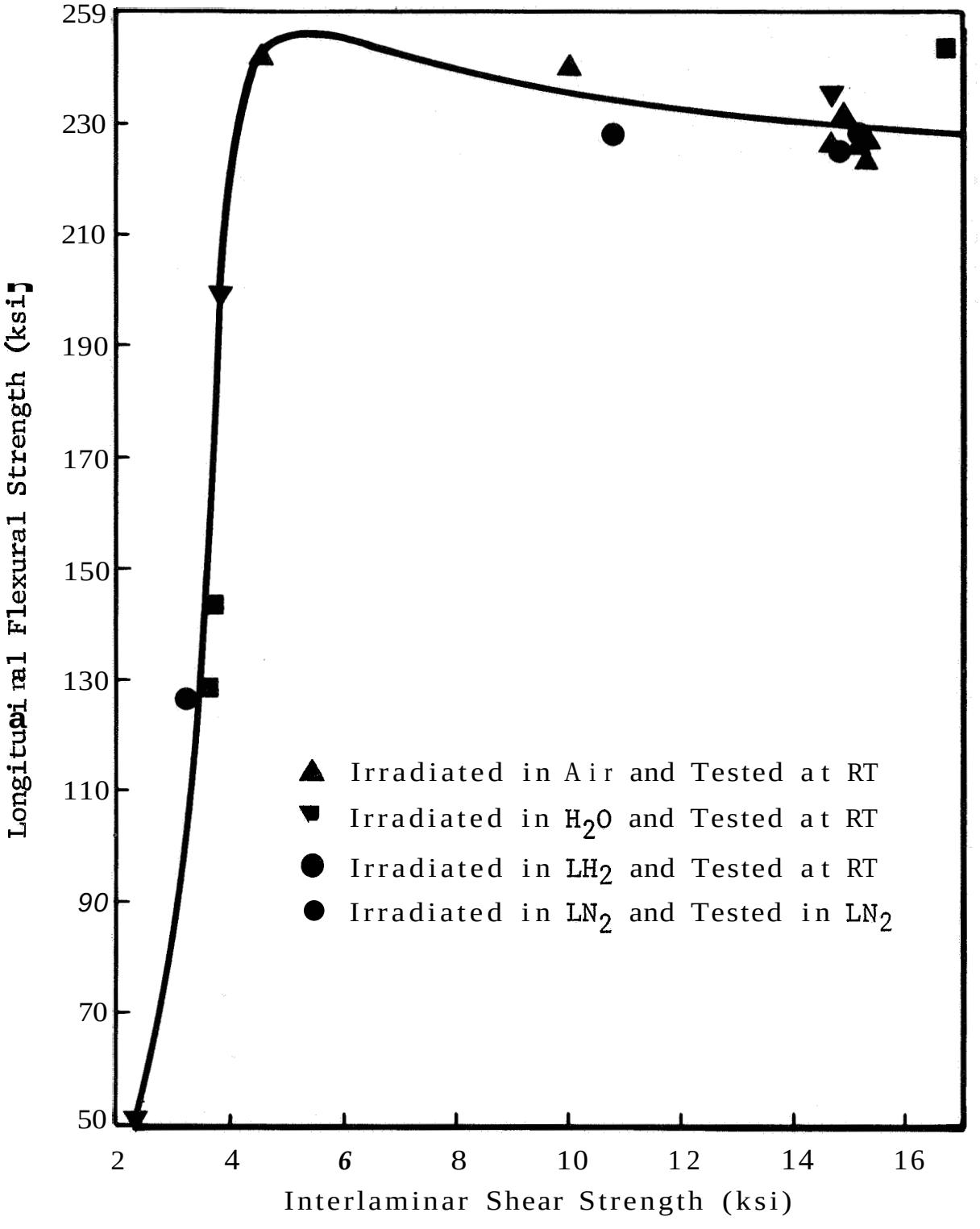

Figure 3 Dependence of the Longitudinal Flexural Strength of Irradiated Boron-Epoxy Composite on its Interlaminar Shear Strength

three specimen groups, the strength curves of Figure 1 are readily understandable. The shear strength falls below 4 ksi for specimens of group 3 at a smaller thermal-neutron fluence than it does for specimens of group 2, and still a higher fluence is required to reduce the shear strength of group-1 specimens below the 4-ksi value. Therefore, the longitudinal strengths of Figure 1 fall off first for specimens of group 3, next for specimens of group 2, and last for specimens of group 1. Figure 3 was used as an aid in drawing the longitudinal-strength curve of Figure 1 for specimens of group 3.

It is interesting to note that the order in which the transverse flexural strengths of Figure 2 fall off for the various specimen groups is exactly the reverse of that for the longitudinal strengths of Figure 1. The transverse strength holds up best for group 3 in which specimens were irradiated and mechanically tested in LN_2 without warmup. Here, the helium atoms introduced into boron filaments by (n,α) reactions are "frozen" within the filaments and cannot diffuse into the matrix of the composite, so that transverse strengths should be less degraded in this case. In the ambient-temperature irradiation of specimens in group 1, helium atoms can more readily diffuse out of the filaments and collect to form gas bubbles in matrix voids, and the transverse strength is most severely degraded for this case. For specimens of group 2, helium atoms are "frozen" within the filaments during the course of the irradiation in LH2 and are then rapidly released when specimens are returned to room temperature for testing; this gives a matrix damage intermediate to the other two conditions. In other words, for the same radiation exposure, the transverse strength decreases for specimen groups which give increasing helium concentrations in the epoxy matrix at the time of testing, and the longitudinal strength decreases for specimen groups which give increasing helium concentrations in the boron filaments.

For most actual structural applications, composites having boron filaments running in all directions would be used, so that the two most important strength properties of unidirectional composites applicable to such multidirectional composites would be (1) the longitudinal flexural strength and (2) the interlaminar shear strength. On the basis of these two strengths, the three conditions of irradiation and testing would be rated according to decreasing severity as follows: (1) irradiation and testing at cryogenic temperature without intermediate warmup, (2) irradiation at cryogenic temperature and testing at RT, and (3)

irradiation at ambient temperature and testing at RT. Boron-epoxy composites in a nuclear-powered spacecraft using a hydrogen propellant, for example, would be most susceptible to radiation damage if irradiated and stressed while in contact with the cryogen, they would be less damaged if irradiated in contact with the cryogen and then slowly raised in temperature before being stressed,* and they would be still less damaged if irradiated and stressed near room temperature.

The curves of Figures 1 and 2 were measured for continuous, constant-flux irradiations in the various environments. If these same radiation exposures were achieved in a series of shorter irradiations in the appropriate environments, as might occur with the restartable NERVA engine, then mechanical properties of boron-epoxy materials would still be expected to roughly follow the degradation curves shown in the figures. Curves 2 and 3 for cryogenic irradiations should hold almost exactly, and curve 1 should be approximately correct if irradiation times are long in comparison to the time required for specimens to reach equilibrium temperatures during irradiation. Different degradation curves would be expected if test environments were changed during cyclic irradiations, of course, for the curves of Figures 1 and 2 are all for a given irradiation environment.

The lowest damage threshold for the most severe irradiation environment on a particular mechanical property should still define lower damage thresholds for cyclic irradiations in different environments, however, for damage thresholds could only be raised by switching to less severe environments (except possibly for specimens warmed after irradiation in LN_2). If composite specimens first irradiated to a thermal fluence of 10^{17} n/cm^2 in LH_2 were allowed to gradually return to RT and were then irradiated

*Boron-epoxy composites irradiated in LN_2 disintegrate explosively when removed from LN_2 and allowed to warm. This does not occur in LH_2, and an explanation for this behavior has not yet been determined with certainty. However, it is believed to be caused by the absorption and decomposition of nitrogen trioxide (NO_3) which is formed from small oxygen impurities (< 20 ppm) in irradiated LN_2. The NO_3 radical probably forms and decomposes through the chemical reactions $NO + O_2 + M \rightarrow NO_3 + M$ and $NO3 + NO_3 \rightarrow 2NO_2 + 02$. The explosive decomposition of absorbed NO3 on warmup may well be initiated by the pressure buildup from trapped helium gas in the composite specimens.

to an additional fluence of 10^{17} n/cm2 at ambient temperature. for example, then the longitudinal strength (at RT) should be roughly twice that for a specimen irradiated to 2 x 10^{17} n/cm^2 in LH2 and mechanically tested without warmup, assuming that the property curves would not differ too much from curve 3 for irradiation and testing in LN_2. Likewise, the interlaminar shear strength should be considerably greater for the two-cycle irradiation, but the transverse strength should be only about one half that of the one-shot irradiation of the same exposure dose. Therefore, change of environments during cyclic irradiation can greatly affect strengths of boron-epoxy composites, and rough estimates of these temperature effects can be determined from Figures 1 and 2.

4.2 Mechanisms of Damage

The boron nucleus has a large cross section for interacting with a low-energy neutron and being "split" into two high-energy charged particles which on escaping from boron filaments are extremely damaging to the epoxy matrix and its bonding with reinforcement filaments. Because of this nuclear interplay between boron atoms and epoxy molecules of a composite, it is not possible to determine reliable radiation-exposure thresholds for strength degradations in a reactor field by considering only the gamma-ray component and its ionizing effects on the more radiation-sensitive epoxy matrix of the composite.

Boron-10 atoms have a cross section of 3840 barns for absorbing neutrons which are in energy equilibrium with atoms of a room-temperature, low-absorbing medium with which the boron atoms have an interface. An alpha particle is emitted when such a "thermal" neutron (0.025 eV) is absorbed and the excited boron atom is transmuted into a lithium-7 ion. The charged particles from this (n,α) reaction will divide an average kinetic energy of 2.34 MeV in inverse proportion to their masses, so that the He^4 and Li^7 ions have average initial kinetic energies of 1.49 MeV and 0.85 MeV, respectively. These energetic charged particles have extremely short ranges in boron filaments ($<10\mu$), but some of the charged particles from reactions which take place near outer surfaces of the 100-μ filaments will escape and cause extensive ionization damage over short ranges into the epoxy matrix of the composite, and the bond strength between filament and matrix would seem to be particularly sensitive to this type of intense localized damage.

In any case, neutral impurity atoms of He^4 and Li^7 initially rest in the near neighborhood of each (n,α) reaction site. The Li atoms probably remain near these sites, but the gaseous He4 atoms, being chemically inert, tend to diffuse out of the boron filaments at elevated temperatures and collect in matrix voids at filament interfaces to form gas bubbles which grow during irradiation (Refs. 8-12). These gas bubbles exert high localized pressures which tend to cause separation of filaments from the matrix. Thus, in summary, some few percent of the high-energy charged particles from (n,α) reactions in boron filaments promptly escape from the filaments and expend their remaining kinetic energies in less than 10 μ of epoxy, where this energy is largely expended in ionizing atoms of epoxy molecules over these short ranges. Of the majority of the particles which are initially stopped in filaments, another several percent of the gaseous-helium atoms slowly diffuse out of the filaments during high-temperature irradiations.

There are, then, two sources of damage from (n,α) reactions at elevated temperatures, but the second of these sources is largely eliminated in cryogenic irradiations where impurity atoms are frozen into place after once coming to rest. This suggests that there might be significant differences in radiation damage of boron-epoxy composites between ambient and cryogenic irradiations, and that the postirradiation temperatures at and prior to strength measurement are likely to be important, as was found to be the case.

The (n,α) cross section for natural boron (19.8% B^{10}) is essentially due entirely to the B^{10} isotope, so that the thermal cross section for the average natural boron atom of filaments is 760 barns. Therefore, the mean free path of a thermal neutron in natural boron is about 100 μ, the diameter of a boron filament, so that virtually every such neutron which strikes a 15-ply composite laminate undergoes reaction. In addition to the damaging effects of reactor gamma rays on the epoxy matrix of a composite reinforced with boron filaments, then, there is also thermal-neutron damage which is sensitive to the temperatures at which the composite specimens are irradiated and mechanically tested. Moreover, this thermal-neutron contribution is quite important in strength degradation, since a great many low-energy neutrons are produced in nuclear reactors and since all such neutrons incident on composites undergoe (n,α) reactions. The (n,α) cross section of natural boron is inversely proportional to the square root of

the neutron energy (going as the reciprocal of velocity) for energies below 165 keV, and does not depart too much from this relationship for energies considerably higher. Therefore, fast neutrons from reactors are not nearly so important a source of radiation damage in boron-epoxy composites as are thermal neutrons.

V. CONCLUSIONS

Strengths of boron-epoxy composites are primarily affected by gamma-ray and thermal-neutron components of reactor radiation. The transverse flexural strength and the interlaminar shear strength are improved by cross-linking of the epoxy matrix for gamma doses below 10^{11} ergs/g(C), provided that the thermal-neutron fluence is below some few 10^{15} n/cm^2. The thermal-neutron fluence begins to dominate radiation effects on strengths above 10^{16} n/cm^2, however, and from there up to fluences of 10^{17} n/cm^2 the transverse strength and the shear strength decrease rapidly, while the longitudinal flexural strength increases somewhat. Finally, the longitudinal strength begins to decrease rapidly somewhere above thermal-neutron fluences of 10^{17} n/cm^2, and the other two strengths continue to fall off.

The more important longitudinal strength is degraded at 10^{17} n/cm^2 only for specimens which are irradiated and tested at cryogenic temperature without warmup; this threshold increases to 2 x 10^{17} n/cm^2 when specimens are irradiated at cryogenic temperature and mechanically tested at room temperature (RT), and it increases to 4 x 10^{17} n/cm^2 when specimens are irradiated at ambient temperature and tested at RT. These damage thresholds correspond roughly to the thermal-neutron fluences which are required to reduce the controlling interlaminar shear strengths of the composites below about 4 ksi for the various temperatures of irradiation and testing. Apparently, then, only a shear strength somewhat in excess of 4 ksi is required to develop the full strength of the boron reinforcement filaments in a composite laminate.

The most important strength properties of unidirectional composites which would be applicable to multidirectional composites used in actual structural applications would be the longitudinal flexural strength and the interlaminar shear strength. These two strength properties appear to be interrelated for all temperature conditions of irradiation and testing, and the more radiation-sensitive shear strength seems to largely determine when the longitudinal strength will be degraded, with the threshold being the 4-ksi shear strength previously mentioned. On the basis of these two unidirectional strengths, the three temperature conditions of irradiation and testing for multidirectional composites would be expected to rate in order of increasing severity as follows: (1) irradiation

at ambient temperature and testing at **RT,** (2) irradiation at cryogenic temperature and testing at **RT,** and **(3)** irradiation and testing at cryogenic temperature without warmup. Flexural strengths of multidirectional composites would be expected to show little degradation below a thermal-neutron fluence of 1×10^{17} n/cm^2, no matter what the temperatures of irradiation and testing, and they might be adequate up to 1×10^{18} n/cm^2 when irradiated at ambient temperature and tested at RT.

REFERENCES

1. ASTM Standards (ASTM, Philadelphia, 1966) Part 27, Designation D790-66, p. 299.

2. ASTM Standards (ASTM, Philadelphia, 1967) Part 26, Designation D2344-65T, p. 499.

3. Ishai, O. and Lavengood, R. E., Composite Materials: Testing and Design, ASTM-STP-460 (ASTM, Philadelphia, 1969), p. 62.

4. Hanna, G. L. and Steingiser, ibid., p. 182.

5. Gatti, A., Mullin, J. V., and Berry, J. M., ibid., p. 573.

6. Tetelman, A. S., ibid., p. 473.

7. Zweben, C., ibid., p. 528.

8. Barnes, R. S., and Redding, G. B., Atomics 9 (1958) 166.

9. Barnes, R. S., and Greenwood, G. W., Progress in Nuclear Energy, Series V, Metallurgy and Fuels, Vol, 3, edited by H. M. Finniston and J. P. Howe (Pergamon Press, New York, 1961) p. 195.

10. Foreman, A. J. E., ibid., p. 897.

11. Willis, A. H., ibid., p. 729.

12. Barnes, R. S., Radiation Damage in Solids, edited by D. S. Billington (Academic Press, New York, 1962) p. 860.

Part V

RADIATION ANALYSIS OF EXPLOSIVE MATERIALS AND BIFUELS FOR RNS APPLICATIONS

FZK-389

By

H. G. CARTER
W. A. GREENHOW

SUMMARY

A study has been made to examine and summarize the results of other experimentors in regard to explosive materials and bifuels which may be considered for RNS applications. The objective of the study was to determine the compatibility of candidate materials with an expected maximum gamma-ray exposure of 2×10^9 ergs/gm(C) and to assess the importance of potential problems that are not encountered in Saturn V applications.

The explosive materials considered are TNT, PETN, RDX, HMX, DATB, and UDMH. The bifuel reducing agents considered for secondary propulsion systems are hydrogen, hydrazine, and monomethylhydrazine. The bifuel oxidizing agents considered are nitrogen tetroxide and oxygen.

In many cases the various reported results on the effects of radiation on explosive materials were found to be ambiguous or mutually inconsistent. Such discrepancies are to be expected in view of the dissimilar radiation sources used in the experiments, the wide range of dose rate levels employed, and the diversity of methods used to analyze such radiation effects characteristics as volume and composition of evolved gas and impact sensitivity changes.

It is possible, nevertheless, to draw some distinct inferences from the available data. In general, it appears that doses on the order of 2×10^9 ergs/gm(C) do not produce catastrophic changes in any of the explosives or bifuels that would normally be considered for such applications. A summary of specific conclusions is given in Section IV.

I. INTRODUCTION

This report contains a radiation effects evaluation of some flight-qualified S-II stage materials and components which may be considered for possible pyrotechnic and auxiliary power applications on a Reusable Nuclear Shuttle (RNS). The objectives of this study were (1) to determine those pyrotechnic materials, propellants and associated components currently contained in the Saturn V which are suitable for use in the RNS environment; (2) to examine and summarize results of radiation effects tests performed by other experimentors regarding candidate explosive materials and bifuels; and (3) to qualitatively assess potential problems and, where possible, establish radiation tolerance limits, i.e., the maximum radiation exposure to which the component or material can be subjected without incurring significant degradation in its material performance characteristics.

This report is directed to the potential problems associated with:

1. Applications regarding explosive or pyrotechnic materials for stage and equipment separation systems.

2. Bifuels and pyrotechnic materials required for the auxiliary propulsion and gas generation systems.

3. The effects of the nuclear environment inherent to RNS missions on non-explosive organic materials used in the ordnance systems of the S-II stage of Saturn V. This investigation supplements the study conducted under Contract NAS8-25848 and reported in FZK-378 (Ref. 1).

For purposes of this analysis, the RNS mission is assumed to be of two-years duration and require ten full-power engine operations of the NERVA (1575 MW) reactor, each of 1-hour duration. The RNS configuration is based on the nuclear flight system definition studies performed by McDonnell Douglas (Ref, 2). The explosive materials and systems contained on the S-II stage of the Saturn V were selected as reference systems for performing analyses on components representative of current liquid-hydrogen fueled vehicles,

II. EFFECTS OF RADIATION ON EXPLOSIVES

The RNS and its supporting chemical boosters will require explosive and pyrotechnic materials for various applications, many of which are common to systems such as those contained on the Saturn V vehicle, and some applications which are unique to the RNS. The types of explosives that might be used and the range of radiation environments to be considered can be illustrated by considering a few of these applications.

Separation of Propellant Tank Stages. The use of explosives as gas generators would be one method of performing this function. In this application, the explosive materials would be exposed to gamma doses as high as 2.5×10^9 ergs/gm(C) at rates as high as 2.5×10^8 ergs/gm(C)-h. Materials considered as possible candidates include DATB, RDX, and PETN. As discussed later, none of these materials have exploded prematurely in irradiation tests, and each of these candidate materials has performed satisfactorily in air at 20°C when subjected to radiation exposures greater than that predicted. Only slight degradations were noted in these tests; however, their response at low temperatures is unknown.

Equipment Separation and Replacement. The periodic replacement of large equipment items such as the auxiliary propulsion system could be achieved by the use of linear shaped charges and explosive bolts. The explosive materials and the supporting mechanical components should be capable of reliable operation to gamma doses of up to 2×10^9 ergs/gm(C).

Space Capsule Separation. The separation of the manned capsule will require the separation of all lines and mechanical connections to the propulsion system followed by operation of a propulsion system to move the capsule away from the reactor. Since the manned capsule will be located forward of the propellant tanks and well away from the engine, the radiation exposure will be relatively low. No radiation effects problems with explosives are to be expected in this application.

The following subsections present a general discussion of the effects of radiation on explosives and give experimental data for several explosives believed to be the most suitable for use on the RNS. An overall summary of the observed radiation

effects is given in Table 1. In a number of cases data appearing in various references are ambiguous or mutually inconsistent. The Table 1 data correspond to the exposures and environments which most closely approximate those expected in RNS applications.

2.1 General Radiation Effects on Explosives

2.1.1 Radiation Induced Ignition

Crystals of lead azide, silver azide, cadmium azide, silver acetylide, and nitrogen iodide have exploded when irradiated with an intense beam of electrons; however, the experimentors have attributed this result to thermal effects (Ref. 3). Nitrogen iodide has also exploded under exposure to alpha particles and fission fragments. This effect is believed to be due to the relatively high linear energy transfer associated with irradiation by these particles. Exposure of TNT, HMX, and blends of RDX and TNT to 90-μsec neutron pulses from the Godiva reactor failed to produce detonation even though the peak flux levels were as high as 1×10^{17} n/cm^2-sec (Ref. 4). This neutron flux is several orders of magnitude higher than the maximum fast-neutron flux anticipated in regions outside of the NERVA.

Radiation induced ignition of explosives might be enhanced at cryogenic temperatures by the possible formation and accumulation of ozone, acetylene, and unstable reaction products. This potential problem is considered later for RDX and generalized conclusions are presented for other materials.

2.1.2 Pressure Buildup of Radiolytic Gases

Nuclear radiation causes the decomposition of organic explosives and the subsequent release of radiolytic gases. In many instances, gases continue to be released after termination of irradiation. Such evolution could result in excessive pressure buildup in containers similar to those employed for storing propellants for the auxiliary propulsion system. It could also interrupt electrical continuity of explosive trains containing encapsulated explosives if the end caps separate from the explosive.

Candidate auxiliary propulsion system oxidizers and propellants, e.g., monomethylhydrazine, nitrogen tetroxide, and UDMH (unsymetrical dimethyl hydrazine) evolve radiolytic gases when

Table 1

RADIATION STABILITY OF PYROTECHNIC MATERIALS
(Irradiated to 2×10^9 ergs/gm(C) in Air at 20°)

Material	Weight Loss (%)	Gas Evolution (ml/gm)	Decomposition Gases (in order of abundance)	Change in Impact Sensitivity	Change in Melting Point (°C)	Remarks
TNT	1	0.04	CO_2, N_2, CO, N_2O, H_2	No change	-3	Explosive power not affected appreciably by 2×10^{10} ergs/gm(C) (Ref. 7).
PETN $C(CH_2ONO_2)_4$	1 (based on 0.2% at 0.5×10^9 ergs/gm(C)	(0.3 at 10^{15} nvt & 0.5×10^9 ergs/gm(C)	CO_2, N_2, N_2O, CO, H_2	(-2% at 10^{16} nvt & 0.5×10^9 ergs/gm(C)	-2	d
RDX	0	3.5	N_2, CO_2, N_2O, CO, NO	+10%	-1	Increases in impact sensitivity up to 60% due to 4.4×10^9 ergs/gm(C) gamma exposure (Ref. 7).
HMX/EXON	0.6	0.3	N_2, CO_2, CO, N_2O	No change	-3	Condensed decomposition products; slightly more stable than TNT or PETN (Ref. 6).
DATB	(0.15% at 2×10^{16} nvt, 2×10^{10} ergs/gm(C))	-	-	-	(-2 at 2×10^{16} nvt & 2×10^{10} ergs/gm(C))	Anomolous decomposition isotherm (Ref. 6).
UDMH	-	4.0	N_2, CH_4	-	-	Non-gaseous decomposition products probably include ammonia.
N_2H_4	-	30	H_2, N_2	-	-	Non-gaseous decomposition products probably include ammonia.

subjected to nuclear radiation, In many instances these gases are insoluble in the liquid phase and cause an increase in pressure (Ref, 5).

The resultant pressure rise can be approximated by

$$P = p_1 \left(\frac{1 - \mu}{\mu} \right) \rho R$$

where
- P = resultant pressure rise in psia
- p_1 = standard pressure = 15 psia
- μ = ullage fraction
- ρ = density of propellant (gm/cm^3)
- R = gas evolution (ml/gm at STP) which is a function of both gamma exposure and time elapsed since cessation of irradiation

The pressure rise is plotted in Figure 1 for UDMH at various gas evolution rates. From data on the pressure rise induced in UDMH at ullage fractions of 20% and 80% (Ref. 5), it is found that the gas evolution due to a gamma dose of 1×10^9 ergs/gm(C) would be approximately 2 ml/gm. Figure 1 shows that the corresponding pressure rise at the predicted maximum exposure of 2×10^9 ergs/gm(C), corresponding to 4 ml/gm, would be approximately 400 psia at an ullage fraction of 10%. Several minor design modifications are available to alleviate this problem:

1. The propellants could be stored in a region of lower radiation intensity.

2. Vent valves could be installed which would periodically be actuated to release gases formed due to decomposition of propellants,

3. The tank structure could be reinforced for the higher pressures.

The pressure rise for the other candidate materials could be sufficiently large to cause structural damage. This problem must be investigated in more depth when materials are selected and the propellant storage systems are designed,

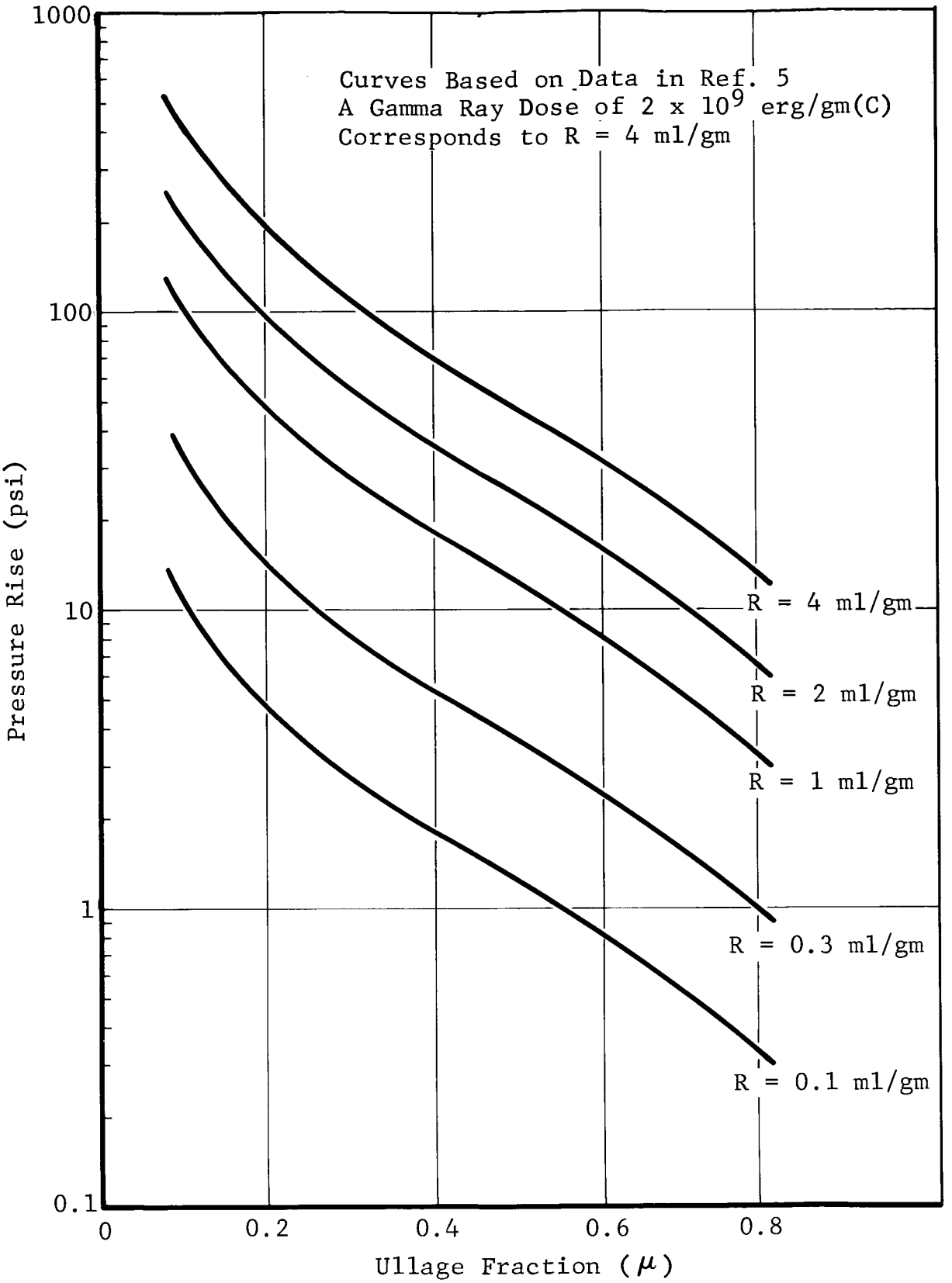

Figure 1 Pressure Rise Due to Off-Gassing of UDMH

2.1.3 Formation of Corrosive Products

Nuclear radiation causes the decomposition of organic explosives resulting in the production of radiolytic gases and other reaction products. In systems such as the auxiliary propulsion system, these gases and reaction products could come into intimate contact with seals, gaskets, and O-rings of Teflon TFE and FEP, Kel-F, Buna N, and Viton A. However, tests performed at 20°C resulted mainly in the formation of gases such as H_2, N_2, N_2O, NO, CO, CO_2, and H_2CO - none of which are corrosive or harmful to organic compounds. Although the radiation-induced evolution of NO_2 is theoretically possible in many cases and this gas and its related products are often corrosive, only the data on the irradiation of PETN suggest that nitrogen dioxide is produced (Ref. 4). Inasmuch as a spot test on irradiated PETN gave a strong indication of NO_2 and/or NO_2^-, this material should be regarded as a possible source of corrosion in materials that are attacked by nitric acid.

2.2 Radiation Effects Test Data

The explosives investigated in this analysis are complex nitrogen-containing organic compounds with an inherent high degree of chemical instability. Considerable experimental work has been performed to investigate the effects of radiation on:

1. Gas evolution, both during and after irradiation
2. Peak pressure during detonation
3. Propagation velocity
4. Impact sensitivity
5. Melting point
6. Auto-ignition temperature
7. Weight loss
8. Explosive power

Most of the experimental data are for explosives irradiated and tested in air at room temperature. Since the RNS environment would be much different, comments regarding the limitations of the data are included in the following discussions.

The Saturn V ordnance system uses PETN and RDX explosive materials. Four additional materials that are representative of explosives that could be used on the RNS - TNT, HMX, DATB, and UDMH - have been included in the study.

2.2.1 TNT

Although 2,4,6 Trinitrotoluene (TNT), which is the most widely used explosive, is relatively radiation resistant and has been irradiated and tested by more experfmentors than any other explosive material, it is doubtful if TNT will be employed for RNS applications due to improved characteristics possessed by other explosives. It is included primarily for purposes of comparison.

TNT has been irradiated to exposures as high as 1×10^{11} ergs/gm(C) at several temperatures ranging between 230% and 344% (Refs. 6 and 7). The volume of gas evolved during irradiation, which, to a certain extent, is an indicator of decomposition, is quite small for TNT when compared to other explosive materials. Gas evolution, which stops when irradiation is terminated, is shown in Figure 2 at three different temperatures. These data illustrate that gas evolution varies directly with temperature, thus implying even greater radiation stability in the RNS environment than the data below indicate.

Although the color of TNT changes considerably and minor changes occur in the elemental composition of TNT as a result of irradiation, it is believed that TNT would be relatively unaffected at the maximum exposure anticipated for components located above the reactor/propellant tank interface, i.e., 2×10^{9} ergs/gm(C). At this exposure, nuclear radiation affects TNT as follows:

Gas volution	0.04 ml/gm at 230% and considerably less at RNS temperatures. Gas evolution stops when irradiation is terminated.
Melting point	approximately $3^{\circ}C$ decrease.
Weight loss	less than 1%.
Impact	sensitivity characteristics relatively unaffected.
Sand-test	relatively unaffected.

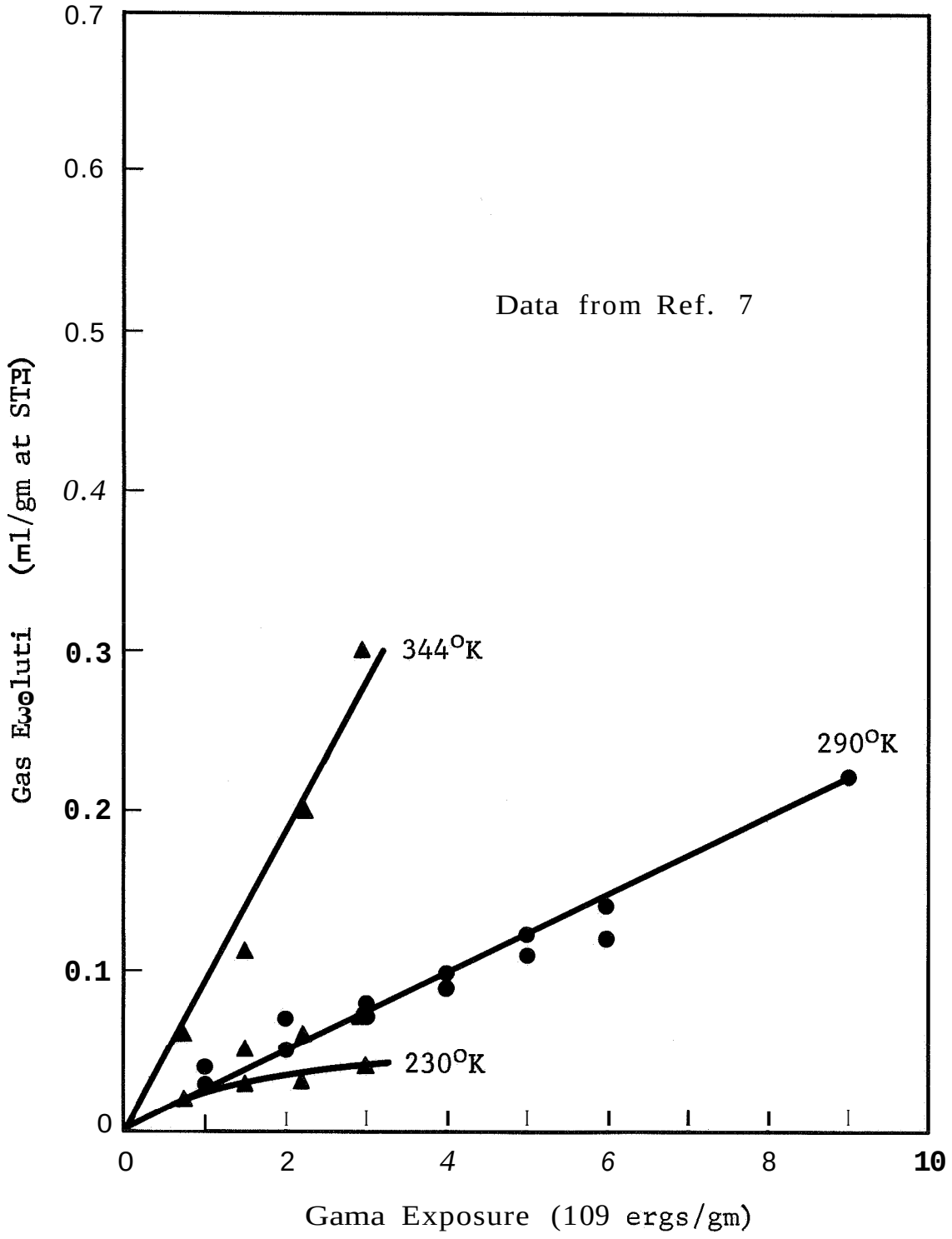

Figure 2 Volume of Gas Evolved by TNT During Irradiation

Radiation effects test experience with TNT is summarized below:

1. TNT irradiated in a pure gamma environment to 1×10^{11} ergs/gm(C) showed a 17°C decrease in melting point and its decomposition, as determined by chromalographic analysis, amounted to approximately 30% (Ref. 6).

2. When irradiated at room temperature to an exposure of 9×10^{9} ergs/gm(C), TNT exhibited a 5°C decrease in melting point and a weight loss of approximately 1%; however, no decomposition products were noted during melt tests (Ref. 6). The decomposition exotherm showed a decrease of about 15°C at this exposure.

3. TNT was exposed to high radiation fluxes (fast-neutron flux = 1×10^{17} n/cm^2-sec and a gamma dose rate of 5×10^{12} ergs/gm(C)-h) during a 90-μsec pulse of the Godiva II reactor. Examination of the sample showed negligible damage, and in particular none of the samples exploded during irradiation (Ref. 4).

4. 'impact sensitivity tests indicated a slight decrease in sensitivity for TNT irradiated at 210°K and a slight increase for that irradiated at 310%. The height of fall required for detonation changed from 150 cm to 160 cm for TNT irradiated to 2.4×10^{10} ergs/gm(C) at 210%; when irradiated to 5×10^{8} ergs/gm(C) at 210° and 310% the impact distances were 166 and 144 cm, respectively (Ref. 4).

5. The explosive power of TNT as measured by its sand crushing ability (the weight of sand crushed by a 200-gm bomb) was relatively unaffected after an exposure of 2×10^{10} ergs/gm(C) (Ref. 7).

6. A decrease in the melting point of 1.2°C after an exposure of 2×10^{10} ergs/gm(C) indicates the presence of about 2 wt% of impurity formed as a result of irradiation.

2.2.2 PETN

Pentaerythritoltetranitrate (PETN) is a high explosive which is employed throughout the Saturn V ordnance system. It is used in safety and arming devices, fuse assemblies, and ordnance tees. It is a candidate for similar RNS applications. PETN is regarded as one of the most stable organic esters of nitric acid and has a high velocity of detonation; however, it is much less stable than TNT, HMX, and **DATB** when evaluated on the basis of radiation induced decomposition and gas evolution. Based on the data presented below, it is believed that the characteristics of PETN, when irradiated to the maximum exposure predicted for regions above the reactor/propellant tank interface, i.e., 2×10^7 ergs/gm(C), will be affected as follows:

Melting point	decrease by approximately 3°C.
Weight loss	approximately 0.4%.
Gas evolution	0.5 ml/gm at 290%; however, the volume of gas evolved by PETN could be considerably less at the RNS temperature.
Impact sensitivity	relatively unaffected.

Radiation effects test experience with PETN is summarized below:

1. The data in Table 2 indicate significant decreases in melting point are experienced by PETN.

2. The decomposition of PETN increases rapidly with exposure as indicated by Table 3. Based on data concerning Pentolite (50/50 mixture of PETN and TNT), off-gassing is believed to continue after termination of irradiation.

3. A chemical analysis of decomposition gases are presented in Table 4, None of these decomposition products are considered corrosive or present any potential hazard to components located adjacent to PETN. However, a spot test of an irradiated sample gave a strong indication of NO_2 and/or NO_2^-, which implies that irradiated PETN may not be compatible with materials that are attacked by nitric acid,

Table 2

MELTING POINT OF IRRADIATED PETN

Gamma Exposure (ergs/gm(C)	Neutron Fluence E > 0.18 MeV (n/cm^2)	Decrease in Melting Point (°C)	Ref.
3×10^9	2×10^{15}	3	6
5×10^9	-	4	7
6×10^9	7×10^{15}	7	6
2×10^{10}	-	10	6
2×10^{10}	2×10^{16}	11	4

Table 3

GAS VOLUME AND WEIGHT LOSS OF IRRADIATED PETN

Gamma Exposure (ergs/gm(C)	Neutron Fluence E > 0.18 MeV (n/cm^2)	Gas Volume Evolved (ml/gm)	Wt. Loss (%)	Ref.
5×10^8	9×10^{13}	0.3	0.2	4
1×10^9	-	0.2	-	8
2×10^9	-	0.5	-	8
3×10^9	-	1.0	-	8
4×10^9	-	2.7	-	7
4×10^9	-	2.4	-	8
2×10^{10}	2×10^{16}	-	10.5	6
2×10^{10}*	5×10^{15}	71.7	13.8	4

*Irradiated at -80°F

Table 4

GAS COMPOSITION OF IRRADIATED PETN

Radiation Exposure	Ref.	Composition (mole percent)						
		$H_2(CH_4)$	N_2	N_2O	NO	CO	CO_2	H_2O
a	4	6	29	3	22	17	0	5
b	4	1	23	19	-	5	53	-

[a] 5×10^8 ergs/gm(C) and 9×10^{13} n/cm^2

[b] 2×10^{10} ergs/gm(C) and 5×10^{15} n/cm^2

4, Impact sensitivity tests performed on PETN indicated a slight decrease in sensitivity after irradiation. The drop-height distance required to initiate detonation increased from 13.0 cm to 13.2 cm after irradiation to 5 x 10^8 ergs/gm(C) and to 13.8 cm after irradiation to *2.4* x 10^{10} ergs/gm(C) (Ref. 4).

5. After an exposure of 2 x 10^{15} n/cm^2 (E > 0.18 MeV) and 3 x 10^9 ergs/gm(C), PETN liberated red fumes indicating NO_2 during the melting point determination (Ref. 6).

6. Microscopic examinations of the sample irradiated to 5.0 x 10^8 ergs/gm(C) and 8.7 x 10^{13} n/cm^2 (E > 2.5 MeV) revealed only minor changes in color or opacity of the crystals, However, for samples irradiated to 2.4 x 10^{10} ergs/gm(C) and 4.8 x 10^{15} n/cm^2 (E > 2.5 MeV) the most prominent changes were the changes in transparency of the crystals. The original crystals were clear except for gross imperfections while the irradiated crystals were white and opaque. Numerous small voids could be seen in the crystals of these materials (Ref. 4).

7. IR spectra run on the *2.4* x 10^{10} ergs/gm(C) and 4.8 x 10^{15} n/cm^2 specimens showed distinct changes after irradiation consisting of increased OH-stretching absorption and new bands in the carbonyl region at 5.75 μ (Ref. 4).

2.2.3 RDX

Cyclotrimethylene trinitramine (RDX) is employed throughout the Saturn V ordnance system in exploding bridge wire (EBW) detonators, linear shaped charges, and destruct assemblies. RDX is considered to be a prime candidate for similar RNS functions. At the maximum exposure predicted in regions above the reactor/propellant tank interface (*2* x 10^9 ergs/gm(C)), it is estimated that RDX will be affected as follows:

Melting point	decrease by approximately $1^{\circ}C$.
Weight loss	approximately 0.7%.
Gas evolution	3.5 ml/gm at $18^{\circ}C$. (Gas evolution should be considerably less in the RNS environment.)
Impact sensitivity	approximately 10% increase in sensitivity.

Radiation effects test experience with RDX is summarized below:

1. Data regarding the effects of radiation on the melting point, weight loss, and gas evolution are presented in Table 5,

2. Various blends of RDX with Kel-F and TNT showed no evidence of any synergistic effect caused by high dose rates (10^{17} n/cm^2 and 5 x 10^{12} ergs/gm(C)-h) during a 90-μsec pulse of the Godiva reactor (Ref. 4).

3. In one set of reported results for $-80^{\circ}F$ and at $+100^{\circ}F$ (Ref. 4), the drop-weight impact sensitivity decreased with increasing radiation, requiring a drop height of 29.4 cm for detonation after an exposure of 2.4 x 10^{10} ergs/gm(C) and 4.8 x 10^{15} n/cm^2 at $-80^{\circ}F$ as compared to a drop height of 22.8 cm for the unirradiated material. However, in other experiments at ambient temperature (Ref. 7), a gamma exposure of 4.4 x 109 ergs/gm(C) caused increases of impact sensitivity which varied from 10 to 60%.

4. RDX evolved relatively large amounts of gas (1.8 ml/gm) during a 44-day irradiation to 4.4 x 10^9 ergs/gm(C); it continued to evolve 1.5 ml/gm during the first 20 days after the irradiation and 1.0 ml/gm during the next 20 days (Ref. 7). In this set of experiments the colorless gas evolved was found to be a mixture of N_2, CO_2, and a small percentage of H_2. Tests for ammonia, nitrogen oxides, oxygen, and carbon monoxide were negative (Ref. 7). In other experiments (Ref. 4), RDX irradiated to 2 x 10^{10} ergs/gm(C) and 10^{16} n/cm^2 was found to evolve N_2O in the amount shown in Table 5.

Table 5

CHARACTERISTICS OF IRRADIATED RDX

Neutron Fluence E >2.9 MeV (n/cm^2)	Gamma Exposure (ergs/gm(C))	Irradiation Temperature (^oC)	Change in Melting Point (^oC)	Weight Loss (%)	Gas Volume Evolved (ml/gm)	Ref.
8.7×10^{13}	5×10^8	38	0	0.2	0.24	4
1.1×10^{14}	5.2×10^8	-62	0	0.1	0.10	4
0	4×10^9	18	-	-	1.8	7
4.8×10^{15}	2.4×10^{10}	-62	0	14.3	69.0	4

		Gas Product	H_2	N_2	N_2O	NO	CO	CO_2	HCHO	H_2O	
1×10^{16}	2.4×10^{10}	Mole %	0.19	54.80	13.45	0.24	2.74	28.54	0.03	-	4

5. The explosive power of RDX as measured by the sand test was unchanged after an exposure of 4.4 x 10^9 ergs/gm(C) (Ref. 7).

6. RDX evolved a very strong odor reminiscent of a hydroxylamine derivative (Ref. 7).

7. A microscopic examination of irradiated RDX showed the same structural changes, viz., numerous small voids, as reported for PETN (Ref. 4).

On the basis of maximum free energy charges, the gamma irradiation of RDX might be expected to promote the net reaction

$$(CH_2)_3\ N_3(NO_2)_3 + \gamma \longrightarrow (2N_2 + CO_2 + H_2O) + (N_2O + 2HCHO)$$

This reaction is consistent with the fact that the observed N_2 yield (Ref. 4) is about twice the CO_2 yield. The product represented by the last term on the right, formaldehyde, tends to form stable polymers and would not show up strongly in the gas analysis. However, the above reaction indicates that N_2O would be evolved to about twice the extent given in Table 5. It is therefore possible that RDX irradiation also leads to net reactions such as

$$(CH_2)_3\ N_3(NO_2)_3 + \gamma \longrightarrow (2N_2 + CO_2 + H_2O) + (2CNOH + H_2O)$$

and

$$(CH_2)_3\ N_3(NO_2)_3 + \gamma \longrightarrow (2N_2 + CO2 + H_2O) + (CNOH + CO + NH_2OH)$$

Cyamelide, CNOH, forms a polymer which is a stable solid at ordinary temperature. The latter reaction would explain the appearance of CO and the indication of hydroxylamine, NH_2OH. The latter compound melts at 34°C, boils at 110°C and explodes at 130°C. It is therefore conceivable that an accumulation of NH_2OH could increase the impact sensitivity of RDX in accord with some of the available data (Ref. 7).

If RDX were irradiated at cryogenic temperature it is conceivable that a number of intermediate reaction products which lead to the above net reactions at normal temperatures could be stabilized. Although these intermediates might include potentially explosive products such as O_3, N_2H_4, and C_2H_2-O_2 mixture, it is doubtful that the concentrations of these would be large enough to effect a large increase in impact sensitivity. In the case of ozone, for example, it is known that the G-value for radiation induced destruction is over twice as large as the G-value for ozone production (see Sec. III).

2.2.4 HMX

Tetranitrooctahydro - 1,3,5,7 - tetrazocine (HMX) is a high explosive which has potential application in detonators and destruct assemblies. At the maximum exposure predicted in regions above the reactor/propellant tank interface, 2×10^9 ergs/gm(C), it is believed that HMX will be affected as follows:

Melting point	decrease by approximately $3^{\circ}C$.
Weight loss	approximately 0.6%.
Gas evolution	0.3 ml/gm at $18^{\circ}C$; however, gas evolution could be considerably less in the RNS environment.
Impact sensitivity	not affected.

Radiation effects test experience wfth HMX and a mixture of HMX/EXON (95%/5%) is summarized below:

1. Data regarding the effects of radiation on the weight loss and gas evolution are presented in Table 6. A decrease in melting point of $9^{\circ}C$ was reported for the irradiation of HMX to 2×10^{10} ergs/gm(C).

2. The impact sensitivity of HMX was not affected when irradiated and tested at 5×10^8 ergs/gm(C) and also at 2.4×10^{10} ergs/gm(C); however, the HMX/EXON (94/6) material exhibited approximately a 15% reduction in detonation sensitivity at the higher exposure.

Table 6

CHARACTERISTICS OF IRRADIATED HMX AND HMX/EXON (94/6)

Material	Gamma Exposure (ergs/gm(C))	Neutron Fluence E >2.5 MeV (n/cm^2)	Irradiation Temperature (°C)	Weight Loss (%)	Gas Volume Evolved (ml/gm)	Ref.
HMX	5×10^8	8.7×10^{13}	60	0.2	-	4
HMX	5×10^8	8.7×10^{13}	-32	0.1	0.02	4
HMX	2×10^{10}	4.8×10^{15}	-32	9.1	9	4
HMX/EXON	5×10^8	8.7×10^{13}	68	0.1	0.35	4
HMX/EXON	5×10^8	8.7×10^{13}	-32	0	0.24	4
HMX/EXON	6×10^9	7.2×10^{15}	18	2	-	6
HMX/EXON	1.7×10^{10}	2×10^{16}	10	10	-	6
HMX/EXON	2×10^{10}	4.8×10^{15}	-32	11.5	71	4

3. HMX was subjected to high radiation rates (fast neutron fluences of 10^{17} n/cm^2 and a gamma dose rate of 5 x 10^{12} ergs/gm(C)-h during a 90-μsec pulse of the Godiva reactor with no evidence of any synergistic effects or radiation induced detonations (Ref. 4).

4. Based upon chemical analyses, etc., Ribaudo et al. concluded that HMX/EXON is slightly more stable to reactor irradiation than TNT or PETN (Ref. 6).

2.2.5 DATB

Diaminotrinitrobenzene (DATB), based upon a few irradiation experiments performed to date (Ref. 6), is the most radiation resistant explosive and has a high potential for RNS applications. At the maximum exposure predicted in regions above the reactor/propellant tank interface, 2 x 10^9 ergs/gm(C), radiation should not measurably affect the physical or chemical properties of DATB.

Radiation effects test experience with DATB is as follows:

1. After an exposure of 2 x 10^{10} ergs/gm(C) and 2.0 x 10^{16} n/cm^2 (E >0.18 MeV), the weight loss was about 0.2%, the melting point decreased by 2°C, and there was some evidence of decomposition; at 9 x 10^{10} ergs/gm(C) and 1 x 10^{17} n/cm^2 (E >0.18 MeV), the weight loss was 0.7% and the melting point decreased by about 4°C.

2. Infrared spectra for irradiated DATB samples show no evidence of decomposition and x-ray diffraction data do not indicate any solid decomposition products.

2.2.6 UDMH

Unsymmetrical dimethylhydrazine, $NH_2N(CH_3)_2$, has been irradiated to a dose of 1 x 10^9 ergs/gm(C) (Ref. 5). The composition of the propellant was not significantly affected by this exposure, although H_2, N_2, and CH_4 gases were evolved. On the basis of pressure rise, it is estimated that the total gas evolution for this exposure was 2.0 ml/gm.

III. EFFECTS OF RADIATION ON BIFUELS

The RNS system will require an auxiliary propulsion system for: (1) vehicle attitude control during powered flight in the roll axis, (2) vehicle attitude control in the pitch yaw and roll axes during coast periods, and (3) thrust to settle main stage propellants both before and after each main engine operation.

Conceptual designs for the APS include an APS similar to that presently employed for the S-IVB stage of the Saturn V vehicle, i.e., two modules located 180 degrees apart on the aft end of the vehicle, each containing four hypergolic engines, three 150-lb thrust attitude engines, and one 70-lb thrust ullage engine. Each APS module contains its own propellant supply and pressurization system. The hypergolic propellants used by the engines are monomethylhydrazine (MMH) for the fuel and nitrogen tetroxide (N_2O_4) for the oxidizer. Helium is the pressurant used in the system.

The Saturn V gas generation system, which is a hypergolic fueled engine, produces gases for starting the turbopumps as well as pressurizing the hydraulic system reservoir and valve/seal system. A similar system could be employed in the RNS for pressurizing the hydraulic and pneumatic systems as well as being a backup system for pressurizing the LH_2 tanks if the boil-off rate is less than required,

A radiation hardening analysis for all radiation sensitive materials, components, and systems which might be employed in such RNS applications - excluding the propellants and solid motors - is presented in Reference 1. The effects of radiation on some bifuels that might be used for auxiliary power are discussed below.

Of bifuels that have been considered for secondary propulsion applications, the gaseous O_2/H_2 combination has received the most attention in regard to application on the nuclear stage. The advantages of this system are reasonable performance, absence of ignition problems, and a well-developed Apollo-based technology. However, the preferred method of storage of these components, viz., supercritical storage, requires superinsulated

storage tanks and a series of heat exchangers, and gas generators to maintain tank pressure during the mission. It is therefore conceivable that another combination of oxidizing and reducing agents might be used, e.g., nitrogen tetroxide and monomethyl-hydrazine, or nitrogen tetroxide and hydrazine.

The combinations of oxidizing and reducing agents cited above could be stored separately and employed as true bifuels, or they could be stored in combination as hypergolic monofuels, Unfortunately, no irradiation data are available for hypergolic mixtures of oxidizing and reducing agents. It is quite possible that the effects of radiation on such mixtures could include spontaneous detonation. Since nitric oxide (NO) is probably a decomposition product in the irradiation of N_2O_4 and since even as stable a compound as ammonia burns easily in the presence of NO (Ref, 9), it is reasonable to expect that the ignition temperature of a N_2O_4/hydrazine mixture might be drastically lowered by irradiation, especially if NH and NH_2 radicals were produced in addition to NO.

In the following discussion, the effects of radiation on pure oxidizing and pure reducing agents are considered separately. Reducing agents are discussed first.

3.1 Reducing Agents

3.1.1 Hydrogen

The irradiation of hydrogen produces radicals such as H_2^+ and H which recombine rapidly to form H_2 molecules, Although some evidence exists for a relatively long-lived H_3 state in irradiated liquid hydrogen (Ref. 10), there is no direct experimental evidence that the energy stored in this way is significant. It is possible that species such as H or HB could carry over to an O_2/H_2 mixture and thereby lower the ignition temperature by accelerating the production of HO_2 radicals, which process determines the ignition point, but such an effect would not constitute a problem.

3,1.2 Hydrazine

The radiation induced decomposition of solid hydrazine at liquid nitrogen temperature has been investigated using 20-keV electrons and ions of undetermined energy (Ref. 11). A stepwise

evolution of H_2, N_2, and NH_2 was noted during warmup of the irradiated samples, the appearance temperatures being 113% for H_2 and N_2 and 146°K for NH_2. The results indicated the presence of triazene which decomposed according to

$$H_2\text{-}N\text{-}N = N\text{-}H \longrightarrow NH_3 + N_2$$

Irradiation of liquid hydrazine to 1×10^9 ergs/gm(C) with Co^{60} gamma rays (Ref. 5) resulted in the evolution of N_2 and H_2 gases. On the basis of the observed pressure rises it is inferred that the total gas evolution was about 1.5 ml/gm. According to these results, there is no reason to expect that the irradiation of N_2H_4 to 2×10^9 ergs/gm(C) or less will have detrimental effects on its use as a reducing agent.

3.1.3 Monomethylhydrazine

No data are available on the effects of radiation on monomethylhydrazine. This compound. NH_3NHCH_3, is expected to be slightly less stable than the dimethyl compound UDMH (see Sec. 2.2.6), viz., H2, N_2 and CH_4. As in the case of UDMH, no significant degradation of monomethylhydrazine is expected for doses of 2×10^9 ergs/gm(C) or less.

Only two oxidizing agents are expected to be considered for use with the above reducing agents. These are nitrogen tetroxide and liquid oxygen.

3.2 Oxidizing Agents

3.2.1 Nitrogen Tetroxide

Nitrogen tetroxide is the dimer of NO_2 to which it partly dissociates in the gas phase. Fission fragment irradiations of the monomer have revealed (Ref. 12) an unusual mode of decomposition, namely, that the G-value for NO_2 destruction varies from G = 0.5 molecules per 100 eV at a dose of 5×10^9 ergs/gm(C) to G = 1.2 molecules per 100 eV at a dose of 3×10^{11} ergs/gm(C). The explanation of this effect is that after long exposures the NO_2 starts to be "autocatalytically" decomposed by the radiation induced secondary decomposition of its products. The assumed reactions axe:

$$NO_2 + E \rightarrow NO_2^+ + e^-$$

$$NO_2^+ + e^- \rightarrow NO + O$$

$$NO_2^+ + e^- \rightarrow N + 2O$$

$$N + N + M \rightarrow N_2 + M$$

$$N_2 + E \rightarrow 2N$$

$$NO_2 + N \rightarrow 2NO$$

$$NO_2 + N \rightarrow N_2O + O$$

The radiation products are therefore NO, N_2, O_2 and N_2O. These last three products were also evolved from neutron irradiated NO_2 (Ref. 13) in the proportions $N_2:O_2:N_2O = 1:1:2$.

Irradiation of N_2O_4 in the liquid phase to a dose of 1×10^9 ergs/gm(C) (Co^{60} gamma rays) resulted in the evolution of NO and N_2O gases with only slight decomposition of the sample (Ref. 5). But in another irradiation of N_2O_4 by gamma rays, the evolved products were found to be N_2 and N_2O in the proportions $N_2:N_2O = 2:1$ (Ref. 14). The G-value for N_2O_4 destruction in the latter experiments was found to be only $G = 0.075$ molecules/100 eV. On the basis of this G-value, it is found that the destruction of N_2O_4 due to a gamma ray dose of 2×10^9 ergs/gm(C) would only amount to about 0.01%.

3.2.2 Liquid Oxygen

The exposure of liquid oxygen and LO_2-LN_2 mixtures to ionizing radiation has long been known to produce ozone. The molecular yields of O_3 produced by the irradiation of liquid oxygen have been investigated by Brown and Wall (Ref. 15), who found that the O_3 yield for Co^{60} gama rays is about $G_p = 6$ molecules per 100 eV. They also determined that radiation destroys ozone molecules with a G value of $G_D = 26$ molecules per 100 eV deposited in the ozone fraction of an LO_2-LO_3 solution. From these results it can be shown that the ozone concentration in liquid oxygen after an irradiation time t is

$$n = \frac{\rho G_p}{48 G_D} \left[1 - \exp\left(-4.8 \times 10^{-13} G_D \dot{E} t\right)\right]$$

where

n = number of moles of ozone per cm^3

ρ = density of LO_2 (gm/cm^3)

$\dot{E}$ = dose rate (ergs/gm(C)-h)

From the above values it is found that the limiting ozone concentration for any dose rate level is

$$n_\infty = \frac{\rho G_p}{48\, G_D} = 0.00442 \text{ moles/cm}^2$$

This value represents an ozone fraction of about 14% in the LO_2-LO_3 solution. Actually the solution would separate into a two-phase liquid at an ozone level of about 12%, thereby forming a highly explosive ozone-rich phase (Ref. 16).

However, for a maximum dose of only $\dot{E}t = 2 \times 10^9$ ergs/gm(C) the time dependent equation shows that $n = 1.1 \times 10^{-4}$, corresponding to an ozone fraction of only 0.35%. Since this value is well below the explosive limit for ozone-oxygen mixtures, it can be concluded that use of liquid oxygen as one component of a bifuel cannot lead to an ozone explosion in RNS applications.

IV. CONCLUSIONS

It is concluded that for the 2 x 10^9 ergs/gm(C) maximum dose expected in RNS applications:

1. None of the explosive or pyrotechnic materials considered for RNS applications will explode.

2. None of the materials considered will undergo an appreciable reduction in impact sensitivity or explosive power (the impact sensitivity of RDX may increase by about 10%).

3. All of the materials considered can be expected to evolve stable gases at levels ranging from 0.04 ml/gm for TNT to 4 ml/gm for UDMH; adequate allowance for possible pressure rises accompanying such evolution must be made by the installation of vents or by reinforcing the tank structures.

4. Corrosive radiation products are expected only in the case of PETN; irradiated PETN may be incompatible with materials that are attacked by nitric acid.

In regard to the effects of a 2 x 10^9 ergs/gm(C) dose on the oxidizing and reducing agents which may be considered for bifuels, it is concluded that:

5. None of the candidate materials will be degraded significantly.

6. In the case of liquid oxygen, a potentially explosive compound, namely ozone, will be produced, but the ozone/oxygen ratio will be well below that corresponding to separation into two liquid phases and no explosion can occur.

APPENDIX A

RADIATION EFFECTS ANALYSIS OF NON-EXPLOSIVE MATERIALS IN SATURN V ORDNANCE SYSTEMS

Components and systems of the S-II stage of the Saturn V vehicle which contain pyrotechnic materials were selected as reference systems for analysis since they are representative of systems envisioned for liquid hydrogen fueled vehicles. The purpose of this analysis was to determine those components which can be used as designed, or present the modifications necessary to radiation harden them for analogous RNS applications.

Ordnance systems that are used on the S-II stage of the Saturn V have been identified and analyzed to determine the effects of radiation on the non-explosive constitutents of these components.

A.1 Radiation Hardening Procedures

The analysis of the non-explosive radiation sensitive materials is basically an extension of work previously reported in Reference 1, which analyzed the effects of radiation on mechanical components of the S-II and S-IVB stages of Saturn V. The radiation hardening procedures employed, which are the same as those described in Reference 1, are summarized below:

1. S-II stage assembly drawing V7-000002-2691 was examined. All components and systems containing explosive materials were identified and selected for detailed investigation.

2. The radiation-sensitive materials contained in each selected system and their applications were identified.

3. Each of the materials identified in step 2 (except the explosives) had previously been investigated (Ref. 1). The recommended radiation tolerance limits (Table A-1), i.e., the maximum radiation exposure to which the material, when employed in a particular application, can be exposed without incurring significant degradation in its physical or mechanical properties are identical with those determined in Reference 1.

Table A-1

RECOMMENDED RADIATION TOLERANCES FOR ORGANIC MATERIALS IN S-II ORDNANCE SYSTEMS

Material	Application	Recom. Tolerance (ergs/gm(C))
Diallyl Phthalate	Insulation, electrical	2×10^{10}
Epoxy	Adhesive	1×10^{10}
	Potting	2×10^{10}
Mylar	Insulation, electrical	1×10^{10}
Nylon	Fabric, tape	3×10^{9}
Polysulfide Rubber	Adhesive	5×10^{9}
Polyurethane	Insulation	1×10^{10}
Polyolefin, Irradiated	Tubing	3×10^{9}
Polyvinylchloride	Sleeving	4×10^{9}
Silicone Rubber	O-ring	8×10^{8}
	Insulation, electrical	1×10^{9}
	Spacer, tubing, potting, molding	2×10^{9}
	Adhesive	1×10^{10}
Teflon TFE	Backing strip	5×10^{7}
	Insulation, electrical	1×10^{8}
	Washer	1×10^{8}

4. Each component or subsystem analyzed was examined with respect to its relative placement if it were utilized on the RNS. The predicted nuclear environment of each Saturn V component and system was determined by superimposing the assumed locations of each component onto the predicted RNS radiation flux profile shown in Figure A-1.

5. The recommended limit for each component was established by the lowest recommended radiation tolerance of material applications critical to flight safety or the functional performance of the specific component.

6. The recommended tolerance for each component was then compared to the predicted nuclear environment. If the tolerance exceeded the predicted environment by a factor of ten or more, it was considered suitable for the application under investigation and no additional analysis was performed. If the recommended tolerance was at least as great as the predicted environment but exceeded it by less than a factor of 10, a radiation hardening procedure was considered desirable. Radiation hardening was considered mandatory for all critical applications if the recommended tolerance did not meet the predicted environment. Modifications were recommended for both critical and non-critical applications; however, the assigned classification for non-critical applications is denoted "non-critical."

The assumptions used in this analysis result in what is probably a worst-case since the maximum radiation levels (unattenuated) for 10 hours of engine operation were used, and the recommended radiation tolerances for each material application were chosen to be conservative.

The analysis is assumed to be unaffected by the time sequence in which the total dose is applied. The effects of shorter operating times or different reactor power levels can be evaluated simply by scaling down the given doses. This, of course, ignores the possibility of more serious adverse effects resulting from periodic engine operation spread over a period of, say, three years. It can be presumed that material degradation resulting from other environmental or operational factors

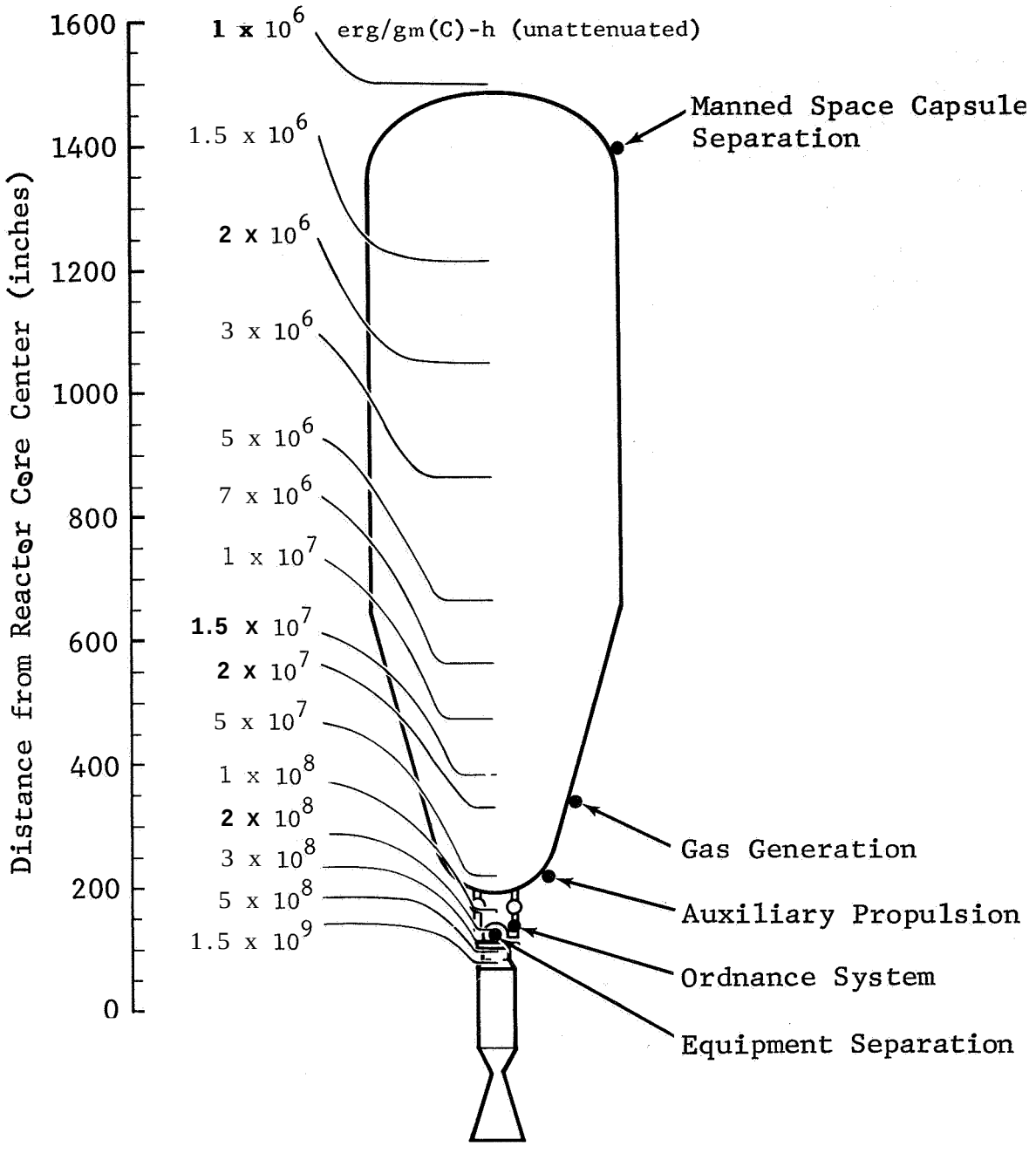

Figure A-1 **Assumed Location of Systems Containing Explosive Materials**

would act in addition to the radiation, but the consequences of cyclic operation are largely unexplored, However, radiation induced changes in organic materials are irreversible and annealing does not occur, so in this respect the assumption of accumulation of dose is valid. Also, vacuum and cryotemperature alter (usually favorably) the radiation response of some organic materials.

Radiation hardening was accomplished primarily through material substitution, i.e., replacing the radiation sensitive materials which have low recommended tolerances with radiation stable materials have mechanical properties thought to be compatible with the requirements of the particular application; however, it is recognized that redesigning a component with new materials to have the same operating characteristics and size envelope as originally designed may not be easy. Material processing techniques, which may have been the criteria employed in the original material section, might prevent usage of materials selected on the basis of radiation stability. Engineering judgment was the basis for recommended material substitutions; however, the component or material might be required to satisfy a unique design or system requirement, Therefore, component designers, familiar with all design aspects, must examine the recommended design modifications and in some instances must select alternate materials.

A.2 Radiation Environment

The nuclear radiation environment employed in this analysis, Figure A-1, is from Reference 1. It was based upon an extrapolation of data for the 1575-MW NERVA-I full-flow engine (Ref. 17) assuming a total of 10 hours of full-power engine operation. The radiation flux data are unattenuated (by fuel or structure), thus providing additional conservatism in the analysis,

A.3 S-V Ordnance System Components

Table A-2 lists the radiation sensitive components contained in the S-II stage ordnance system. The recommended radiation tolerance limits for all material applications (except explosive materials) are based upon limits established in Reference 1. These ancillary materials and components can be radiation hardened by the modifications recommended in Table A-3 such that reliable performance of these non-explosive materials and components can be expected at gamma exposures up to 1×10^{10} ergs/gm(C).

TABLE A-2

RADIATION SENSITIVE COMPONENTS - S-II ORDNANCE SYSTEM

Part Number	Subsystem	Component	Material	Critical Application	Gamma Environment (ergs/gm(C))		Specification or Vendor
					Predicted	Tolerance	
V7-540676	Detonator, Separation Sys - First Plane		--	yes	2.5×10^9	$2 \times 10^{9*}$	
DAC7865742-501		Detonator-EBN	--	yes		$2 \times 10^{9*}$	P/N 513014; Aerojet General Corp.
--		Potting	Silicone Rubber	yes		2×10^9	P/N RTV-11; General Electric
515466-1		Detonator Assy	--	yes		$1 \times 10^{10*}$	
--		Adhesive	Epoxy Base	no		1×10^{10}	MMM-A-132; Type I
--		Explosive	RDX	yes		See Sec.II	MIL-R-00398; Type B (0.162 grains)
515684		Body	--	yes		2×10^{10}	
--		Insulator, Elec.	Diallyl Phthalate	yes	2.5×10^9	2×10^{10}	MIL-M-14
V7-540677	Detonator, Separation Sys - Second Plane (Same as V7540676)			yes	2.5×10^9	$2 \times 10^{9*}$	
V7-540174-11	Detonator, Propellant Dispersion		--	yes	2.5×10^9	$1 \times 10^{8*}$	
DAC786542-501		Detonator (Same as V7540676)	--	yes		$2 \times 10^{9*}$	
1B33735-503		Safety & Arming Device	--	yes		$1 \times 10^{8*}$	
--		Explosive	PETN	yes		See Sec.II	MIL-P-387A (5 grains)
1P20001		Adhesive	Epoxy	no		1×10^{10}	1P20001; Type 2
--		Adhesive	Polysulfide Rubber	no		5×10^9	MIL-S-8802; Class B2
1B66895-1		Washer	Teflon TFE	no		1×10^8	
1A22201-1		Wire Instl.	--	yes		1×10^8	
78		Wire, Elec	Teflon TFE	yes		3×10^9	MSFC-276
--		Tubing	Irradiated Polyolefin	no		3×10^9	MIL-T-713
--		Tape	Waxed Nylon	no		$1 \times 10^{8*}$	
1A02322-1		Rotor Assy	--	yes		$1 \times 10^{8*}$	
1A00913		Explosive Assy	--	yes		See Sec.II	MIL-P-387; Class 4
1A00913-3		Explosive	PETN	yes		1×10^{10}	MIL-A-14042
--		Adhesive	Epoxy	yes		1×10^8	
1A02398-1		Solenoid Assy	--	yes		1×10^8	P/N 126002-001; LEDEX Inc.
1A35497-1		Solenoid	--	yes		1×10^8	
--		Insulation	Teflon TFE	yes		1×10^8	MIL-S-6743
MS24547-1		Switch	--	yes		8×10^8	
		Insulation	Teflon TFE	yes		8×10^8	P/N PT02H14-19P; Bendix Corp.
PT02H14-19P		Connector	--	yes	2.5×10^9	1×10^8	
--		O-Ring	Silicone Rubber	no	2.5×10^9	N/R	
V7-540672-21	EBW Firing Unit Instl.			yes		1×10^8	P/N 41503-P; General Lab. Assoc.
40M39515-123		Firing Unit	--	yes		1×10^8	
40M02852		Pulse Sensor	--	yes		2×10^{10}	P/N 224L-1-201; Bourns
224L-1-201		Potentiometer	Diallyl Phthalate	yes		8×10^8	
16552		Insulation	Silicone Rubber	no		3×10^9	
34732		O-Ring	Nylon	no		1×10^8	
16518		Cover	Teflon TFE Insul.	yes		2×10^9	P/N RH-5; Dale Electronics Co.
--		Wire, Elec.	--	yes		2×10^9	
RH-5		Resistor	Silicone Rubber	yes		1×10^{10}	
--		Molding	Mylar	yes		2×10^{10}	P/N Scotch Cast 2651; Emerson & Cuming
40M03344		Insulator, Electrical	Epoxy Base	no		1×10^8	MIL-W-16878/1
--		Potting	Teflon TFE	yes		4×10^9	MIL-I-7444B; Type I
--		Wire, Electrical	polyvinylchloride	no		8×10^8	P/N PT107A-12-8P; Bendix Corp.
--		Sleeving	--	yes		8×10^8	
PT107A-12-8P		Connector	Silicone Rubber	no		8×10^8	P/N 1042212; Bendix Corp.
--		O-Ring	--	yes		8×10^8	
1042212-3P		Connector	Silicone Rubber	no	2.5×10^9	8×10^8	
--		O-Ring					

TABLE A-2

RADIATION SENSITIVE COMPONENTS - S-II ORDNANCE SYSTEM (Cont'd)

Part Number	Subsystem	Component	Material	Critical Application	Gamma Environment (ergs/gm(C))		Specification or Vendor
					Predicted	Tolerance	
V7-540691-21 Ordnance, Separation Sys.			--	yes	2.5x10	5x10	
V7-540381		Spacer	Silicone Rubber	no		$2x10^9$	
V7-540666-X		Spacer	Silicone Rubber	no		$2x10^9$	
MD364-0004-0001		Insulator	Mylar	yes		$1x10^{10}$	
ME901-0019-0013		LSC Assy	--	yes		$5x10^{7}$*	
--		Backing Strip	Teflon TFE	yes		$5x10^7$	
--		Explosive	RDX	yes	$2.5x10^9$	See Sec.II	MIL-R-398
V7-540681-51 Ordnance, Propellant Dispersion			--	yes	$2.5x10^9$	$1x10^{9}$*	
MS35490-XX		Grommet	Synthetic Rubber	no		$1x10^9$	
ME901-0061-0001		Destruct Assy	--	yes			
--		Explosive	RDX	yes		See Sec.II	MIL-R-398
ME901-0060-0001		Destruct Assy	--	yes		$3x10^{9}$*	
--		Explosive	RDX	yes		See Sec.II	MIL-R-398
--		Fabric, Insulation	Nylon	yes		$3x10^9$	
--		Adhesive	Silicone Rubber	no		$1x10^{10}$	V7-53045
ME901-0052-XXXX		Fuse Assy	--	yes		$1x10^{9}$*	
--		Explosive	PETN	yes		See Sec.II	MIL-P-387A
--		Bonding-Adhesive	Silicone Rubber	yes		$1x10^{10}$	MB 0130-019C
--		Tubing	Silicone Rubber	no		$2x10^9$	RB 0120-006
--		Insulation	Silicone Rubber	yes		$1x10^9$	
ME901-0051-XXXX		Ordnance TEE		yes			
		Explosive	PETN	yes		See Sec.II	
MD364-0003-0001		Insulator	Polyurethane	yes	$2.5x10^9$	$1x10^{10}$	MB 0130-069
V7-540351 Detonator, Ullage Ignition Sys.			--	yes	$2.5x10^9$	N/R	
V7-540361 Ordnance, Ullage Ignition Sys.			--	yes	$2.5x10^9$	N/R	

N/R Vendor drawings were not available for review
* Tolerance might be limited by explosive materials. See Section II

Table A-3

RECOMMENDED RADIATION HARDENING PROCEDURES FOR S-II ORDNANCE SYSTEMS

Subsystem	Part No.	Application	Assigned Category of Modification	As Designed		Modified	
				Material	Tolerance (ergs/gm(C))	Recommended Material	Tolerance (ergs/gm(C))
Detonator - First Plane	V7-540676						
	-	Potting	Critical	Silicone Rubber	2×10^{9}	Epoxy	2×10^{10}
Detonator	V7-540174-11						
	1B66895-1	Washer	Not critical	Teflon TFE	1×10^{8}	Silicone/glass	2×10^{11}
	1P20001	Adhesive	Not critical	Polysulfide rubber	5×10^{9}	Epoxy	1×10^{10}
	-	Wire insulation	Critical	Teflon TFE	1×10^{8}	Polyimide	1×10^{10}
	-	Tubing	Not critical	Irradiated polyolefin	3×10^{9}	Kynar	3×10^{10}
	-	Tape	Not critical	Waxed nylon	9×10^{9}	Silicone/glass	2×10^{11}
	-	O-ring	Not critical	Silicone rubber	8×10^{8}	Kynar	3×10^{10}
EBW Firing Unit	V7-540672-21						
	34732	O-ring	Not critical	Silicone rubber	8×10^{8}	Kynar	3×10^{10}
	16518	Cover	Not critical	Nylon	3×10^{8}	Silicone/glass	2×10^{11}
	-	Wire insulation	Critical	Teflon TFE	1×10^{8}	Polyimide	1×10^{10}
	-	Molding	Desired	Silicone rubber	2×10^{9}	Silicone/glass	2×10^{11}
	-	Sleeving	Not critical	Polyvinyl chloride	4×10^{9}	Kynar	3×10^{10}
Ordnance Separation	V7-540691-21						
	V7-540381	Spacer	Not critical	Silicone rubber	2×10^{9}	Silicone/glass	2×10^{11}
	-	Backing strip	Critical	Teflon TFE	5×10^{7}	Mylar	1×10^{10}
Ordnance System	V7-540681-51						
	MS 35490	Grommet	Not critical	Synthetic rubber	1×10^{9}	Kynar	3×10^{10}
	-	Fabric	Desired	Nylon	3×10^{9}	Fiberglass/epoxy	3×10^{10}
	-	Tubing	Not critical	Silicone rubber	2×10^{9}	Kynar	3×10^{10}
	-	Insulation	Critical	Silicone rubber	1×10^{9}	Polyimide	1×10^{10}

REFERENCES

1. Greenhow, W. A., Lewis, J. H., Evaluation of Insulation Materials and Composites for Use in a Nuclear Radiation Environment, Radiation Analysis of Saturn V Materials, Systems, and Components, General Dynamics, Convair Aerospace Division Report FZK-378, June 1971.

2. Nuclear Flight System Definition Study Final Report, McDonnell Douglas Astronautics Co. Report MDC-C0585, May 1970.

3. Bowden, F. P., "The Initiation of Explosion by Neutrons, Alpha Particles, and Fission Products," Proc. Royal Society, A246, 1958, p. 216.

4. Urizar, M. J., et al., "The Effects of Nuclear Radiation on Organic Explosives," Exposiostoffe No. 3, 1962, p. 55.

5. Gray, D., et al,, Rockets in Space Environment, Phase II - Individual Component Investigation, Aerojet-General Report AGC-2263, 1962.

6. Rebaudo, C., et al., The Effects of Reactor Irradiation on the Chemical Characteristics of Solid Explosives, Picatinny Arsenal Report TR 3893, 1970.

7. Rosenwasser, H., Effects of Gamma Radiation on Explosives, USAEC Report ORNL 1720, 1955.

8. Kaufman, J. B. R., "The Effects of Nuclear Radiation on Explosives," Proc. Royal Soe., A248, 1958, p. '219.

9. Wolfhard, H. G., and Strasser, A., J. Chem. Phys. 28 (1958) 172.

10. Carter, H. G., and Bullock, R. E., NERVA Hydrogen Conversion Problems, General Dynamics Fort Worth Division Report FZK 351-5, 9 June 1970.

11. Papazian, H. A., J. Phys. Chem. 65 (1961) 53.

12. Harteck, P., and Dondes, S., J. Chem. Phys. 27 (1957) 546.

13. Harteck, P., and Dondes, S., J. Chem. Phys. 27 (1957) 953.

14. Schrader, R., et al., Z. Chem. 4 (3) (1964) 108.

15. Brown, D. W., and Wall, L. A., J. Phys. Chem. 65 (1961) 915.

16. Cook, G. A., et al., Industrial and Engineering Chemistry 48 (1956) 736.

17. NERVA Reference Data (Full-Flow Engine), Aerojet Nuclear Systems Company Report SBO-CP-090290-F1-Prel, April 1970.

Part VI

TEST OF THERMAL INSULATION

FZK-391

By

R. D. CRABTREE
P. R. CHEEVER
E. E. KERLIN

FOREWORD

The test described in this report is a part of the technology studies conducted at the Nuclear Aerospace Research Facility in support of nuclear rocket development. The test article, a polyurethane foam insulated tank (5400-gal RIFT-model tank) had originally been prepared by MSFC for an irradiation test with liquid hydrogen. However, subsequent events precluded the use of the Aerospace Systems Test Reactor for performing the irradiation. Therefore, the various materials and devices, other than the foam insulation, which had been scheduled as an integral part of the RIFT tank test were irradiated by means of the Ground Test Reactor. The objectives of these tests were met and are reported in General Dynamics reports **FZK-372** (pressure transducers), **FZK-386** (liquid-level sensors and fission thermopiles), and **FZK-387** (valve-seal materials).

The foam thermal insulating material, CPR **285-2,** had been irradiated and tested previously on a smaller liquid hydrogen tank, and although the larger RIFT tank could not be irradiated, it was decided that a useful test would be the thermal cycling of the large insulated cryogen tank to evaluate the ability of the foam to retain its integrity under the stress of thermal

and pressurization cycling. The tank was therefore subjected to five fill, drain, and warmup cycles using liquid nitrogen as the cryogen. Temperature, boiloff, and strain measurements were used to aid in the evaluation.

SUMMARY

A 5400-gal RIFT-model tank (9-ft diameter and 15-ft height with a conical bottom) insulated with a 2-in.-thick layer of sprayed-on polyurethane foam insulation has been thermal cycled with liquid nitrogen. Five fill, drain, and warmup cycles were conducted over a period of about a month. During each fill with LN_2, temperatures were measured at several levels in the insulation and the tank was pressurized to a maximum of 27 psi.

Although there was considerable wrinkling and puckering of the outer glass cloth covering over the foam during the fill cycles, there was no evidence, either visual or from temperature data, that the insulation was damaged or its effectiveness impaired. The measured boiloff rate was approximately 22 gal LN_2 per hour and the computer thermal conductivity was 0.014 Btu/h-ft-^{o}F.

Data from strain gages mounted internally on the tank wall indicated that strains were within expectations during the pressure cycles. Data from gages mounted on the outer surface of the insulation tended to have large variability, generally going from large positive values to large negative values during the different cycles. This is probably a reflection of the considerable movement that obviously occurred due to the lowering

of the pressure and partial condensation of the freon gas in the foam.

I. INTRODUCTION

A test has been performed in which a 5400-gal RIFT-model tank insulated with sprayed-on polyurethane foam has been subjected to five fill-and-drain cycles with liquid nitrogen. Temperatures were measured at several depths in the 2-in.-thick foam and strain was measured during pressurization cycles with the tank filled with liquid nitrogen. The ability of the insulation to withstand repeated thermal cycles without serious loss of effectiveness was then evaluated.

The insulation system consisted of a 2-in.-thick layer of CPR 385-2 polyurethane foam enclosed in glass cloth impregnated with Narmco 7343 urethane adhesive and overcoated with Staco No. 1024 white epoxy enamel. This insulation system had been selected on the basis of an irradiation test previously conducted at General Dynamics. The irradiation of a tank (30-in. cube) containing liquid hydrogen verified the radiation stability of the foam. The following is a summary of results taken from Reference 1:

> A tank (Cube B) insulated with urethane spray foam (CPR 385-2) has been irradiated while filled with liquid hydrogen, subjected to six 1-h postirradiation acoustic vibration tests while filled with liquid nitrogen, and finally given nine thermal cycles with liquid hydrogen. The irradiation was made with the Ground Test Reactor with the maximum exposure to the

insulation being a gamma dose of 2×10^{10} ergs/g(C) and a neutron fluence of 2.3×10^{16} n/cm^2 (E > 1.0 MeV). The principal results were:

- No detonations occurred during this test; this is in contrast with the earlier Cube A experiment during which two detonations occurred in the cork-board insulation of that tank.

- The tank withstood the irradiation and postirradiation tests with a probable maximum increase of 35% in the thermal conductivity of the insulation system.

- Separation of the vapor barrier from the foam insulation was observed at one of the faces exposed directly to the acoustic horn after the third LH_2 cycle following the irradiation and acoustic vibration tests, Post-test examination also revealed damage to the foam insulation and separation of a small section from the aluminum tank on same face.

The radiation exposure to the insulation in the Cube B test exceeded by more than a decade that predicted at the bottom of the propellant tank in ten missions of the Reusable Nuclear Shuttle utilizing a 1575-MW NERVA (Ref. 2). Radiation damage to the insulation, per se, was therefore not of prime concern, but some question remained as to the ability of the foam to adhere to the tank under thermal cycling. Under the conditions of this test, at least, this does not appear to be a problem.

This work was conducted at the Nuclear Aerospace Research Facility (NARF) operated by the Fort Worth operation of the Convair Aerospace Division of General Dynamics for the George C.

Marshall Space Flight Center of the National Aeronautics and Space Administration under Contract NAS8-18024. Under Contract NAS8-18024, the Fort Worth operation has performed numerous radiation effects experiments on organic materials and thermal insulations as a part of the technology program supporting the development of a nuclear rocket vehicle.

II. DESCRIPTION OF TEST

2.1 Test Article

The insulation material under evaluation consisted of Upjohn CPR 385-2 polyurethane foam enclosed in glass cloth. A 2-in.-thick layer of foam was sprayed on the tank and enclosed in two layers of No. 16 glass cloth impregnated with Narmco 7343 urethane adhesive. The glass cloth was overcoated with a thermal-control coating of Staco No. 1024 white epoxy enamel (Stabler Paint Mfg. Co.).

The insulated and instrumented tank was supplied by NASA-MSFC. The 5400-gal tank is 9 ft in diameter and slightly over 15 ft in length. The tank material is 0.25-in.-thick 5456-H321 aluminum. It was mounted vertically in a four-column stand just south of the Irradiated Materials Laboratory (IML) (Fig. 1). The plumbing (Fig. 2) consisted of liquid nitrogen fill and gravity-drain line and gaseous nitrogen vent and relief lines with pressure gages.

2.2 Instrumentation

Strain gages were mounted along four lines running from top to bottom along the tank wall. As viewed from above, the lines were spaced 90° apart and CCW numbered I, II, III, and IV. The gages were mounted in biaxial pairs, one horizontal and

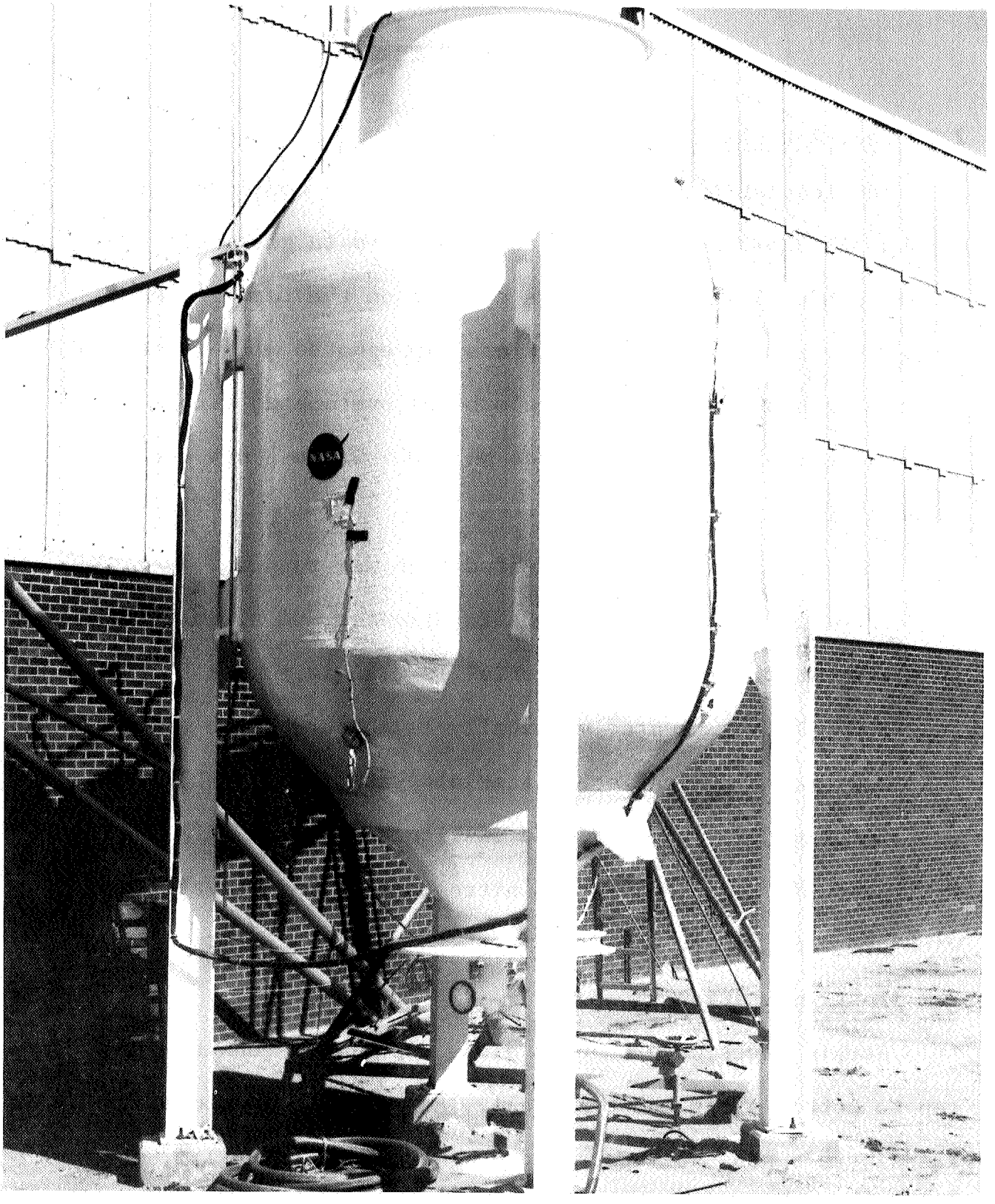

Figure 1 Tank Mounted in Test Position

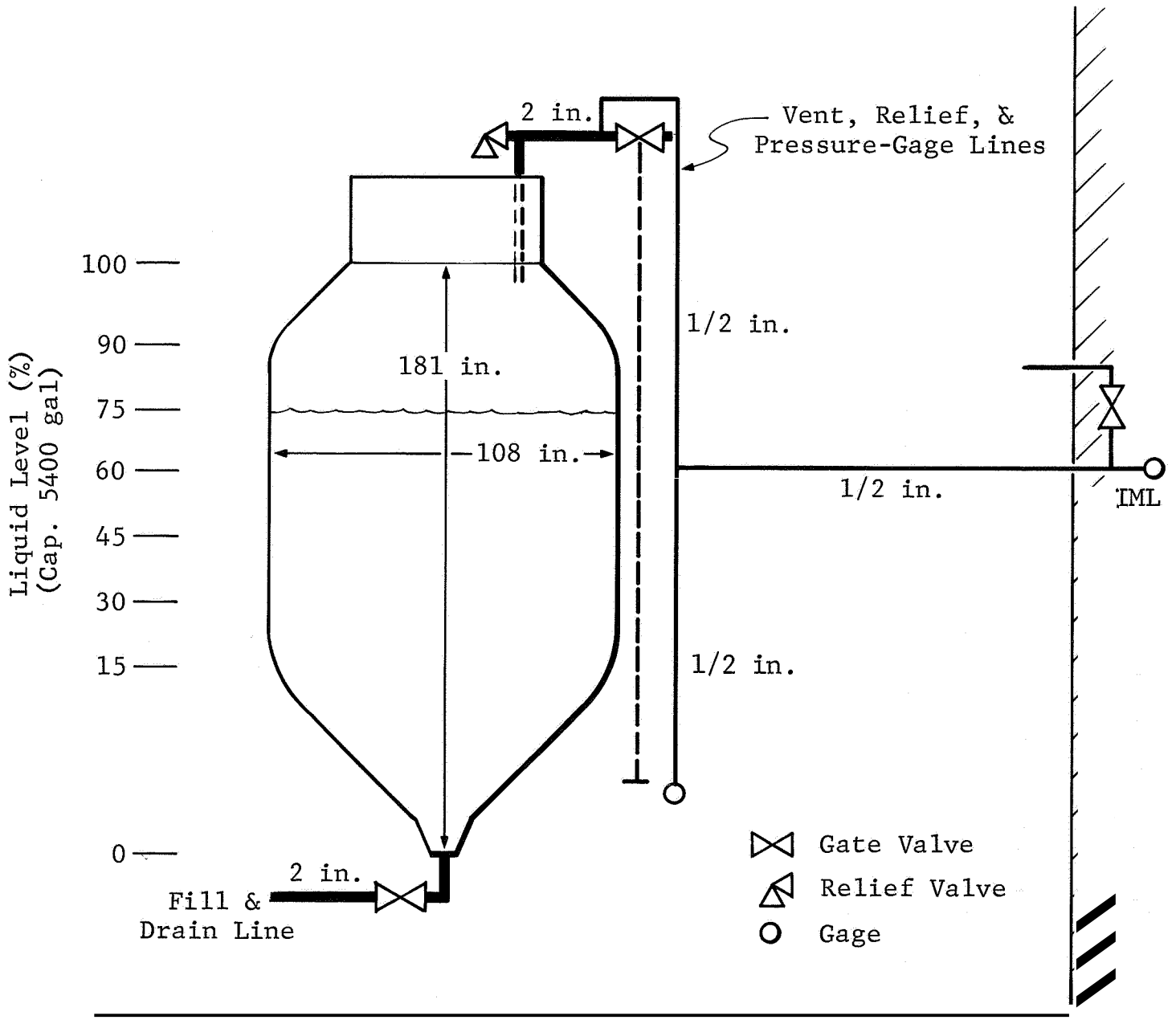

Figure 2 Schedmatic of Tank and Piping

one vertical, at station locations corresponding to inches above the tank base. The gages were Budd Metalfilm Type S-740, temperature compensated for magnesium alloy with an expansion coefficient of 15 ppm/°F, and having a gage factor of 2.65 at 75°F and resistance of 281.3 ±2 ohms. Eight strain gage pairs were mounted on the tank inner surface and eight pairs on the insulation outer surface just under the glass fabric. Strain gage measurements were made by recording of the strain gage d.c. voltage and the d.c. voltage drop across a standard resistor as measured with a digital voltmeter.

Copper-constantan thermocouples were mounted along the above lines at various locations. The couples were made of 10-mil wire with 32-mil leads. In addition to single thermocouples along line II at the tank and insulation interface (0-in. level), sets of nine tempered thermocouples were embedded to different depths in the insulation at four locations. The nine thermocouples in each of these four sets were arranged in two groups and positioned as illustrated in Figures 3 and 4. The tempering methods were such that one group had a constant length (– 3 in.) of T/C wire embedded at each level (tempering Method A). The other group had different lengths of embedded T/C wire but all the thermocouples were lined upon a direct path through the insulation (tempering Method B). As indicated in the figures, the embedding

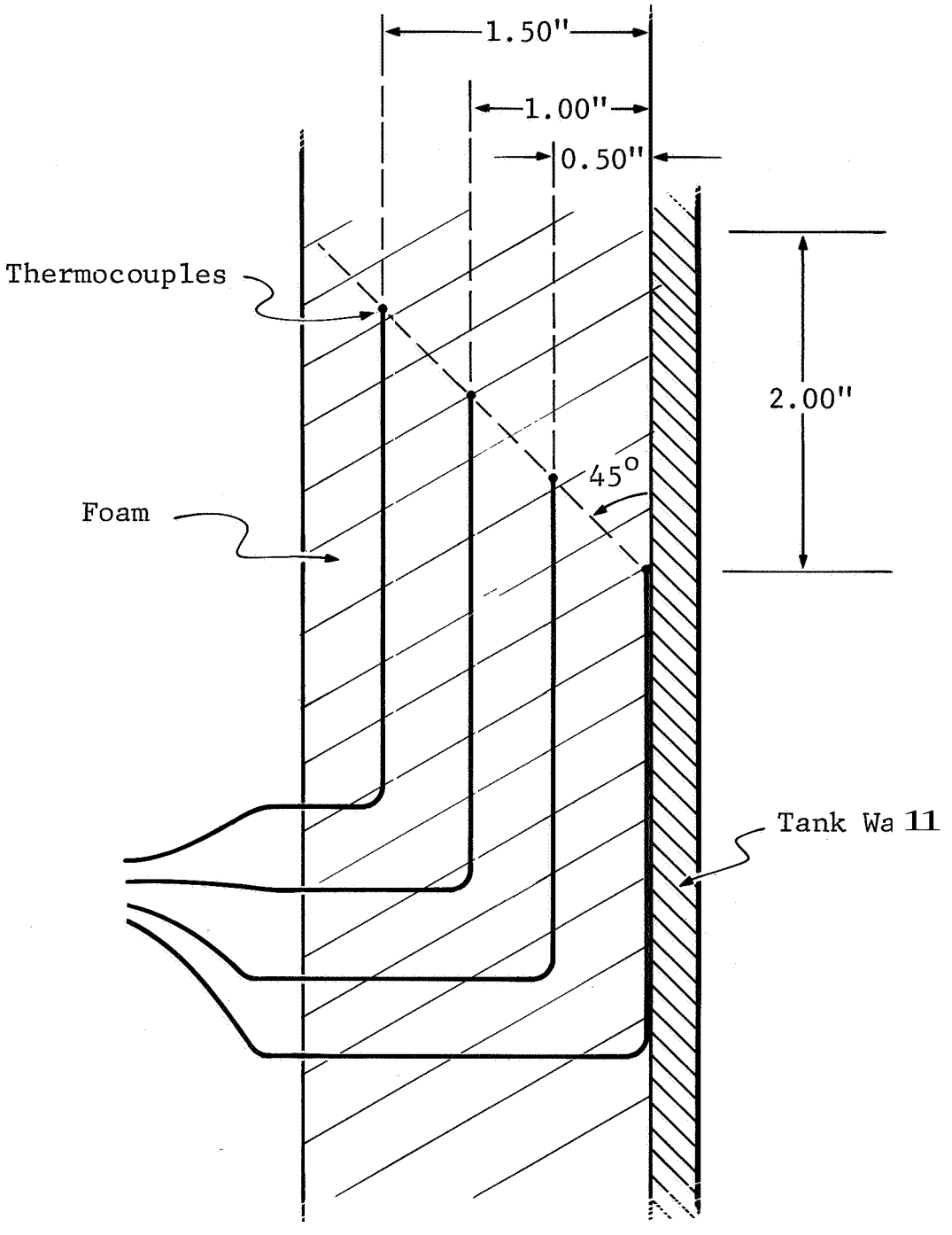

Figure 3 Thermocouple Arrangement for Tempering Method A

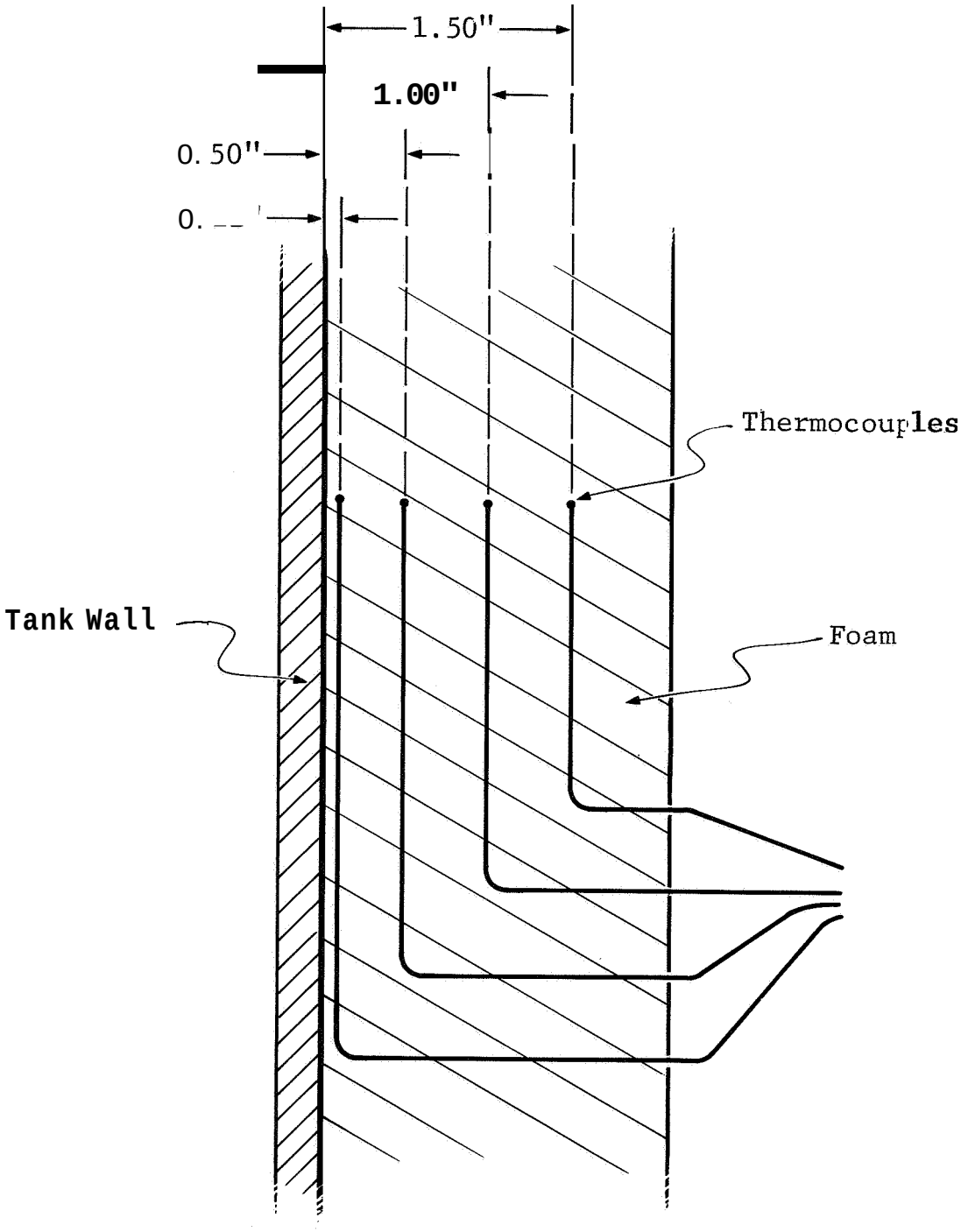

Figure 4. Thermocouple Arrangement for Tempering Method B

levels were 0, 0.5, 1.0, and 1.5 in. for the thermocouples of tempering Method A and 0.12, 0.5, 1.0, and 1.5 in. for tempering Method B. The single common thermocouple at the 2-in. level, i.e., the insulation surface, was under the glass fabric.

The locations on the tank of the individual and sets of thermocouples are given in Table 1. A Brown multipoint temperature recorder was used for thermocouple readout.

In addition to the strain gages and thermocouples, a cryogen level probe consisting of 18 resistors was installed in the tank for monitoring the LN_2 level. The resistors were each 860-870 ohms. Two copper-constantan thermocouples were installed at the two lowest resistor levels on the probe for verifying resistor immersion in LN_2 during calibration of the cryogen liquid level indication and control panel. The probe resistor stations and tankage in gallons and percent are given in Table 2.

Table 1

THERMOCOUPLE LOCATIONS ON TANK

Line	4	12	24	36	48	60	72	96	120	144	168
I					9						
II											
III											

Table 2

SENSOR LOCATIONS IN LIQUID LEVEL PROBE

Station (in.)	Quantity		Station (in.)	Quantity	
	Percent	Gal		Percent	Gal
12*	-	-	84	33.8	1830
26	1.0	54	99	45.0	2430
30	1.8	97	124	64.2	3460
38	3.9	211	138	75.0	4050
46	7.0	378	139	75.8	4090
48	8.0	432	140	76.6	4130
54	11.5	621	141	77.4	4180
62	17.2	929	149	83.3	4500
66	20.0	1080	158	89.8	4850

*Reference resistor station

III. RESULTS AND DISCUSSION

The insulated tank was subjected to five fill-and-drain cycles with liquid nitrogen. During each period that the tank contained liquid nitrogen, the tank was pressurized (by closing the exhaust valve) and strain measurements were made as a function of tank pressure up to a maximum of 27 psi. Temperature measurements in the insulation were also made during each fill cycle and the tank insulation was visually inspected.

Data pertaining to the fill-and-drain cycles are the following:

Date of Fill	Initial Quantity gal	Duration h
2-14-72	4850	46
2-18-72	3400	98
2-24-72	4850	105
3- 6-72	4850	
3-14-72	4850	190

3.1 Heat Transfer Data

3.1.1 Temperature Measurements in the Insulation

Data on the temperature gradient through the insulation were taken at two points on the tank (line II, station 12 and line 11, station 120) during each of the five fill cycles. Two sets of thermocouples were used at each point, each set using different tempering methods. Figures 3 and 4 show the placement through the insulation and illustrate the two tempering

methods used. As discussed in the previous section, the placement method using constant tempering length is called tempering method A, and the placement method using various tempering lengths is called tempering method B.

Tables 3 through 6 show the temperature gradient data. Each set of data shown was recorded toward the end of the cycle when thermal equilibrium appeared to be established. As can be seen from the temperature values for the same placements from cycle to cycle there was no significant degradation of the effectiveness of the insulation with time. Although some considerable variation is noticeable from cycle to cycle in measured values at placements toward the outside of the insulation, this is believed to be merely a reflection of the changing ambient conditions.

On the whole, tempering method A appears to be the better method of thermocouple placement. Figure 5, which is a plot of measured temperature versus location through the insulation for cycle 1, station 120, clearly illustrates the superiority of tempering method A. The radius of the tank wall is so large that the insulation can be effectively treated as a plane slab and, assuming homogeniety, the temperature profile through the slab should therefore be linear. It can then be seen how much more closely the temperatures values measured with thermocouples

Table 3

TEMPERING METHOD A THERMOCOUPLE DATA, STATION 12

Distance from Tank Wall (in.)	Temperature (OF) Fill Cycle				
	1	2	3	4	5
0.0	-308	-308	-312	-310	-312
0.5	-184	-180	-192	-177	-190
1.0	-104	- 97	-114	- 92	-110
1.5	- 48	- 38	- 52	- 32	- 55
2.0	62	78	48	84	62

Table 4

TEMPERING METHOD A THERMOCOUPLE DATA, STATION 120

Distance from Tank Wall (in.)	Temperature (°F) Fill Cycle				
	1	2	3	4	5
0.0	-308	-300	-292	-311	-312
0.5	-210	-205	-194	-199	-208
1.0	-105	- 96	-114	- 92	-116
1.5	- 49	- 96	-114	- 92	-116
2.0	64	82	43	86	60

Table 5

TEMPERING METHOD B THERMOCOUPLE DATA, STATION 12

Distance from Tank Wall (in.)	Temperature (OF) Fill Cycle				
	1	2	3	4	5
0.12	-286	-288	-292	-286	-292
0.5	-174	-175	-186	-173	-184
1.0	- 96	- 98	-106	- 82	-102
1.5	- 65	- 58	- 78	- 54	- 74

Table 6

TEMPERING METHOD B THERMOCOUPLE DATA, STATION 120

Distance from Tank Wall (in.)	Temperature (°F)				
	'1	2	3	4	5
0.12	-286	-296	-296	-295	-296
0.5	-168	-162	-160	-160	-166
1.0	- 40	- 30	- 50	- 26	- 52
1.5	-16	- 6	-28	1	- 26

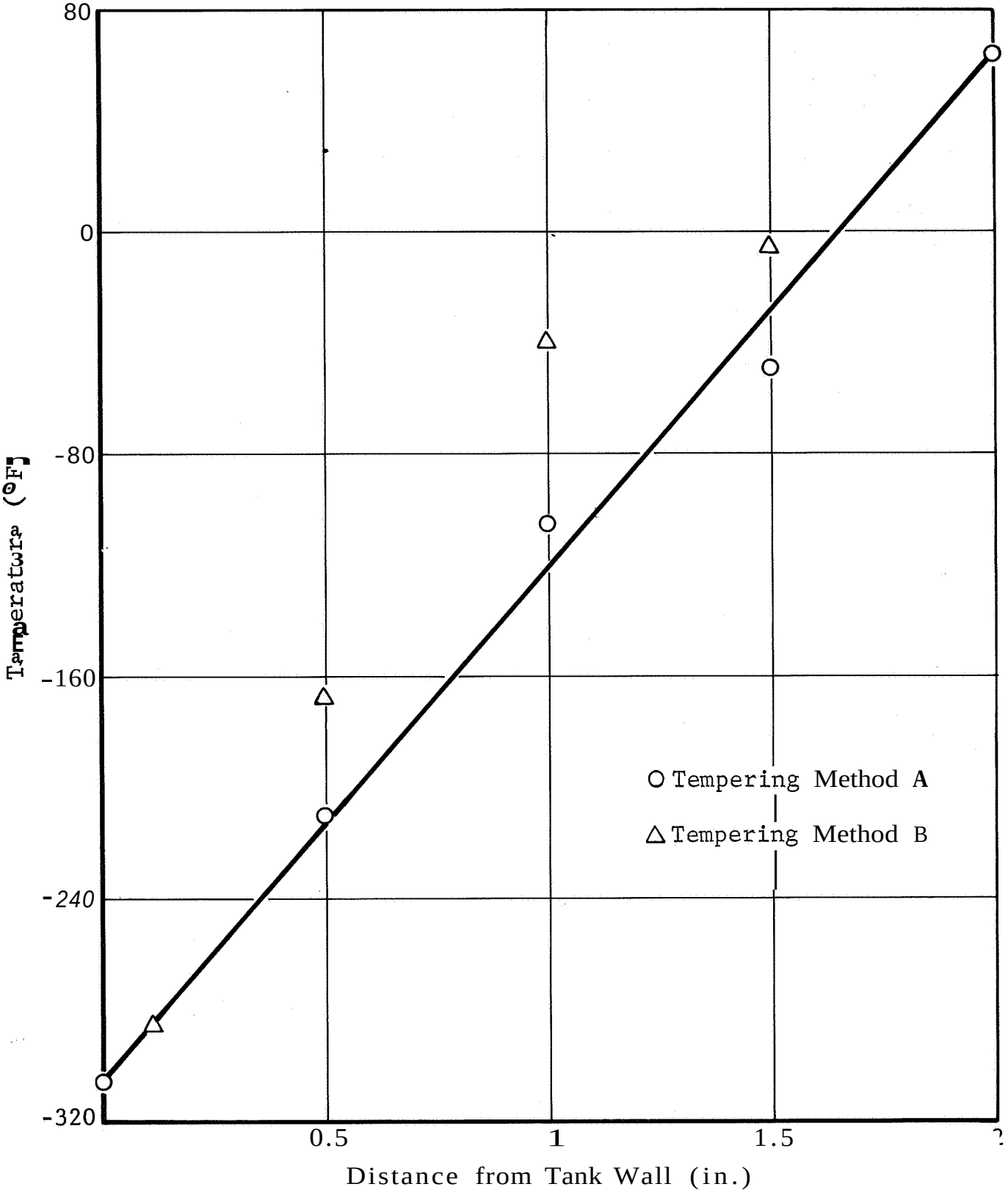

Figure 5 Typical Results of Temperature Measurements through the Insulation Using Two Tempering Methods

placed according to tempering method A approach the theoretical straight line function than do the temperature values measured with thermocouples placed according to tempering method B. The shorter the tempering lengths the greater the departure of measured values from the theoretically expected values. This departure is also always in the direction of too high a measured value, and the overall results are exactly what would be expected if the tempering lengths of tempering method B were insufficient.

3.1.2 Effective Thermal Conductivity of the Insulation

The surface area of the tank is known, the thickness of the insulation is known, and the temperature difference across the insulation has been measured. In order to calculate the effective thermal conductivity of the tank insulation it is then only necessary to ascertain the average heat flow into the tank.

Boil-off data were accumulated over a seven day period after the last cycle, and from these data it was determined that the average boil-off rate of the liquid nitrogen contents was approximately 22 gal/h. Assuming that all of the heat entering the tank was rejected by vaporization of the liquid nitrogen, it is then possible to estimate the effective thermal conductivity of the tank insulation by using the equation

$$k = \frac{QX}{A\Delta T}$$

where k = thermal conductivity in Btu/h-ft-^{o}F

X = thickness of insulation = 1/6 ft

Q = heat flow into tank = 12,600 Btu/h

A = surface area of tank = 400 ft^2 (including uninsulated cop plate and shroud, Fig. 1)

AT = average temperature difference across the insulation = 374^{o}F

Substitution of values into the equation yields

$$k = 0.014 \text{ Btu/h-ft-}^{o}\text{F}$$

which is in general agreement with data from the literature.

3.2 Strain-Gage Data

The RIFT tank strain measurements were made by the voltage-ratio technique. This technique is based on the principle that the ratio of the individual voltage drops across two resistors in series is independent of power supply variations, thus eliminating variations in the input power as a source of error.

The strain gage equation is expressed as

$$\epsilon F = \frac{\Delta R}{R} \qquad (1)$$

where F = gage factor (2.65 for gages used)

R = resistance of strain gage at zero strain

ΔR = change in resistance of Strain gage due to strain

ϵ = strain

Using the voltage ratio technique with R_s constant, Equation 1 may be expressed in terms of the voltage ratios at zero (0) strain, $E_{R_S}(0)/E_{R_G}(0)$, and the voltage ratios at a value of strain, $E_{R_G}(P)/E_{R_S}(P)$. With the ratio substitutions, Equation 1 becomes

$$\epsilon = \frac{1}{F}\left[\left(\frac{E_{R_G}(P)}{E_{R_S}(P)} \times \frac{E_{R_S}(0)}{E_{R_G}(0)}\right) - 1\right] \qquad (2)$$

Figures 6 and 7 are typical plots showing the relationship between strain and pressure build-up inside the tank. The slopes of the strain-pressure plots showed deviations from the average of up to +15% for station 56 and ±6% for station 90 over the five thermal cycles. The deviations in slope were apparently due to creeping, which was more apparent during some cycles than others because of the greater lapse of time between data points. Overall, the data did not indicate strains sufficient to structurally damage to the tank.

The output from strain gages located on the outer surface of the insulation showed large variations within a pressurization cycle and also between cycles. Strains varied from large positive values to large negative values at various times with no consistency with tank pressure. This probably reflects the shifting of the foam and the cloth fiber coating as evidenced

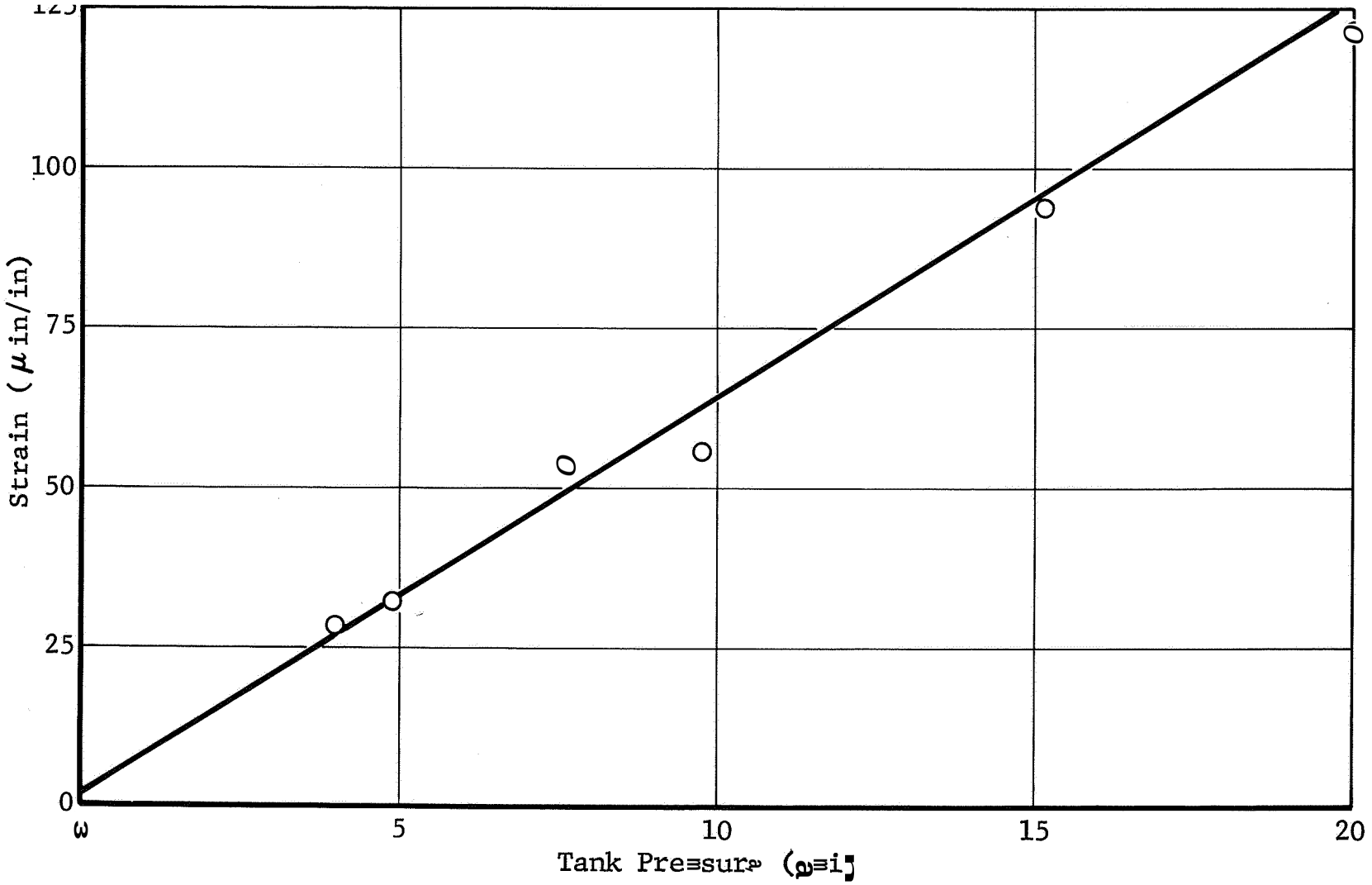

Figure 6 Strain in Tank Well Measured with Gage 3 (Vertical) at Station 56 During Pressure Cycle 4

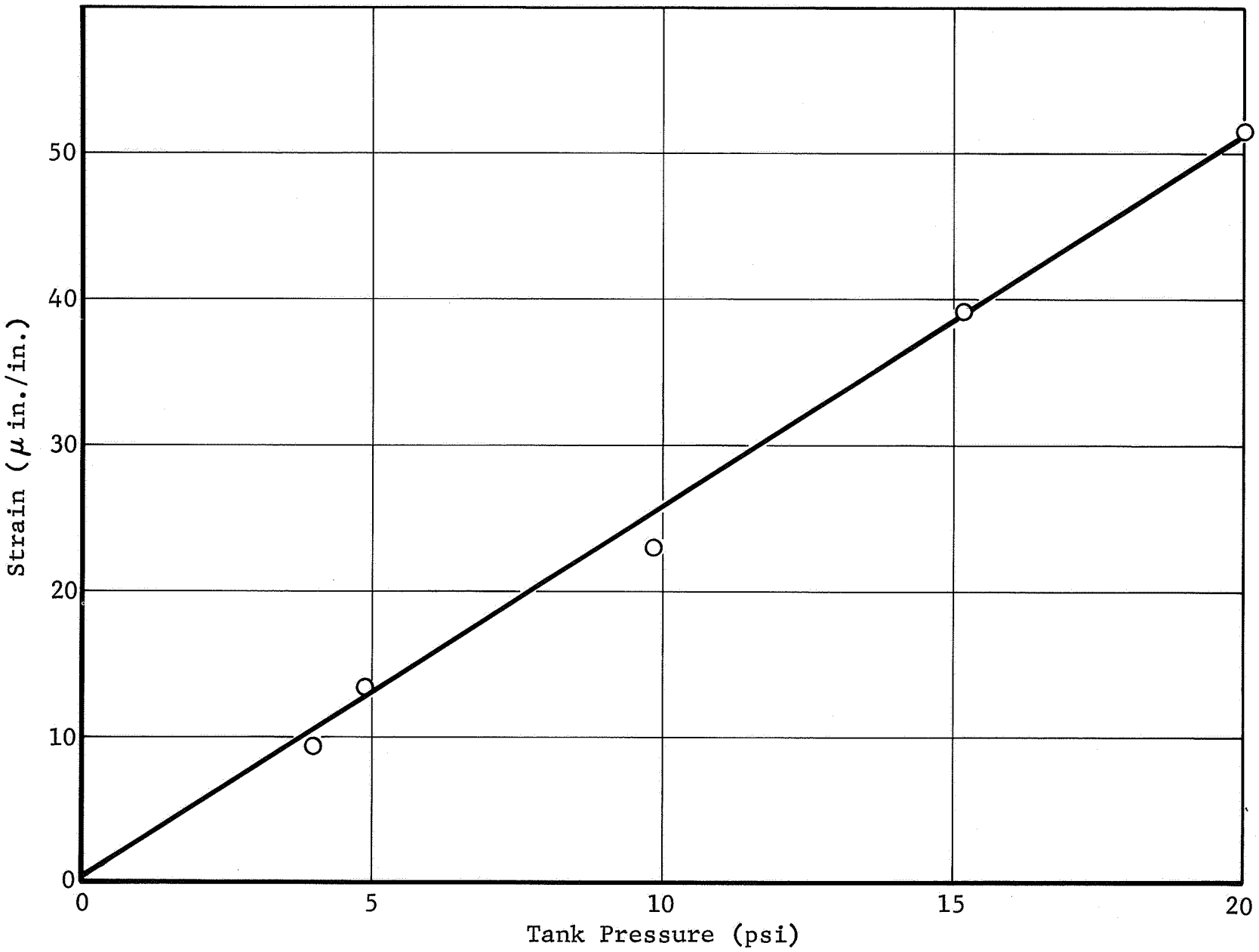

Figure 7 Strain in Tank Wall Measured with Gage 4 (Horizontal) at Station 90 During Pressure Cycle 4

by the wrinkling of the surface. These movements may have been sufficient to exceed the gage'limits or cause failure of the bonding.

3.3 Visual Appearance of Insulation

With liquid nitrogen in the tank, the glass fabric cover over the foam insulation became wrinkled and puckered. Figures 8, 9, and 10 are views of the tank during the third fill cycle. The appearance was essentially the same during all five cycles. No serious deterioration of the insulation or coating was evident. After completion of the test, the coating retained slight creases at the locations of the deeper wrinkles. However, there was no visual indication of insulation separation from the tank or other deterioration.

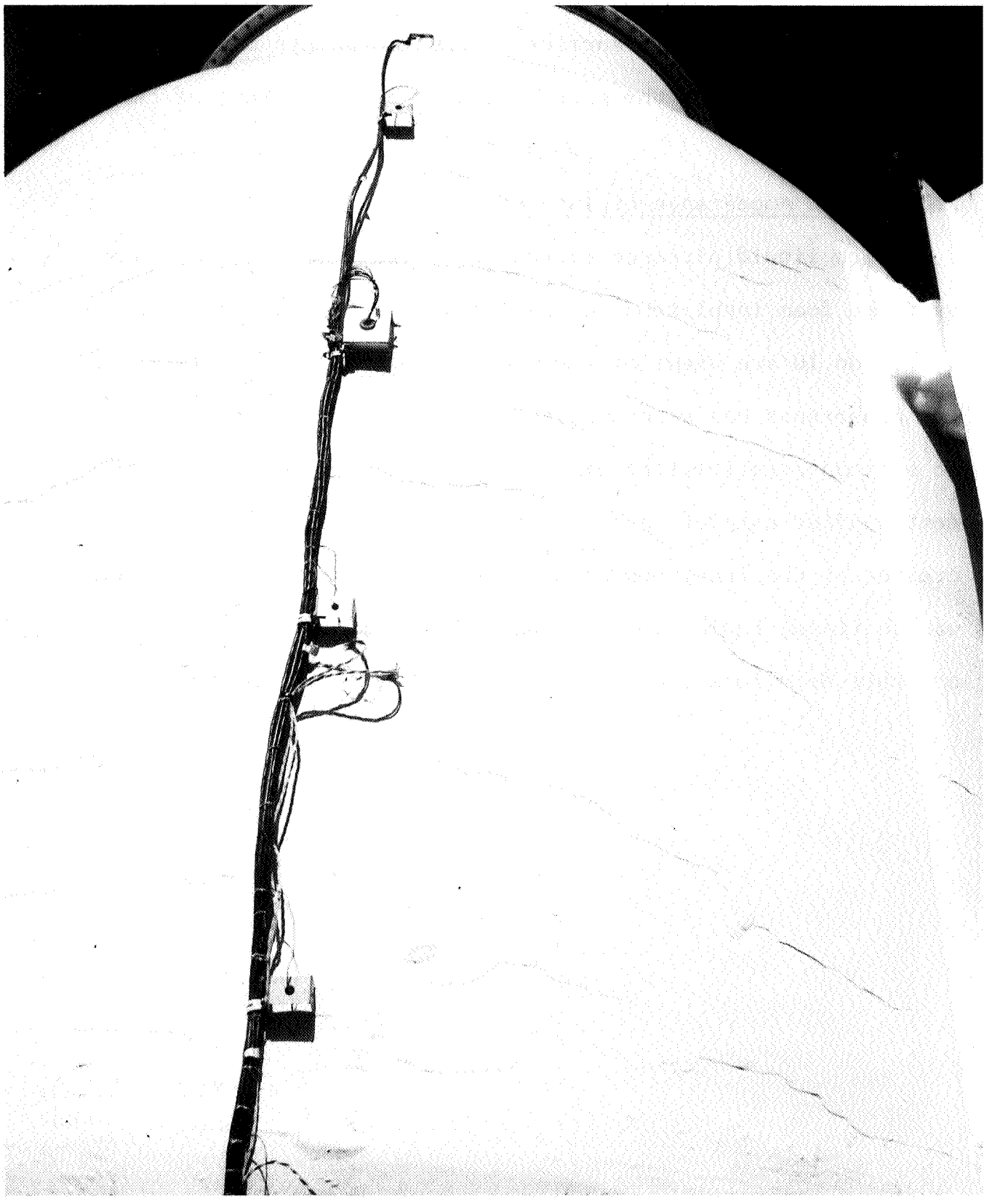

Figure 8 View of Insulation Surface During Third Fill Cycle

Figwre 9 Detail of Insulation Coating During Third Fill Cycle

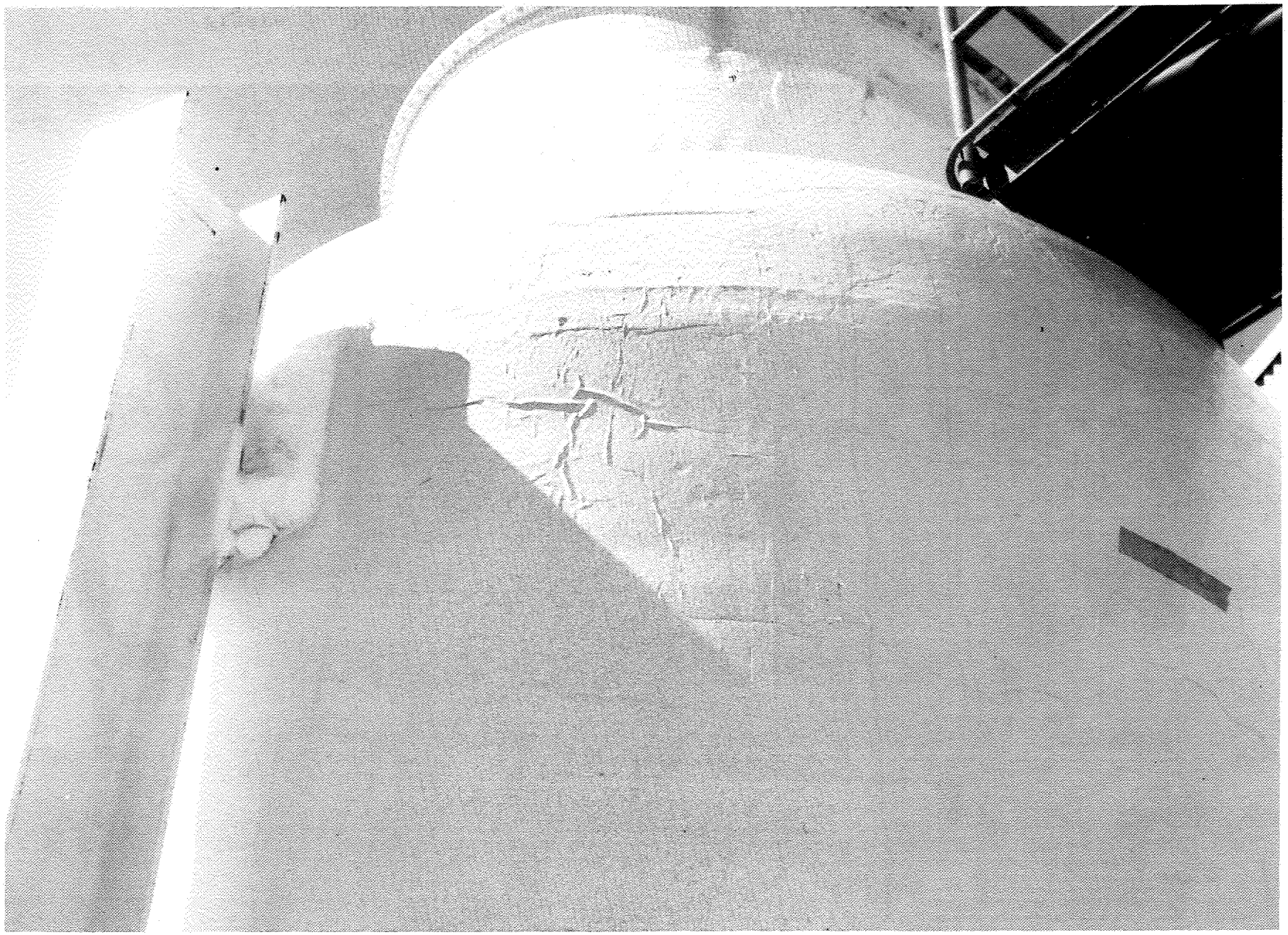

Figure 10 Puckering of Insulation Coating During Third Fill Cycle

REFERENCES

1. McMillan, W. D., Carter, H. G., and Lightfoot, R. P., Evaluation of Cryogenic Insulation Materials and Composites for Use in Nuclear Radiation Environments - Insulation System Tests, General Dynamics Fort Worth Division Report FZK-348, June 1968.

2. Greenhow, W. A. and Lewis, J. H., Evaluation of Insulation Materials and Composites for Use in a Nuclear Radiation Environment - Radiation Analysis of Saturn V Materials, Systems, and Components, General Dynamics, Convair Aero-Space Division Report FZK-378, June 1971.